FLUORIDE LEVELS IN WATER SOURCES OF GILGIL AREA IN KENYA: DEFLOURIDATION USING LOCALLY AVAILABLE GEOMATERIALS

WAMBU ENOS WAMALWA (MSc, Chemistry)

I84/1277/2009

A Thesis Submitted in Partial Fulfilment of the Requirements for the Award of the Degree of Doctor of Philosophy (Chemistry) in the School of Pure and Applied Sciences, Kenyatta University

MAY 2015

DECLARATION

This thesis is my original work and has not been presented for a degree in any other university

Signed……Date 13/6/2015

Wambu Enos Wamalwa (I84/12777/2009)
Department of Chemistry
Kenyatta University

We confirm that the work reported in this thesis was carried out by the candidate under our supervision and it has been submitted with our approval as university supervisors

Signed……Date 15th June 2015

Dr. Charles O. Onindo
Department of Chemistry
Kenyatta University, Nairobi, Kenya

Signed……Date June 15, 2015

Dr. Willis J. Ambusso
Department of Physics,
Kenyatta University, Nairobi, Kenya

Signed……Date June 15, 2015

Prof. Gerald K. Muthakia
Department of Chemistry,
Dedan Kimathi University of Technology, Nyeri, Kenya

DEDICATION

To my dad, Wilson Wambu Murambakania (1917-2012)

ACKNOWLEDGEMENTS

This work was made possible by research funds from the International Foundation for Sciences (IFS) and from the National Commission for Science, Technology and Innovations of Kenya (NACOSTI). Nonetheless, I must thank the Department of Geology and Mines in the Ministry of Mining of Kenya for allowing me to perform XRD and AAS analyses on their instruments.

Very special thanks are due to my lead supervisor Prof Gerald K. Muthakia of the Department of Chemistry, Dedan Kimathi University of Technology and to my other supervisors Dr. Charles Onindo of the Department of Chemistry, Kenyatta University and Dr. Willis Ambusso of the Department of Physics, Kenyatta University for their constant interest, encouragement, support, and friendship throughout the course of this work. Their excellent guidance, kind criticism and novel thoughts made this work a pleasurable and gratifying experience. It is my genuine pleasure then to thank my mentors: Prof Paul M. Shiundu of the Departments of Chemistry in Technical University of Kenya and Dr Joseph Karanja wa-Thiong'o of the Department of Chemistry, Kenyatta University, for their invaluable thoughts during the designing of the initial proposal for this work. I sincerely thank Prof Alex Machocho, Department of Chemistry, Kenyatta University, for sparing his precious time to proof read the final draft of not only this thesis but of the initial proposal as well. Notwithstanding, I must express my gratitude to all the members of the Department of Chemistry of Kenyatta University for their academic and technical support throughout the time I worked on this project.

A very special 'thank you' is, however, owed to Ms Grace W. Gachagua and to my sister Ms Rose Namachanja Wambu for assisting me in the collection of the adsorbent materials from Nakuru and Bungoma counties, respectively. Finally, it suffice to mention that indeed I owe this work to the unrestricted love, patience and support of my wife Sare, my daughters Abida and Hope, my son Joacquim and to my parents Dinah and Wilson Wambu Murambakania, his soul rest in eternal peace.

TABLE OF CONTENTS

LIST OF TABLES

LIST OF FIGURES

ABBREVIATIONS AND ACRONYMS

AAS	Atomic absorption spectrophotometry
DIME	Acid treated diatomaceous earth
b	Langmuir thermodynamic equilibrium constant'
C	Weber-Moris intercept
C_0	Initial adsorbate concentration
CDC	Centre for Disease Control and Prevention
C_e	Equilibrium adsorbate concentration
C_v	Effluent adsorbate concentration at a particular volume
DDW	Doubly de-ionized water
EDL	Electrochemical double layer
ΔH^*_a	Activation enthalpy
HAp	Hydroxyapatite
IHP	Inner Helmholtz Plane
ISE	Ion selective electrode
$k_{1,ads}$	First order adsorption rate constant
$k_{2,ads}$	Second order adsorption rate constant
K_f	Freundlich adsorption constant
K_{Th}	Thomas adsorption rate constant
$K_{w,1}$	Weber-Moris intraparticle constant in the initial stages
$K_{w\cdot2}$	Weber-Moris intraparticle constant in the later stages
LAG	Locally available adsorbent geomaterial
LOI	Loss on ignition of a mineral
m	Adsorption batch adsorbent mass
NSIM	Siliceous mineral adsorbent
FEPM	Ferric poly-mineral adsorbent
FELS	Lateritic adsorbent mineral
MLC	Magnesia-loaded cenospheres
n	Freundlich intensity parameter
OHP	Outer Helmholtz plane
PZNC	pH of zero net charge of a mineral
q_e	Equilibrium adsorption
q_m	Langmuir maximum adsorption capacity
q_t	Amount of adsorption per unit time
q_{Th}	Thomas maximum adsorption capacity
r_L	Langmuir dimensionless parameter
TiSAB	Total ionic strength adjustment buffer
V_t	Break through volume
WHO	World health organization
XRD	X-ray diffraction

ABSTRACT

High prevalence of fluorosis resulting from consumption of drinking water containing excessive fluoride levels continues to affect many communities in Kenya. Low-income rural communities are most affected because of inadequate water treatment and high costs of necessary medication. As part of the on-going search for efficient and affordable water defluoridation protocol, which has intensified in the most recent past, soil adsorbents have attracted a near-global acclaim as the most promising low-cost media for water defluoridation. Nevertheless, it is still unclear whether certain Kenyan clays and soil minerals could be applied as inexpensive adsorbents in defluoridation of household water. The present study was, therefore, designed to assess the capacities of selected locally available geomaterials (LAGs) to remove fluoride from water with a view to develop an efficient and affordable water defluoridation technology. The adsorbent materials, which included a naturally occurring siliceous mineral (NSIM), a diatomaceous earth (DIME), a ferric poly-mineral (FEPM) and iron enriched lateritic soils (FELS) were sampled from their natural deposits in Bungoma and Nakuru counties of Kenya. The minerals were pulverized to pass through 0.5-mm sieves and less than 1.0-μm fractions isolated by mechanical agitation and sedimentation of the pulverized samples in doubly de-ionized water (DDW). After the initial pre-treatment in dilute HCl solution, the chemistry and mineralogy of the LAGs were analyzed by atomic absorption spectrophotometry (AAS) and by X-ray Diffraction Analysis (XRD). The fluoride adsorption properties of the LAGs were then assessed with respect to changes in initial fluoride concentration, contact time, mixing ratios, presence of interfering ions, and solution pH and temperature. The efficacy of the LAGs to sorb fluoride from natural high-fluoride water was verified in batch and column tests. Fluoride adsorption onto the acidified LAGs was found to be controlled by the mineralogy and chemical composition of the adsorbents as well as by the solution parameters. The equilibrium fluoride adsorption onto the LAGs was adequately fitted by the Langmuir and the Freundlich adsorption isotherms indicating heterogeneity in the fluoride adsorption mechanisms. Acidified DIME had highest fluoride adsorption capacity (51.1 mg/g) and the capacities of NSIM, FEPM and FELS to sorb fluoride from simulated batch solutions were in range of 10-13 mg/g. The adsorption kinetic data showed that for fluoride adsorption by NSIM and FEPM followed both pseudo-first order and pseudo-second order kinetic models. The adsorption of fluoride onto DIME could, however, be described by intraparticle diffusion kinetics whereas that for FELS by both the pseudo-second order and intraparticle diffusion models. Highest fluoride removal from high-fluoride natural water was achieved using FELS. Fluorides desorption from the LAGs, which was assessed using aqueous solutions of NaCl and Na_2CO_3, demonstrated the reversibility of the processes. The LAGs showed good fluoride adsorption capacities and they could be utilised as inexpensive adsorbents to defluoridate high fluoride drinking waters and help to alleviate endemic of fluorosis among the communities. Results of this study will be useful as a basis for future scale up using these inexpensive materials as low-cost adsorbents to develop affordable technology for easy and safe defluoridation and sustainable cleaning of drinking water.

CHAPTER ONE
INTRODUCTION

1.1 Background information

Sufficient dietary fluoride is essential for the development of healthy teeth and bones. Fluoride deficiency increases teeth decay but prolonged exposure to excessive fluoride attracts detrimental effects such as colorization of teeth surfaces, staining, pitting and loss of teeth enamel (Boldaji *et al.*, 2009). Severe crippling deformations and death result in chronic cases of exposure to excessive fluoride (Xu *et al.*, 2000). Non-skeletal effects of long-term consumption of excessive fluoride range from neurological, kidney, endocrine, thyroid and liver disorders to chronic disruption of metabolic processes when the fluoride dosage is high (Ayoob and Gupta, 2006; Adelana *et al.*, 2010). At the moment, however, fluorosis remains the most noxious effect of long-term exposure to excessive fluoride levels (Sushela *et al.*, 1993).

The primary pathway by which people get exposed to excessive fluoride is by continuous consumption of high-fluoride water, when safer drinking water sources are not readily available (Mascarenhas, 2000). For this reason, the drinking water standards for fluoride, which are recommended by the World Health Organization (WHO) are 0.7 mg/L (Centre for Disease Control and Prevention (CDC), 2005). Even so, natural waters, normally, linked with high fluoride levels occur in calcium-deficient groundwater aquifers, in geothermal springs, and in certain sedimentary drainage basins (Teutli-Sequeira *et al.*, 2011). Constant monitoring of fluoride content of community water in such areas is, therefore, recommended.

Increasingly more communities are being exposed to elevated levels of fluoride through high-fluoride household water (Burt, 1992). Thus, about 200 million people, in over 25 countries world-over, are now under constant threat of fluorosis due to excessive fluoride in their household water sources (Ayoob and Gupta, 2006). Thus, In view of the high toxicities associated with excess consumption of fluoride, the fate of excessive fluoride in groundwater sources continues to raise serious public health concerns world over (Nielsen and Dahi, 1995; Emekli-alturfan *et al.*, 2009; Arveti *et al.*, 2011; Borgnino *et al.*, 2013). In Kenya, for instance, endemic forms of fluorosis are to be found in the rural areas along the volcanic belt associated with the Great East African Rift Valley (Gikunju *et al.*, 2002; Moturi, 2004). The latest evidence have, however, reveals that the riparian communities along the shorelines of Lake Victoria could be at increased risk of severe forms of fluorosis and associated fluoride toxicities caused by excessive fluoride in their household water sources (Wambu *et al.*, 2014). In all cases, children under the age of 8 years, in whom teeth and bones are still developing, are most liable to all forms of fluorosis (Kahama *et al.*, 1997).

Prevention by controlling human exposure to fluoride remains the most efficient way of combating fluorosis among the communities. However, since it is not always practicable to change the water sources for the entire community, defluoridation of water from the existing sources to remove excessive fluoride while allowing adequate levels to safeguard against dental caries is currently the most realistic option.

Adsorption has emerged as the most appropriate technology for defluoridation of household water (Mohapatra *et al.*, 2009). This is because it is normally simple, cost-

effective and it offers satisfactory results (Bhatnagar *et al.*, 2011). Whereas several adsorbents have been applied to water defluoridation by adsorption to varying degrees of success, clays and certain soil minerals have attracted the highest research interest as ultimate fluoride adsorbents. It is because soil adsorbents are, normally, available in abundance and they are stable, easy to prepare and use and they can be applied in a wide range of conditions (Nath and Dutta, 2010). Notwithstanding, it is not immediately clear whether certain Kenyan clays and soil minerals could be used as inexpensive adsorbents in household water defluoridation so as to combat the runaway effects of excessive fluoride water in the country.

The current study was designed to interrogate the adsorption properties of particular Kenyan clays and to assess their capacities and efficiencies for water defluoridation. The locally available geomaterials (LAGs) that were selected for the current study included: a natural siliceous mineral (NSIM), a ferric poly-mineral (FEPM), ferric laterites (FELS) and diatomaceous earth (DIME). The mineral surfaces of the LAGs were initially pre-enhanced by physicochemical treatment in dilute HCl solution. Their fluoride adsorption capacities were then assessed on batch basis as a function of the adsorption time, adsorbent dosage, interferent anions, solution pH, and temperature. The Langmuir and Freundlich isotherms were then applied to analyze the fluoride adsorption equilibrium and the batch adsorption results verified in batch and column tests using natural high-fluoride water from a source in Gilgil, Nakuru County, Kenya (Kahama *et al.*, 1997). The results, which are presented in the current work demonstrated that the LAGs could be utilized as inexpensive media for easy and safe removal of excessive fluoride from drinking water.

1.2 Statement of problem

The undesirable effect of fluoride on human teeth was first formally documented in Kenya, independently, by Neville and Brass (1953), and by Williamson (1953). The authors described severe forms of fluorosis attributed to excessive fluoride in water in many parts of the country. Later the subsequent studies reported endemic levels of fluorosis by regions. Central (57%), Eastern (47%), and Rift Valley (34-80%) regions had the highest water fluoride levels in the country (Gitonga and Nair, 1982), while Nyanza (20%), Nairobi (18%), Northern-Eastern (17%), Coast (14%) and Western (12%) showed more modest prevalence levels (Chibole, 1987).

Newer evidence indicates progressively higher fluorosis prevalence in parts of Kenya. Ng'ang'a and Valderhaug (1993), for instance, reported 92% fluorosis prevalence among school-going children in Nairobi, which was higher than values reported earlier on by Nair *et al.* (1984) and Chibole (1987). In initial surveys conducted in 2010, which are reported in relevant sections of the current work, the values of water fluoride in the Gilgil-Elementaita area of Nakuru County of Kenya have been found to be greater than those earlier reported by Kahama *et al.* (1997) in the same area.

Water defluoridation by filtration using magnesium oxide and bone meal (Opinya and Pameijer, 1987; Opinya *et al.*, 1987), bone charcoal (Mwaniki, 1992), clay pot chips (Moturi *et al.*, 2002) and bone char (Korir *et al.*, 2009) have all been applied in previous initiatives to defluoridate household water so as to combat fluorosis in Kenya. Widespread fluorosis, however, continues to trouble communities in rural areas of the country (Kahama *et al.*, 1997; Kaimenyi, 2004; Moturi, 2004).

Since the previous initiatives are not creating much impact in controlling fluorosis in the country, there is need to rethink the approaches to provision of more quality point-of-use water for the rural communities in the high fluoride areas of the country. The current work has proposed a tailored adsorptive protocol based on locally available geomaterials (LAGs) for defluoridation of drinking water. It is anticipated that effective and affordable water defluoridation using the proposed media would improve access to safe drinking water, reduce human exposure to excessive fluoride and lessen the adverse effects of excessive water fluoride on public health among the rural communities in the Kenya.

1.4 Objectives

1.4.1 General objective

The general objective of this work was to determine the fluoride levels in selected water bodies in Gilgil area of Nakuru, Kenya, and the efficiency and capacity of selected geomaterials for fluoride from water with a view to develop affordable technology for easy and safe defluoridation and cleaning of drinking water.

1.4.2 Specific objectives

Specifically the study sought:

a. To determine the concentration of fluoride in drinking-water sources in the Gilgil-Elementaita area of Nakuru County of Kenya and so to assess typical magnitudes of the water-fluoride problem in Kenya.

b. To optimize activation conditions and determine the defluoridation efficiency and capacity of acid-activated geomaterials with respect to variations in

solution pH, temperature, contact time, initial fluoride concentrations, adsorbent dosage and co-existing ions so as to optimize the fluoride adsorption protocol using these adsorbent materials.

c. To characterize the fluoride adsorption data for the LAGs based on selected equilibrium and kinetics models so as to quantify the adsorptivity of the ion, elucidate the principal adsorption mechanism and evaluate the feasibility of practical use of this adsorption protocol in water defluoridation and sustainable cleaning of water.

1.3 Justification

According to the 2008 United Nations report on Millennium Development Goals, more than half of world's population faces water scarcity (United Nations, 2008). About 1.2 billion people in this category experience physical water scarcity but a bigger proportion of 1.6 billion others live under conditions of economic water scarcity, where even though water in nature is locally available to meet human demand, institutional and financial capital limits access to safe drinking water. The latter conditions are prevalent in South-Eastern Asia and Sub-Saharan Africa, where large proportions of the communities in rural areas suffer acute water shortage.

In Kenya, for instance, many communities in the volcanic belts of the rift valley are faced with acute water shortage due to excessive fluoride and salinity in natural groundwater sources. In such areas, fluorosis is a major public health concern and excessive fluoride in water sources has become the main impediment to water supply programmes and expansion of related economic agenda.

Whereas previous efforts to control household water fluoride levels have been applied to varying degrees of success in improving the quality of water for the communities, replication of the efforts to community scale has not been successful due to low efficiencies, high cost implications and fouling of the treated water (Opinya *et al.*, 1987; Korir *et al.*, 2009). There is, therefore, urgent need to device more innovative approaches towards defluoridation superior efficiencies and ease of replication and industrial scale-up for easy water defluoridation at household level.

The current work was designed to assess the efficacy of four particular locally occurring geomaterials from parts of Kenya to remove excessive fluoride from water by adsorption. The defluoridation protocol was envisaged to provide an innovative tailored approach to treatment of fluoride-contaminated water in the country. It was anticipated that this would help to expand access to safe drinking water and, complement on-going efforts to combat endemic fluorosis among fluoride afflicted communities in the country.

CHAPTER TWO
LITERATURE REVIEW

2.1 The theory of adsorption

2.1.1 Electrical double layer (EDL)

When solid adsorbents are contacted with electrolyte solutions, an electrical potential is set up across the interface between the adsorbent and the adsorbate solution phase. The magnitude of the resulting potential depends on the extent of charge separation between the two phases. The ensuing polarization makes counter-ions in the solution to move to the adsorbent surface as co-ions are repelled from the interfacing layer. This creates a pair of parallel sheets of oppositely charged ions at the adsorbent surface referred to as an electrical double layer (EDL) (Malvern Instruments, 2014).

The concept of EDL is important in explaining reactions that occur at charged surfaces in electrolytic solutions. It is assumed that the ions that first arrive at the adsorbent surface shed their solvation to approach and bond strongly to the sites in the adsorbent surface. However, because of their large excess in the solution, solvent molecules adsorb alongside and get oriented on the adsorbent surface. Together with the specifically adsorbed ions, the solvent molecules, therefore, constitute the first part of the EDL. This layer is followed by a layer of more loosely sorbed solvated electrolyte ions, which are in turn linked to a diffuse layer of ions into the solution as illustrated in figure 2.1 (a).

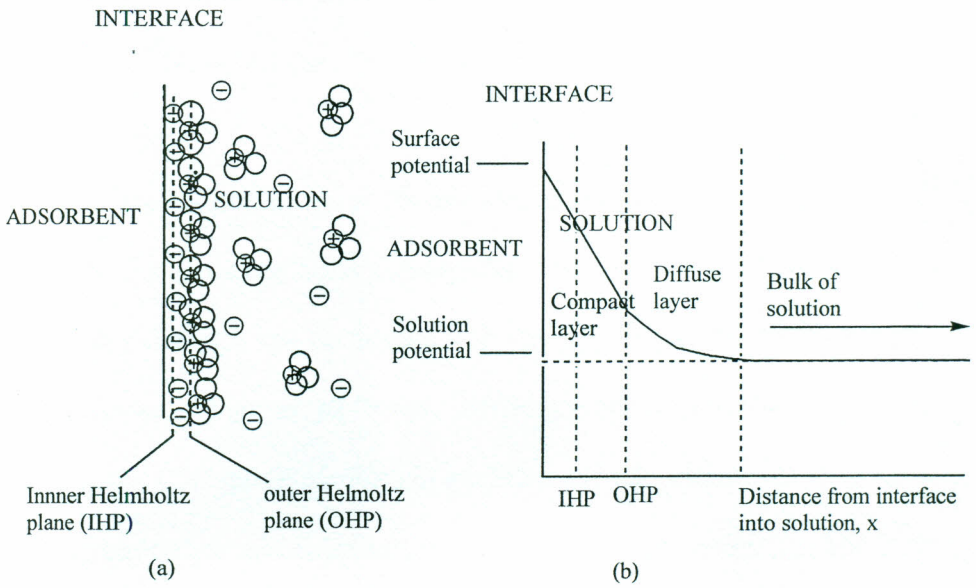

Figure 2.1: An electrical double layer (EDL) showing (a) arrangement of ions on either sides of interface (b) variation of surface potential, o_A, with distance, x, from the adsorbent surface.

A plane passing through the centres of adsorbed solvent dipoles and the specifically sorbed ions close to the adsorbent surface constitute what is called the inner Helmholtz plane, IHP. On the other hand, the plane through the centres of the solvated ions and loosely adsorbed electrolyte ions, which separate the compact inner regions of the EDL from the diffuse region, is referred to as the outer Helmholtz plane, OHP. The concentration of ions in the diffuse layer, C_x, varies with distance from the solid surface according to Boltzmann's law as:

$$C_x = C_B e^{[(-z_i \Phi_D)/kT]} \qquad 2.1$$

In addition to the IHP and OHP, there is a shear plane, which does not necessarily coincide with the OHP. It is the zone where the rigid holding of ions due to the surface charge of the solid adsorbent ceases to operate. The potential of the shear plane is called the zeta or the electro-kinetic potential. The potential varies linearly

with distance until the OHP and then exponentially within the diffuse layer as illustrated in figure 2.1 (b).

2.1.2 Types of potentials at the adsorbent surface

The distance across an EDL is, normally, less than 1.0 nm. Given that the potential across this distance can be several volts in magnitude, the field strength within the EDLs can be as high as 10^7 V/cm. Different types of potentials arising from surface realignment of reactive particles in an EDL when an electro-active solid is contacted with an electrolyte adsorbate solution are illustrated in figure. 2.2. The potential of the interface or of the part of double layer in the solid phase relative to potential in the bulk of the solid adsorbent is called the surface potential. Interfacial potential arises from differences in charge density between the parts of the EDLs in the two phases of the electrochemical system (Bagotsky, 2006). The potential of the shear plane, on the other hand, is called the zeta or electro-kinetic potential; it arises from the differences in charge density between the double layer and the bulk solution.

The total adsorption potential, $\varphi_G^{(A,S)}$ at an adsorbent-solution interface is, the sum of potential set-ups by each part of the EDL according to the relationship:

$$\varphi_G^{(A,S)} = \Phi^{(A,S)} + \chi^{(A)} - \chi^{(S)} \qquad 2.2$$

where, $\Phi^{(A,S)}$ is interfacial potential between the adsorbent and the solution, $\chi^{(A)}$ is adsorbent surface potential and $\chi^{(S)}$ is the surface potential of the solution phase (Bagotsky, 2006).

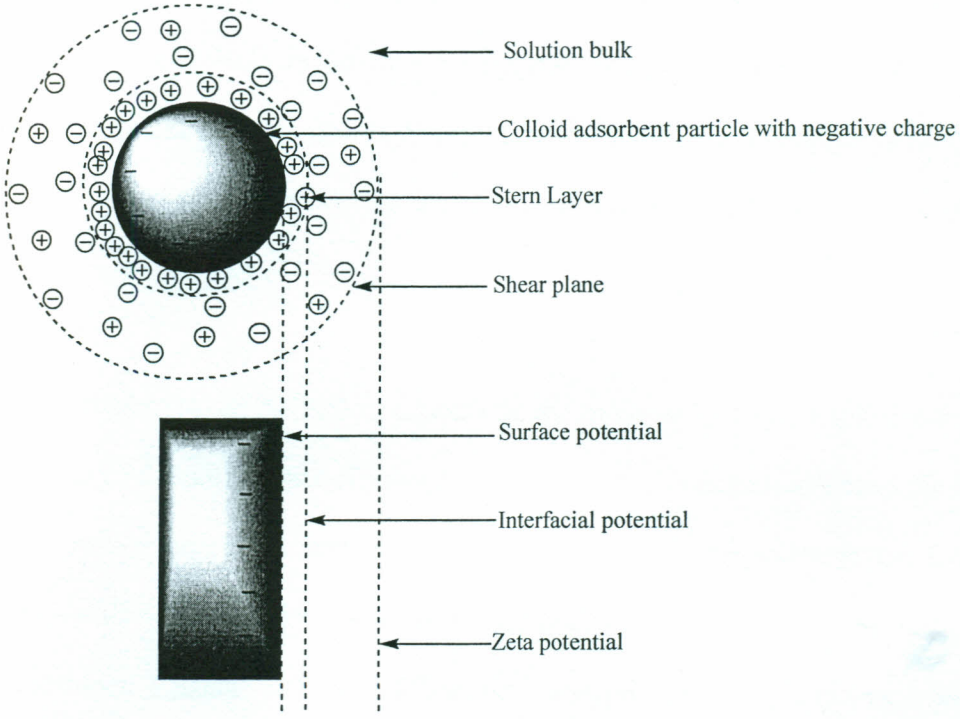

Figure 2.2: Surface, interfacial and zeta potential

2.1.3 The point of zero net charge (PZNC)

The surface potential of the adsorbent $\chi^{(A)}$ arises from surface adsorption of potential determining ions (PDI), χ^{S}_{ads} and orientation of the solvent dipoles, χ^{S}_{or}, at the adsorbent surface. When the solution potential changes, ions move in and out of the EDL until the interfacial potential, $\Phi^{(A,S)}$, has assumed a value that satisfy equation 2.2. Specifically, the interfacial potential change in an appropriate fashion when there has been a change in the adsorption, orientation, or other components of the surface potentials. At a certain value of the adsorbent potential *E*, called the point of zero charge (PZNC), the charge on the adsorbent surface $Q^{S,A}$ and hence the value of $\Phi^{(A,S)}$, drops to zero.

The PZNC is an important parameter of soil adsorbent-adsorbate interface. It determines the nature of surface charge and the surface potential of the soil surface. Normally, soil surfaces assume net positive charge at potential values above the PZNC and net negative charge at values below the PZNC. The quantity of PDI's that sorb to produce the respective net charge at the soil surfaces also depends on the PZNC.

For soil adsorbents, the PZNC depends on the mineralogy and the soil structure in the vicinity of the soil surface (Evangelou, 1998). Thus, so as to understand the chemical and surface properties that control surface charge development in the LAGs, the adsorbents' mineralogy, elemental composition and surface chemistry, were determined using X-ray diffraction analysis (XRD), atomic absorption spectrophotometry (AAS) and alkalimetric titration techniques, respectively. The results of these analyses are discussed in appropriate sections of the current work.

In general, therefore, the adsorption of electrolytic adsorbates onto charge systems of porous adsorbents such as clay systems is a four-step process, which begins with solute transfer from the bulk solution to the boundary film (EDL) close to the adsorbent surface. This is followed by solute transport across the EDL to the adsorbent surface and into the intra-particle active sites inside the porous structure of the adsorbent. The interactions of the adsorbate particles with free adsorbent sites on the internal surface of the adsorbent complete the adsorption process.

2.1.4 Adsorbate transport processes

The adsorbate particles are transported from the bulk solution to the EDL by diffusion, migration, and convection. Diffusion controlled transport is governed by the Fick's first (equation 2.3) and second (equation 2.4) laws of diffusion, which are given as:

$$J = D\frac{\partial C}{\partial x} \qquad 2.3$$

$$\frac{\partial C}{\partial t} = D\frac{\partial^2 C}{\partial^2 x} \qquad 2.4$$

where, J is the diffusion flux, $\partial C/\partial x$ is the concentration gradient in direction x, D is the diffusion coefficient and t is time. Diffusion transport arises whenever there is differential distribution of components in the system. The concentration, C_i, of a solute i varies with distance, x, from the adsorbent surface according to the expression (Bagotsky, 2006):

$$C_i = C_\infty \left\{1 - \mathrm{erfc}\left[\frac{x}{\pi(Dt)^{1/2}}\right]\right\} \qquad 2.5$$

where, C_∞ is the bulk concentration. The diffusion controlled mass transfer is, therefore, limited to a finite distance from the adsorbent surface known as the diffusion layer, δ, which is described by the relationship:

$$D\left(\frac{\partial C}{\partial x}\right)_0 = D\frac{(C_\infty - C_0)}{\delta} \qquad 2.6$$

where, C_∞ and C_0 are the adsorbate concentration at the bulk of solution and at the adsorbent surface, respectively. The smaller the diffusion layer, δ, the larger the concentration gradient, and the greater the rates of adsorbate transfer to the adsorbent surface. Fastest solute transfer from solution to the adsorbent surface are, therefore, achieved under conditions of high bulk concentrations, large availability of adsorbent

surface, high adsorbent affinity and optimum rate of agitation; the latter tends to reduce the diffusion layer thickness.

Migration is the transport of electrochemical particles under the influence of an electrostatic field. The relationship between total flux of ions under the influence of an electrostatic field and a concentration gradient, δC/δx, is described by the Nernst–Planck equation, which is given as:

$$J = J_m \pm J_d = uC\frac{\partial C}{\partial x} \qquad 2.7$$

The minus sign is applied in equation 2.7 when the net diffusion flux is opposite to the migratory flux. For uncharged particles the term J_m is zero and equation 2.7 becomes equation 2.3. This links the parameters u_j and D_j and the expression for the total flux can then be written as:

$$J = D\left(\frac{F}{RT}zCE \pm \frac{\partial C}{dx}\right) \qquad 2.8$$

where, F = Faraday's constant, R = the universal gas constant, T = temperature, z = charge of ions and $\boldsymbol{E}$ = electric field strength.

Convective transport refers to the movement of substances with flux current (Rajeshwar and Ibanez, 1997). The convective flux is given by:

$$J_{kv} - vC \qquad 2.9$$

where, v is the linear velocity of the fluid medium and C is the concentration of the substance in the medium. In electrolyte solutions, the convective flux is always neutral because of the electro-neutrality of the solution. Since convective flux can be to or from the adsorbent surface, the actual change in amount of reactants in the flux

to and fro the adsorbent surface is what is important and equation 2.9 should then be written as:

$$\Delta J_{kv,j} = mAv\left(C_j - C_j'\right) \qquad 2.10$$

where, m is mass of adsorbent, A is the specific surface area of the adsorbent and, C_j and C_j' are the concentration of substance j in the flux to and from the adsorbent surface, respectively.

Ordinarily, the transport process that dominates in an adsorption system depends on the experimental setting of the system (Gupta and Bhattacharyya, 2011). Migration dominates for charged particles under a strong electric field and convective transport get enhanced under conditions of optimum mechanical agitation. Where the migration transport is absent as for uncharged adsorbate particles, convection predominates over diffusion controlled transport. For this reason, optimum constant mechanical agitation has strong kinetic effects on adsorption systems of most adsorbates. The relative significance of each of these processes can be controlled by manipulation of experimental conditions.

2.2 Experimental designs for adsorption tests

Adsorption tests are conducted through batch adsorption, continuous stirred flow or stationary column set-ups (Vannela and Verma, 2006). The type of experimental design for an adsorption protocol is selected to optimise the adsorption process. The batch system is, however, the most popular because it is inexpensive and simple to design and run. A pre-determined mass of adsorbent is contacted with a solution of known adsorbate concentration, C_i (mg/L). After equilibration the final concentration,

C_e (mg/L), of the adsorbate solution is determined and the amount of adsorption, q_e (mg/g), calculated from the mass balance equation as (Wambu *et al.*, 2011):

$$q_e = \frac{v(C_i - C_e)}{m1000} \qquad 2.10$$

where, v is the volume of the solution (mL) and m is the mass of the adsorbent (g) used. The percentage adsorption can then be obtained as:

$$\%adsorption = (1 - \frac{C_{eq}}{C_i}) \times 100 \qquad 2.11$$

Fixed bed column reactors consist of cylindrical steel, glass or plastic columns of suitable height and cross-section dimensions packed with suitable amount of adsorbent. An adsorbate solution of prescribed concentration at set conditions is passed through the column in an up-flow or a downward flow mode at rates controlled through a valve. The effluent is collected and analyzed for residual adsorbate levels at selected time or volume intervals (Xu *et al.*, 2012) and the amount of adsorption determined from a similar mass balance expression as:

$$C_{ad} = (C_0 - C_t), \qquad 2.12$$

where, C_0 and C_t are the influent and the effluent concentrations, respectively.

The adsorption behaviour of a column system is studied through breakthrough curves by plotting the amount of adsorption (C_{ad} or normalized concentration (C_t/C_0) as function of time or volume of effluent solution (Malkoc and Nuhoglu, 2006). From the respective curves, the breakthrough volume (V_B); retention volume (V_R); exhaustion or equilibrium volume (V_E); and total volume (V_0) can then be determined. The Thomas expression is the most useful model for theoretical characterization of an

adsorption processes in fixed bed columns. It is generally used in linearized form as (Murugan and Subramanian, 2006).

$$ln\left(\frac{C_0}{C}-1\right)=\left(\frac{k_T q_T m}{\theta}\right)-\frac{k_T C_0 v}{\theta} \qquad 2.13$$

where, C is the effluent concentration (mg/L), C_0 is the influent concentration (mg/L), k_T is the rate constant (L/mg/min), q_T is the total sorption capacity (mg/g) of the column, m is the mass of adsorbent (g), v is the throughput volume (L) and θ is the flow rate (L/min). The constants q_T and k_T can be calculated from linear regression of $ln\left(\frac{C_0}{C}-1\right)$ versus v according to equation 2.13. The values of the constants are an expression of the efficiency of the adsorbent. Adherence of adsorption data to the Thomas model indicate existence of Langmuir kinetics for the adsorption–desorption protocol and that the rate driving force obeys second-order reversible reaction kinetics.

The stirred-flow method combines aspects of batch and column reactors. Adsorbent solids are kept in suspension as they flow through the adsorption column. The advantages of the method are that the reaction rates are independent of the physical effects of the porous media and the same apparatus can be used to measure both the equilibrium and the kinetic parameters. The column design should, however, ensure proper mixing of the adsorbent-solution mixture and minimize diffusion gradients in the bulk solution (Seyfried *et al.*, 1989).

So as to evaluate the effect of solution parameter such as the pH, temperature, contact time, concentrations, adsorbent dosage and co-existent ions on the efficacies of the

LAGs to sorb fluoride from water and to be able to optimize the fluoride adsorption protocol using these adsorbents, fluoride adsorption onto the LAGs was studied on batch basis as a function of each of the solution variables. Batch results were then verified in fixed bed column tests using natural high-fluoride water.

2.3 Adsorption isotherms

Adsorption isotherms are useful in describing how the adsorbate particles interact with adsorbent sites at equilibrium and they are relevant in optimization of an adsorption protocol. An intensive analysis of adsorption isotherms was conducted by Giles and colleagues (Giles *et al.*, 1960). The authors observed that when equilibrium adsorption is plotted against residual equilibrium concentration, characteristic curves, which have shapes that reflect the dominant adsorption mechanism of the interactions between the solutes and the adsorbent surfaces are obtained. The authors were able to identify four classes of adsorption isotherms based on the shapes of the initial slopes of the curves. These classes were: the sigmoid (*S*), Langmuir (*L*), constant partition (*C*) and high affinity (*H*) curves. Each of the categories of isotherms was further divided into a four-tier sub-classification as presented in figure 2.3. The classes and the sub-classes describe a set of properties that characterise adsorption systems.

In addition, numerous empirical models have been suggested to describe equilibrium adsorption processes. The Langmuir and the Freundlich isotherms are perhaps the most satisfactory models for describing the removal of adsorbates from aqueous systems (Murithi *et al.*, 2014). The Langmuir isotherm is, however, the better known adsorption isotherm, which is often applied to solid/liquid system in describing the saturated monolayer adsorption. It assumes that adsorption takes place by stoichiometric interactions at homogeneous sites within the adsorbent surface.

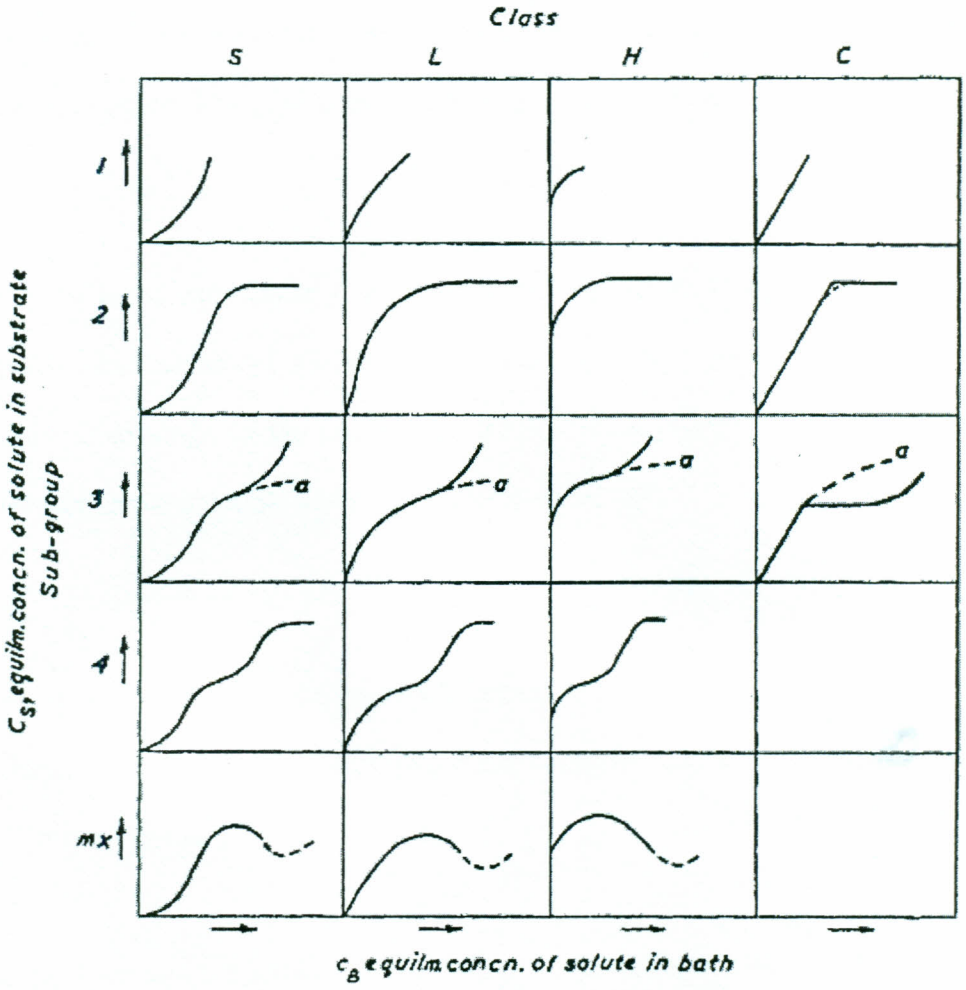

Figure 2.3: Giles classification of adsorption isotherms (Giles et al., 1960)

It presupposes that once an adsorbate ion occupies a site in the adsorbent surface, no further adsorption can take place at that site. As a result, this isotherm describes an adsorption protocol that is chemisorption in nature and one that is limited to monolayer coverage of the adsorbent surface.

In this case, the amount of adsorbate uptake is favoured by increasing temperature, if the overall reactions are endothermic, because the interacting groups must be activated. The rate of adsorption should, therefore, be proportional to the driving

force, which is the adsorbate concentration in the solution, and the amount of free adsorbent surface. Thus, the saturated monolayer isotherm can be represented as:

$$q_e = \frac{q_m b C_e}{1 + bC_e} \qquad 2.14$$

where, C_e is the equilibrium concentration (mg/L), q_e the amount of adsorbate ions sorbed in the adsorbent surface (mg/g) and q_m is the value of q_e for complete monolayer coverage of the material by the adsorbate (mg/g). This equation can be rearranged into the double reciprocal linear form as:

$$\frac{1}{q_e} = \frac{1}{bq_m C_e} + \frac{1}{q_m} \qquad 2.15$$

A plot of $1/q_e$ versus $1/C_e$ should then be a straight line of slope $1/bq_m$ and an intercept of $1/q_m$ from which both the adsorption capacity, q_m, and the thermodynamic equilibrium constant, b, can be derived.

The thermodynamic constant b is related to the adsorption free energy, ΔG, by:

$$\Delta G = RT\ln(b) \qquad 2.16$$

where, R is the universal gas constant, 8.314 J/mol/K, and T is the temperature (K). Both the adsorption enthalpy (ΔH^0) and entropy (ΔS^0) can then be obtained from corresponding van't Hoff's equation as:

$$\Delta G^0 = \Delta H^0 + T\Delta S^0 \qquad 2.17$$

To assess the adsorption efficiency of the system the essential characteristics of the Langmuir isotherm can then be determined using the dimensionless equilibrium parameter, R_L. This is the ratio of unused adsorbent surface, $(q_m\text{-}q_e)$ to the maximum adsorption capacity, q_m, which is given as:

$$R_L = \frac{1}{1+bC_o} \qquad 2.18$$

The slope of the linearized Langmuir isotherm can then be used to interpret the type of adsorption according to the values of R_L as follows: $R_L > 1.0$, uniform not suitable; $R_L = 1.0$, linear; $q < R_L < 1.0$, suitable and $R_L = 0$, irreversible (Umlong *et al.*, 2011).

The Freundlich isotherm is used for describing non-ideal sorption of adsorbate ions onto solid adsorbents. It has a non-linear form of:

$$q_e = K_f C_e^{\frac{1}{n}} \qquad 2.19$$

where, n is the surface adsorption intensity and K_f is the Freundlich equilibrium constant. The equation is normally used in its linear form as:

$$\log q_e = \log K_f + \frac{1}{n}\log C_e \qquad 2.20$$

A plot of $log\ q_e$ against $log\ C_e$ gives a linear graph of gradient $1/n$ and intercept $log\ K_f$. The adherence of adsorption data to the Freundlich isotherm implies a layered physisorption protocol that is completely reversible and based on weak van der Waals type of interactions between the adsorbent surface and the adsorbate particles.

So as to quantify the fluoride adsorption capacities of the LAGs and hence, evaluate the feasibility of fluoride removal from water using the LAGs and elucidate the dominant adsorption mechanisms, the empirical Langmuir isotherm and the Freundlich isotherm were applied to the fluoride adsorption data for the LAGs. The corresponding linear plots were constructed and the adsorption equilibrium constants

computed. The Giles classification of adsorption isotherms was then used to characterize the interaction of fluoride particles with the soil adsorbents.

2.4 Adsorption kinetics

Analysis of the adsorption kinetics provides useful information regarding the resident time required for effective contact between the adsorbent and the adsorbate in the reaction vessel. They are important in determining the influence of different variables on the sorption process and in elucidation the rate determining step of an adsorption protocol. The Lagergren pseudo-first order rate equation, Ho's pseudo-second order equation (Ho, 2014) and the intra-particular diffusion model (Weber and Morris, 1963) are the most popular kinetic equations used in elucidation of the rate determining step of aqueous adsorption systems.

The Lagergren's first-order rate expression is usually given as:

$$\frac{dq_t}{dt} = k_{1,ad}(q_e - q_t) \qquad 2.21$$

where, q_e and q_t are the amount of adsorbate sorbed onto the material (mg/g) at equilibrium and at time t, respectively and $k_{1,ad}$ is the adsorption first-order rate constant (min^{-1}). The integrated rate law resulting from this equation is:

$$\log(q_e - q_t) = \log q_e - \frac{k_{1,ad}}{2.303}t \qquad 2.22$$

A plot of $\log(q_e - q_t)$ against $\log q_e$ should be linear with the first order rate constant $k_{1,ad}$ as the gradient if an adsorption protocol is based on pseudo-first order kinetics.

The rate expression for Ho's pseudo-second-order reactions, on the other hand, is given as:

$$\frac{dq_t}{dt} = k_{2,ad}(q_e - q_t)^2 \qquad 2.23$$

where, $k_{2,ad}$ is the rate constant for the second order adsorption (mg/g/min), q_e, the amount of adsorbate ions adsorbed at equilibrium (mg/g) and q_t the amount of adsorbate on the surface of the adsorbent at any time t (mg/g). This expression yields the integrated rate law for a pseudo-second order adsorption kinetics, which is expressed as:

$$\frac{t}{q_t} = \frac{1}{k_{2,ad}q_e^{\,2}} + \frac{1}{q_e}t \qquad 2.24$$

A plot of $\frac{t}{q_t}$ against t should then give a linear graph from which the second order rate constant, $k_{2,ad,}$ and the equilibrium adsorption, q_e, may be calculated. The initial rate of adsorption, h_0, which is given as $h_0 = k_{2,ad}q_e$, is also obtainable from the plots. Adherence of adsorption data to this model indicates that the rate limiting step is chemisorption reactions involving valence forces through sharing or exchange of electrons between adsorbent and adsorbate.

The second order rate constant of the adsorption process is related to the activation enthalpy, ΔH_{ad}*, by the Arrhenius equation according to the expression (Biswas *et al.*, 2010):

$$k_{2,ad} = Ae^{(-\Delta H^*_{ad}/RT)} \qquad 2.25$$

where, A is the pre-exponential factor. In an aqueous media, the rearrangement of the solvation atmosphere is a necessary step. Thus, if the pre-exponential factor, A, is written in terms of activation entropy, ΔS_{ad}*, as:

$$A = A' e^{\frac{\Delta S^*_{ad}}{R}} \qquad 2.26$$

then,

$$k_{2,ad} = A' exp^{[-(\Delta H^*_a - T\Delta S^*_a)/RT]} = A' e^{[-\Delta G^*_a/RT]} \qquad 2.27$$

The magnitude of the activation energy depends on the nature of adsorption process. Activation energies in the range of 5–40 kJ/mol are typical of physisorption processes whereas higher activation energies (40–800 kJ/mol) are, normally, characteristic of chemisorption. Diffusion-controlled adsorptions have activation energy of adsorption less than 25–30 kJ/mol (Murutu *et al.*, 2009).

Besides the adsorption onto the outer adsorbent surface sites, the adsorbate ions from the solution may be transported to the inner-core pores of the adsorbent by diffusion. In order to assess the existence of intraparticle diffusion in the adsorption processes, the Weber and Morris intra-particular diffusion kinetics model was also employed as:

$$q_t = \frac{k_w}{m} t^{\frac{1}{2}} + C \qquad 2.28$$

where m is the mass of adsorbent (g), q_t the amount of adsorbate ions adsorbed at time t (mg/g), k_w is the initial rate of intra-particular diffusion (mg/L/s$^{0.5}$) and C is the intercept (Weber and Morris, 1963).

Adherence of adsorption data to intra-particle diffusion model is implied by a straight line plot between q_t and $t^{0.5}$ from the slope of which the initial rate of adsorption, k_w,

is obtained. An indication of the boundary layer thickness is obtained from the value of C and the larger value indicates greater boundary layer effect (Goswami and Purkait, 2011). Deviation of the straight line from the origin indicates that pore diffusion is not the sole rate controlling step (Márquez-Mendoza *et al.*, 2011). However, since diffusion is an endothermic process, the rate of adsorption increases with increasing solution temperature when pore diffusion is the rate-limiting step (Weber and Morris, 1963).

In order to characterize the nature of adsorption kinetics and be able to determine the effective resident time of the adsorbents in the batch reactors so as to elucidate the rate determining steps of fluoride adsorption onto LAGs, the time-dependent fluoride adsorption data were analyzed using the Lagergren's pseudo-first order rate law, Ho's pseudo-second order rate expression and the Weber-Moris intra-particle adsorption kinetics. The respective kinetics plots were then constructed and the adsorption kinetics constants computed.

2.5 Application of adsorption to water defluoridation

2.5.1 Aqueous speciation and availability of fluoride

Speciation and, hence, aqueous availability of fluoride in water is controlled primarily by the pH, the concentration, and presence of such cations as: Al^{3+}, Fe^{3+}, Mn^{2+}, Ca^{2+}, and Mg^{2+} (Erdemoglu *et al.*, 2000). The pH effect on aqueous fluoride is illustrated in figure 2.4. Below pH values of 4, the HF molecules predominate and the formation of HF, which favour solubilisation and aqueous availability of fluoride, increase with decreasing pH of the media (Agarwal *et al.*, 2002). Fluoro-aluminium complexes

including AlF^{2+}, $AlF_2^{+}$and AlF_3^{0} exist in natural water systems at pH 4-6. The concentration of free fluoride ions in this pH range is only 21.35% (Jackson *et al.*, 2002). At higher pH values, however, the stability of fluoro-aluminium complexes decrease and the free anions, F^-, predominate. All fluorides exist as free anions, F^-, at pH values of 8–9, where all aluminium form the aluminate, $[Al(OH)_4]^-$, complexes.

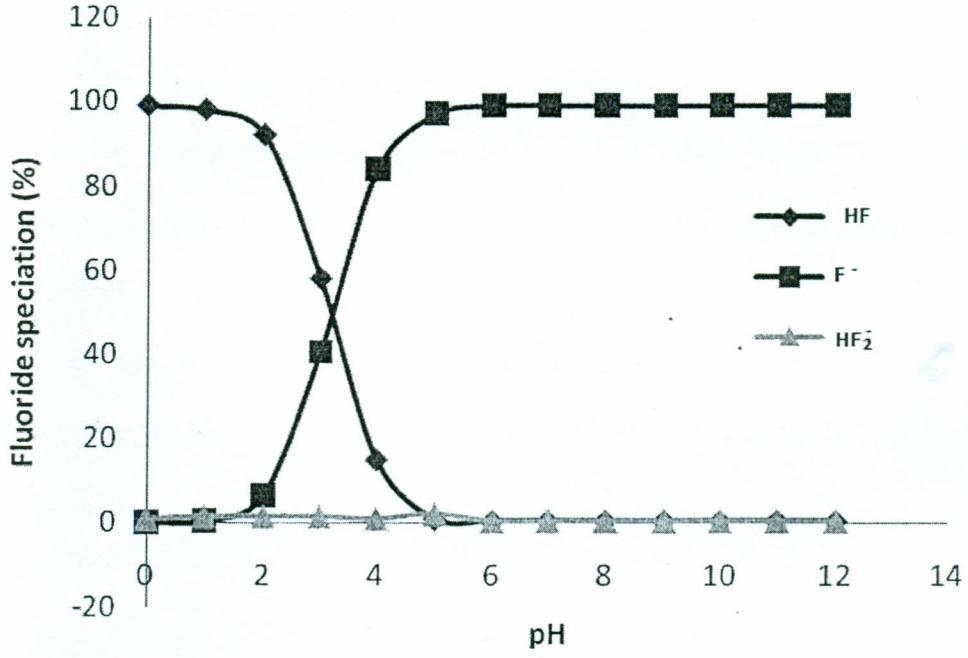

Figure 2.4: Fluoride speciation (Richards *et al.*, 2010)

Calcareous minerals favour fluoride solubilisation according to the mass balance equation related to calcite and fluorite when both salts are in contact with the water (Jha *et al.*, 2013):

$$CaCO_3(s) + H^+(aq) + 2F^-(aq) \rightleftharpoons CaF_2(s) + HCO_3^-(aq) \quad 2.29$$

Clearly, increase in pH and in the concentrations of HCO_3^- increases water fluoride concentrations and vice versa.

2.5.2 Overview of fluoride soil adsorbents

Consumption of high-fluoride water, when safer drinking water is not readily available, is the primary pathway by which people get exposed to excessive fluoride. The primary approach to controlling exposure to unsafe fluoride levels is, therefore, by management of fluoride consumption through drinking water. At the moment, adsorption technology appears to be the most appropriate technology for defluoridation of drinking water. This is because it, normally, is simpler, less expensive, and it results in high quality water (Goromo *et al.*, 2012). Clays and similar soil adsorbents have emerged as the most attractive inexpensive fluoride adsorbents. They have natural capacity to sorb environmental pollutants such as fluoride and they are readily available and usable in a wide range of aqueous conditions (El-Said and Draz, 2010; Nath and Dutta, 2010; Kang *et al.*, 2011; Goromo *et al.*, 2012).

The soil adsorbents that have attracted the highest interest for cost-effective defluoridation of drinking water include aluminosilicates, iron and aluminium (hydr)oxides, apatites, carbonaceous minerals, calcareous soils and zeolites (Bhatnagar *et al.*, 2011). Others are: sordic soils (Robbins, 1986), red soils and serpentine (Chidambaram *et al.*, 2003), fired clays (Bardsen and Bjorvatn, 1996) and Ando soils from Kenya (Zevenbergen *et al.*, 1996).

2.5.3 Aluminosilicate clay adsorbents

Aluminosilicate minerals include montmorillonites (Bia *et al.*, 2012), kaolinites (Wei and Xiang 2012), palygorskite-sepiolite (He *et al.*, 2013) and pumice (Asgari *et al.*,

2012). They are soil materials that have attracted the highest research interest for fluoride adsorption. Montmorillonites are 1:2 layered clay minerals, which belong to the broader class of phyllosilicates. They are the most studied silicate minerals for fluoride adsorption (Mahramanlioglu *et al.*, 2002; Tor, 2006; Achour and Youcef, 2009; Ramdani *et al.*, 2010; Bia *et al.*, 2012). The peak fluoride adsorption by natural montmorillonites occurs at ambient tropical temperatures of 298-303 K (Agarwal *et al.*, 2002; Tor, 2006; Achour and Youcef, 2009; Ramdani *et al.*, 2010) and at pH values of natural waters (Agarwal *et al.*, 2002; Tor, 2006; Ramdani *et al.*, 2010). Even though, longer equilibration intervals up to 180 min have been reported for fluoride uptake by montmorillonites (Tor, 2006; Achour and Youcef, 2009), ordinarily, the adsorption process is fast and the usual time for attainment of equilibrium is just about 30 min (Agarwal *et al.*, 2002; Ramdani *et al.*, 2010).

The usual range of fluoride adsorption capacities of natural montmorillonites is just about 0.265–3.365 mg/g, which is considered low when compared to those of similar materials (Samatya *et al.*, 2007; Sujana and Anand, 2011; Mahvi *et al.*, 2012; Nie *et al.*, 2012;). More enhanced fluoride adsorption capacities have, however, been reported for a number of surface-enhanced montmorillonite adsorbents (Mahramanlioglu *et al.*, 2002; Bia *et al.*, 2012; Karthikeyan *et al.*, 2012).

Aniline modified montmorillonite, PANi-MMT, and pyrrole modified montmorillonite, PPy-MMT, for example, which were both prepared by Karthikeyan and co-workers (2012), have been shown to depict superior fluoride adsorption capacities of 6.0 and 12.3 mg/g, respectively. The highest fluoride adsorption

capacities of the modified adsorbents occurred at temperatures of 303 K and the equilibrium adsorption time in both systems was 50 min. The adsorption equilibrium data could be correlated to the Freundlich isotherm, which showed that physisorption was the preferred mode of fluoride immobilization into the montmorillonite adsorbent surfaces pre-modified by organic groups.

On the other hand, fluoride adsorption capacities of 7.752 mg/g have been reported for spent beaching earth (SBE), a montmorillonite waste from edible oil processing industries. SBE could also be considered under modified class of montmorillonites. The optimum pH value of fluoride adsorption onto SBE was 3.5 and the adsorption data could be fitted by the Langmuir adsorption isotherm indicating a chemisorption process (Mahramanlioglu *et al.*, 2002). It shows that the mode and type of surface modification determines the capacity of the clay to sorb fluoride as well as the kinetics, mechanisms and underlying adsorption thermodynamics. The reuse of SBE in water defluoridation is particularly desired for the need to minimize its generation and preclude its disposal costs on part of the edible oil processing. This could also promote environmental safety as well (Wambu *et al.*, 2009). The use of SBE for water treatment may, however, only be feasible in areas within industrial zones where the SBE wastes are available.

A number of workers have investigated enhancement of fluoride adsorption capacities of montmorillonites by intercalation with inorganic salts. Bia and *et al.* (2012), for instance, studied fluoride adsorption onto an Fe(III)-modified montmorillonite and reported enhanced fluoride adsorption capacity of 9.6957 mg/g for the adsorbent. The

maximum fluoride adsorption using Fe(III)-modified montmorillonite occurred in a media of pH 4.5 at 298 K. The time required for equilibrium adsorption was 160 min. However, the rate of fluoride adsorption onto the Fe(III)-modified adsorbent increased with increasing initial fluoride concentration and decreasing solution pH. It showed that Fe(III)-modification enhanced not only the capacity of montmorillonite but also the affinity of the surfaces for fluoride ions. Fluoride adsorption onto the Fe(III)-modified montmorillonite adsorbent could, therefore, be a diffusion-controlled process.

In general, surface modified montmorillonites have enhanced fluoride adsorption capacities (6.0-12.0 mg/g) over the unmodified montmorillonite adsorbents (0.2-3.6 mg/g). The capacities, kinetics and reaction mechanism of fluoride adsorption onto modified montmorillonites are, however, dependent on the mode and type of the adsorbent modification. Nevertheless, montmorillonite clays are not widely distributed for easy procurement and use in water defluoridation. Moreover, their competing use in bleaching edible oils supersedes their proposed use for water defluoridation at the moment (Murray, 2007). The montmorillonites surfaces are not also very stable in aqueous media. For this reason, the adsorbents tend to have narrow fluoride adsorption edge because they solubilise in aqueous media of very at low pH and get easily poisoned by excess OH^- ions in more alkaline media.

Kaolinites are another class of aluminosilicate clays that have extensively been investigated for fluoride adsorption. They are more widely distributed world over than montmorillonites (Murray, 2007) and they have good sorptive properties towards

several adsorbates (Hyun *et al.*, 2005; Schaller *et al.*, 2009; Reich *et al.*, 2010) because they present more stable surfaces in aqueous solutions than montmorillonite (Clozel *et al.*, 1994). For this reason, kaolinites are usable in a wider spectrum of water conditions than montmorillonites (Agarwal *et al.*, 2002; Sugita *et al.*, 2005; Gogoi and Baruah, 2008; Meenakshi *et al.*, 2008; Ibrahim *et al.*, 2010; Wei and Xiang, 2012). Nonetheless, normally, kaolinites have limited fluoride adsorption capacities of less than 1.0 mg/g (Srimurali *et al.*, 1998; Gogoi and Baruah, 2008; Meenakshi *et al.*, 2008). Kaolinites, therefore, do not usually present very prospective media for practical defluoridation of water (Agarwal *et al.*, 2002; Gogoi and Baruah, 2008; Meenakshi *et al.*, 2008).

Unlike montmorillonites and kaolinites, attapulgite (syn. palygorskite) have highly promising fluoride adsorption capacities in the range of 24.55–71.94 mg/g (Hamdi and Srasra, 2009; Zhang *et al.*, 2009, 2012; Feng *et al.*, 2012; He *et al.*, 2013). Like the montmorillonites and kaolinites, however, palygorskite adsorbents require surface modification using such ions as: $Mg^{2+}$and Al^{3+} (Zhang *et al.*, 2009), Fe^{3+} (He *et al.*, 2013) and ZrO^{2+} (Zhang *et al.*, 2012). The usual conditions for efficient fluoride removal from water using metal-enhanced palygorskite are 323 K temperature, pH values of 3.7–7.5 and equilibrium time of about 110 min (Zhang *et al.*, 2009).

The cation-exchanged attapulgite can be regenerated and reused up to 6–10 cycles by treatment with strong alkalis or by thermal re-activation (Zhang *et al.*, 2009, 2012; Feng *et al.*, 2012; He *et al.*, 2013). The phosphate, sulphate and carbonate ions are the chief interferent species in fluoride removal from water using cation-exchanges

palygorskite (Zhang *et al.*, 2012). Yet, as for montmorillonites, palygorskites are not well distributed world over and their current demand for bleaching vegetable oils surpasses the desire to use the virgin minerals in water defluoridation (Murray, 2007).

2.5.4 Zeolites

The use of zeolites in water purification by adsorption has extensively been studied (Payne and Abdel-Fattah, 2004; Onyango *et al.*, 2004, 2010;Ibrahim *et al.*, 2010). Notwithstanding, natural zeolites have limited sorption capacities for anions because of an intrinsic negative zeta potential that prevails over zeolite surfaces in a wide range of water conditions. To enhance anionic uptake by zeolitic adsorbents, the negative surface potential of the mineral is reversed by impregnation of the zeolite structure with multivalent cations including Al^{3+} (Xu *et al.*, 2000; Onyango and Matsuda, 2006), Al^{3+} and La^{3+} (Onyango *et al.*, 2004), Na^{+}, Ca^{2+}, La^{3+} and Eu^{3+} (Díaz-Nava *et al.*, 2002), Al^{3+}, La^{3+} and ZrO^{2+} (Samatya *et al.*, 2007), and Fe^{3+} (Sun *et al.*, 2011). The ability of ZrO^{2+}, La^{3+}, and Al^{3+} ions to enhance fluoride adsorption of zeolite adsorbents follows the order: ZrO^{2+} (4.13 mg/g) > La^{3+} (2.63 mg/g) > Al^{3+} (2.35 mg/g). The greater capacity of La^{3+}-exchanged zeolites (54.28 mg/g) to sorb fluoride over that of the Al^{3+}-exchanges zeolite (39.52 mg/g) appears to be the usual case in the literature (Onyango *et al.*, 2004). In general, the order of fluoride adsorption capacities of metal-exchanged zeolites decrease in the order: ZrO^{2+} > Eu^{3+} > La^{3+} > Al^{3+} > Fe^{3+} > untreated zeolites > Ca^{2+} ≈ Na^{+} (Díaz-Nava *et al.*, 2002; Onyango *et al.*, 2004).

Fluoride adsorption onto metal-exchanged zeolites occurs over the entire adsorbent surface in just 15 min. It then assumes a steady state of gradual diffusion of fluoride particles into inner core sorptive sites of the adsorbent, which may, however, extend to periods of up to 24 h (Xu *et al.*, 2000; Díaz-Nava *et al.*, 2002; Samatya *et al.*, 2007). The reaction is independent of pH changes and high fluoride adsorption is achieved for metal-exchanged zeolites over the entire pH range of 4–10. In addition, fluoride adsorption onto zeolites is almost independent of the competing anions such as the chloride, nitrate, sulphate and acetate ions (Xu *et al.*, 2000). The zeolite adsorbents are, therefore, stable and can be used to defluoridate water over a wide range of conditions (Xu *et al.*, 2000; Díaz-Nava *et al.*, 2002; Onyango and Matsuda, 2006). However, even though Onyango *et al.* (2004) reported lofty fluoride adsorption capacities of 39.58 and 54.28 mg/g for Al^{3+} and La^{3+}-exchanged zeolite, respectively, modest adsorption capacities of 2.3-4.5 mg/g appear to be more characteristic of fluoride adsorption tests using cation-exchanged zeolite adsorbents in the literature (Xu *et al.*, 2000; Samatya *et al.*, 2007; Sun *et al.*, 2011).

The low fluoride adsorption capacities of most zeolites show that high amounts of the adsorbent is inevitably required to defluoridate significant amount of water. This would, as expected, lead to generation of large amounts of undesirable fluoride-laden sludge increasing the cost of water treatment. Natural and cation modified-zeolites may not, therefore, conform to the general selection criteria for the low-cost adsorbents that are desired for easy and safe defluoridation of water (Wambu *et al.*, 2013).

2.5.5 Pumice

Pumice is a volcanic rock mineral resulting from solidified volcanic lava. It contains 60–70% silica and it is characterized by low density and high porosity, which suits its use as an adsorbent. Furthermore, the mineral is well distributed around the world (Mahvi *et al.*, 2012) and it is one of the most promising media for water defluoridation at the moment. It is characterized by high fluoride adsorption capacities (13.5–41.0 mg/g) and optimum water defluoridation using pumice occurs in the range of natural pH values of water (6–7) at room temperatures (293–303 K), which is desired for easy defluoridation of drinking water (Malakootian *et al.*, 2011; Asgari *et al.*, 2012; Mahvi *et al.*, 2012). Fluoride adsorption onto pumice is rapid and the time required for attainment of equilibrium is just 20–30 min (Asgari *et al.*, 2012; Mahvi, 2012). Few studies have, however, been undertaken to defluoridate water using pumice. More investigations using this material in various conditions are, therefore, desired to establish its efficacy and the scope of its applicability in water defluoridation.

2.5.6 Apatite and hydroxyapatite

Hydroxyapatite or HAps, $Ca_5(PO_4)_3OH$, are among adsorbents with strongest natural affinities for fluoride. The reaction of soluble fluorides with HAps is based on fluoride substitution in the apatite structure, which exchanges the fluoride groups with OH^- groups in the mineral lattice to form fluoroapatite, $Ca_{10}(PO_4)_6F_2$, (Aoba, 1997). This natural exchange occurs in the natural pH range of water (6.0–7.5) over a wide range of temperatures (Fan *et al.*, 2003; Mohapatra *et al.*, 2009; Nie *et al.*, 2012). HAps are, therefore, among the most attractive minerals for water defluoridation at

the moment (Fan *et al.*, 2003; Murutu *et al.*, 2009; Wang *et al.*, 2011; Liang *et al.*, 2011; Mourabet *et al.*, 2012). Fluoride uptake by apatite surfaces is, however, slow and it takes10–24 h for the equilibrium to be established (Murutu *et al.*, 2009; Liang *et al.*, 2011; Nie *et al.*, 2012).

Nonetheless, the fluoride adsorption capacities of natural HAps are in the range 15-22 mg/g (Fan *et al.*, 2003; Mohapatra *et al.*, 2009; Murutu *et al.*, 2009; Liang *et al.*, 2011; Wang *et al.*, 2011; Mourabet *et al.*, 2012; Nie *et al.*, 2012). Besides, the natural fluoride adsorption capacities of HAps can further be enhanced by grafting HAps surfaces with organic groups (Wang *et al.*, 2011; Loganathan *et al.*, 2013) or by impregnating the HAps adsorbents with metal ions (Nie *et al.*, 2012). The capacity of modified HAps to sorb fluoride from water is about 32.57 mg/g (Nie *et al.*, 2012). Fluoride adsorption onto HAps modified with organic groups is a physisorption processes. The amount of fluoride adsorbed increases with increasing concentrations of the reactive organic groups in the HAps surfaces (Wang *et al.*, 2011). The adsorption of fluoride onto cation-intercalated HAps, however, is fitted by Langmuir isotherm indicating existence of chemisorption processes (Nie *et al.*, 2012).

Apatite is one of the hardest natural materials and significant energy amounts and specialized equipment are required to pulverize it to a degree that is suitable for sorption tests. Most of adsorption tests have, as a consequence, been based on laboratory-prepared HAps adsorbents. Larsen and Pearce (2002), for example, developed a fluoride adsorbent by reacting calcite and brushite, $CaHPO_4.2H_2O$. Between 70.5% and 98.8% fluoride adsorption from distilled water containing 5–20

mg/L initial fluoride concentrations and 61.5–76.0% from similar fluoride solutions in background solutions containing 104 mg/L Ca^{2+} were achieved using the brushite-based Hap adsorbents. Murutu and co-workers (2009), on the their part, synthesized an HAp fluoride adsorbent by calcination of limestone at 1073 K and reacting the residues with 50% orthophosphoric acid under controlled conditions at 323 K. Such adsorbents have also been prepared by among other workers, MacDonald (2011) by reaction of commercial lime, CaO, with controlled amounts of 85–90% phosphoric acid and then by Liang *et al.* (2011), who prepared glass-derived hydroxyapatite (G-HAp) by etching sodium calcium borate glass using phosphoric acid.

The adsorption pH values (6.0–7.5), contact time (10–24 h) and derived capacities (11.34–22.22 mg/g) of synthetic HAps are comparable to those of natural HAps (Mohapatra *et al.*, 2009; Murutu *et al.*, 2009;Liang *et al.*, 2011). Thus, fluoride adsorption onto synthetic HAps is also independent of competitor ions and it increases with increasing temperatures depicting endothermic chemisorption reactions. The exception appears to be synthetic HAps samples prepared by Gao and colleagues (2009) from the reactions of $Ca(NO_3)_2.4H_2O$, $(NH_4)_2$-EDTA and $NH_4H_2PO_4$, which perhaps due to the presence of alkaline ammine groups, had maximum fluoride adsorption in acidic media of pH value of 2. It is observed that the efficiency of HAps to sorb fluoride also increases with increasing temperatures depicting endothermic processes.

Accordingly, HAps in all forms: natural, modified or synthetic are highly promising fluoride adsorbents. They have high fluoride adsorption capacities and they are stable

and usable over a wide range of water conditions. They are also among the most distributed minerals globally and they can be procured easily for water defluoridation. Additionally, fluoride adsorption onto HAps adsorbents is independent of anionic competitions, especially from the phosphate, which is a noxious interferent in water defluoridation using adsorption (Tang *et al.*, 2009; Huang *et al.*, 2011).

Natural apatites are, however, not found in a form suitable for direct use as adsorbents for water defluoridation. Apatites are among the hardest natural materials and substantial amounts of energy and specialised equipment are needed to pulverise the adsorbent materials to a form suitable for water defluoridation. Besides, natural HAps are normally associated with potentially labile forms of fluoride. They are, for that reason, among the natural rock systems that control the hydro-geochemistry of fluoride in the environment (Adelana *et al.*, 2010). Natural apatite is, therefore, associated with fluoride contamination of water systems and great care must be exercised in procurement and preparation of natural HAps to ensure that the derived adsorbents do not become point-source of secondary solubilisation and fouling of treated water with fluoride. Synthetic HAps are, therefore, usually more appealing for use as fluoride sorbents.

2.5.7 Aluminium oxide minerals

Bauxite is among the oxide minerals that have most frequently been studied for fluoride adsorption. alongside bauxite minerals that have repeatedly been investigated in this line are refractory grade bauxite (Mohapatra *et al.*, 2004), titania-rich bauxite (Das *et al.*, 2005), mixed Fe/Al hydroxides (Sujana and Anand, 2010), reddish brown

bauxite (Sujana and Anand, 2011), high alumina bauxite (Lavecchia *et al.*, 2012) and calcined bauxite (Thole *et al.*, 2012). Fluoride adsorption onto bauxite is a stoichiometric reaction of fluoride ions with Al^{3+} and other cationic centres in the mineral structure of bauxite. Optimum fluoride adsorption onto bauxite, therefore, occurs in acidic pH range of 5.5–6.5 (Farrah *et al.*, 1987; Sujana *et al.*, 1998; Mohapatra *et al.*, 2004; Das *et al.*, 2005; Sujana and Anand, 2010; Jiménez-Becerril *et al.*, 2011; Lavecchia *et al.*, 2012) where the concentration of F^- ions in the solution is highest. The process is, therefore, relatively independent of effects of such anionic interferents as the SO_4^{2-}, Cl^-, HCO_3^{2-} and NO_3^- (Sujana *et al.*, 1998; Das *et al.*, 2005).

The fluoride adsorption capacities of bauxite ores averages 3.1–5.2 mg/g (Das *et al.*, 2005; Onyango and Matsuda, 2006) but the sorption capacities increase with decreasing particle size (Thole *et al.*, 2012). Remarkably high fluoride uptake capacity of 170 mg/g, which has been reported by Farrah *et al.* (1987) for gibbsite, $Al(OH)_3$ could, therefore, be related to the small particle sizes found in the mineral. It is, however, found that the efficiencies of bauxite adsorbents to sorb fluoride decrease with increasing temperature showing that fluoride immobilization in bauxite surfaces is exothermic (Mohapatra *et al.*, 2004; Sujana *et al.*, 1998). The rates of fluoride adsorption are characterized by an initial rapid phase in the first 5 min followed by gradual approach to the equilibrium after about 120 min as expected for chemisorption processes (Sujana *et al.*, 1998; Mohapatra *et al.*, 2004).

Water defluoridation using boehmite, AlO(OH), is highest in pH range of 4.5–7.5 but unlike for bauxite the reaction may extend to 24 h before an equilibrium is attained (Jiménez-Becerril *et al.*, 2011).

In general, aluminium-based adsorbents are among the most studied media for water defluoridation. This is because they, normally, have strong affinities for fluoride and they are among the most distributed minerals in nature. Yet, the aluminium oxide minerals are not among the adsorbent media with the highest fluoride adsorption capacities and they usually have a narrow sorption edge in the pH range of 5.5–6.5. This is because they tend to solubilise to form $[AlF_x]^{(-x+3)}$ complexes in the medium of lower pH and, at more alkaline pH values; fluoride adsorption onto aluminium oxide minerals is strongly suppressed by excess OH^- ions in the alkaline media.

2.5.8 Calcareous minerals

The term calcareous is used to describe soil samples that are enriched in calcium and magnesium carbonate or soils formed by the weathering of calcium enriched rocks and fossil shell beds (Lagassé *et al.*, 2012). Studies to evaluate capacities of calcareous minerals to defluoridate water have gained momentum in the last few decades. The calcareous minerals studied most in this respect include: calcite (Fan *et al.*, 2003; Turner *et al.*, 2005, 2008, 2010; Patel *et al.*, 2009; El-Said and Draz, 2010; Nath and Dutta, 2010; Sasaki *et al.*, 2013;), quicklime (Patel *et al.*, 2009), marine sediments (El-Said and Draz, 2010), limestone (Nath and Dutta, 2010) and dolomite (Sasaki *et al.*, 2012).

Fluoride adsorption onto pulverized calcareous minerals occurs over the entire mineral surface with surface precipitation of fluorite, CaF_2 (Turner *et al.*, 2005; Sasaki *et al.*, 2013). The fluoride removal from water using calcareous materials is, therefore, fast as expected for a surface precipitation reaction and the equilibrium is attained in 30–60 min (Patel *et al.*, 2009; El-Said and Draz, 2010). Fluoride removal by adsorption using calcareous materials is, therefore, controlled by factors that control availability of $Ca^{2+}$and F^- ions at the mineral-solution interface.

The capacity of calcareous minerals to immobilize fluoride ions from water is, therefore, associated with high temperatures (Yang *et al.*, 1999) and with low pH values of solution. Maximum fluoride adsorption onto Ca-based minerals takes place within pH values of 5–6 (El-Said and Draz, 2010; Nath and Dutta, 2010), which are consistent with highest F^- ions concentration of aqueous fluoride solutions. Fluoride reactions with calcareous minerals is, therefore, site-specific and it is not affected by most of the interferent anions including the phosphate ions (Fan *et al.*, 2003; Turner *et al.*, 2005, 2008, 2010; Patel *et al.*, 2009; El-Said and Draz, 2010; Nath and Dutta, 2010; Sasaki *et al.*, 2013).

Despite earlier studies reporting quite high fluoride adsorption capacities for calcareous minerals (Reardon and Wang, 2000), the more recent studies by Fan *et al.* (2003) and by Gopal and Elango (2007) have shown that calcareous mineral adsorbents, normally, have very limited fluoride uptake capacities in the range of 0.39 mg/g. The minerals may not, therefore, present very prospective media for practical defluoridation of high-fluoride water.

2.5.9 Iron oxide minerals

Such ferric hydr(oxide) minerals as hematite, α-Fe_2O_3; goethite, FeO(OH); magnetite, Fe_3O_4; maghemite, γ-Fe_2O_3; lepidocrosite, γ-FeO(OH); ferrihydride, $Fe_5HO_8.4H_2O$ and schwertmannite, $Fe_{16}O_{16}(OH)_x(SO4)_z.nH_2O$, are some of the most abundant surface geomaterials, especially in the tropics. They are, therefore, among soil materials that have most extensively been studied for water defluoridation in the recent past (Bhatnagar *et al.*, 2011). Removal of fluoride from water using mixed laterite oxides (Sarkar *et al.*, 2006; Sujana *et al.*, 2009; Goromo *et al.*, 2012), haematite (Sarkar *et al.*, 2006; Teutli-Sequeira *et al.*, 2011), goethite (Hiemstra and Riemsdijk, 2000; Mohapatra *et al.*, 2009; Tang *et al.*, 2010) and ferrihydrite (Wei and Xiang, 2012) are some of the studies that have characterized evaluation of fluoride adsorption onto iron oxide minerals in the most recent past.

Natural laterites have fluoride adsorption capacities in the range of 12.0–15.0 mg/g (Sujana *et al.*, 2009). The fluoride adsorption capacities of laterites can, however, be enhanced by acid-base treatment or by calcination at high temperatures. It has been observed, however, that acid-base activated laterites appear to have superior fluoride adsorption capacities of 36.3–39.1 mg/g, (Maiti *et al.*, 2011) compared to thermally activated laterites, which have fluoride uptake capacities of 12.0–20.0 mg/g (Huang *et al.*, 2011). Fluoride adsorption onto heat-treated laterites is, however, concentration-controlled (Huang *et al.*, 2011) whereas that onto acid-base activated laterites is temperature-dependent (Maiti *et al.*, 2011).

The peak fluoride uptake by lateritic adsorbents occurs in the pH range of 3.5–5.2 (Sujana *et al.*, 2009; Huang *et al.*, 2011; Maiti *et al.*, 2011). The adsorption process is also strongly affected by competitor ions and the reduction in fluoride immobilization into laterite surfaces in presence of common anions follows the order: $PO_4^{3-} > SO_4^{2-} > Cl^- > NO_3^-$ (Huang *et al.*, 2011). Fluoride adsorption onto laterites has been found to be consistent with mixed reactions based on heterogeneous sites in the laterite adsorbent surface (Agarwal *et al.*, 2002; Sarkar *et al.*, 2006; Sujana *et al.*, 2009; Maiti *et al.*, 2011).

Hematite and goethite are some of the principal constituents of laterite minerals. Fluoride adsorption onto hematite has been characterised by high adsorption capacities and the adsorption process is not, normally, pH- and temperature-controlled. High fluoride uptakes by hematite, therefore, occur over a wide range of pH (2–7) and temperature, (298–323 K) conditions (Teutli-Sequeira *et al.*, 2011; Mohapatra *et al.*, 2012). The process is, however, slow and it takes up to 48 h before the equilibrium is attained (Teutli-Sequeira *et al.*, 2011). This shows that fluoride adsorption onto hematite is based on strong ion-exchange and chemisorption mechanism rather than on superficial physisorption processes.

Unlike the adsorption of fluoride onto hematite (Fe_2O_3), however, fluoride uptake by pure goethite, α-FeOOH, (Tang *et al.*, 2010) and goethite-enriched minerals (Mohapatra *et al.*, 2009) is pH-dependent. Goethite and goethite enriched minerals have high fluoride adsorption capacities of about 59 mg/g and the reaction of labile fluoride with reactive sites in goethite is reversible (Tang *et al.*, 2010). The fluoride

uptake by goethite is, therefore, time-dependent and the used adsorbent can easily be regenerated or cleansed for reuse before its final disposal into the environment.

In general, therefore, laterites are some of the most promising low-cost adsorbents for water defluoridation due to their high fluoride adsorption capacities. They are also readily available in abundant deposits in nature, especially among the humid tropical climates and they are, normally, stable and usable in a wide range of water conditions (Mohapatra *et al.*, 2009).

2.5.10 Carbonaceous minerals

Carbonaceous minerals represent yet another class of geomaterials that have attracted interest from water defluoridation researchers. The carbon-based minerals that have attracted the highest research interest as fluoride adsorbents are lignite (Pekař, 2008), charfines (Srimurali *et al.*, 1998), coke and coal (Sivasamy *et al.*, 2001; Borah and Dey, 2009) and fly ash (Xu *et al.*, 2011).

Lignite, which is a low quality coal, is a soft brown combustible sedimentary rock formed through natural compression of peat. Whereas previous studies had indicated that lignite could not be a very plausible adsorbent for water defluoridation (Srimurali *et al.*, 1998), subsequent work has revealed enhanced defluoridation capacities of 6.9–17.6 mg/g for the mineral. Furthermore, it has been shown that fluoride adsorption onto lignite is independent of both the interferent anions and variations in the pH of solution. Efficient fluoride adsorption onto lignite, therefore, is achievable over a wide pH range of 6–12 at room temperatures, 303 K. The adsorption process is fast

and more than 90% fluoride sorbs onto the adsorbent sites in just 10 min. However, the contact time required for attainment of the final adsorption equilibrium is about 150 min (Sivasamy *et al.*, 2001; Pekař, 2008). It indicates that there are at least two kinds of adsorbent sites for fluoride sorption onto lignite. The surface exposed sites are filled in the initial rapid phase and the less exposed sites are filled up in the latter phase of prolonged fluoride adsorption.

Charfines is a by-product of coke making from lignite. The efficacy of charfines to sorb fluoride from water has been found to be higher than that of lignite (Srimurali *et al.*, 1998). However, there is greater paucity in data on the use of this adsorbent in fluoride adsorption and more investigative work is desired to establish feasibility of its use as adsorbent in water defluoridation.

Coal is fossilized carbon. Water defluoridation capacities of coal averages 6.9–7.44 mg/g corresponding to 80% fluoride removal from water at most concentrations (Sivasamy *et al.*, 2001; Borah and Dey, 2009). Water defluoridation using coal occurs in acidic media and the defluoridation capacity of the mineral decreases with increasing alkalinity up to pH value of 7 and remains constant thereon. High defluoridation levels are achievable using coal at room temperature over pH values of 4–10 and only a little adsorbent of about 1% mg/mL is required. The sorption process is fast, and as for lignite, more than 90% fluoride sorbs in the first 10 min although the time required for the final attainment of the equilibrium may be more extended up to 60–90 min (Sivasamy *et al.*, 2001; Borah and Dey, 2009).

Fly ash, which is the waste materials generated from combustion of coke, has been associated with low surface areas and low fluoride adsorption capacities. Thus, even though fast rates of fluoride adsorption using this adsorbent have been reported and the time for attainment of the fluoride adsorption equilibrium is just about 30 min, complete fluoride removal from water using fly-ash is not achieved even at low fluoride concentrations (Mahramanlioglu *et al.*, 2002; Chidambaram *et al.*, 2003).

Some workers have, however, reported enhanced fluoride adsorption capacities of about 6.0 mg/g for magnesia-loaded fly ash cenospheres (MLC) prepared by wet impregnation method using magnesium chloride solution (Xu *et al.*, 2011). As for coal, the optimum fluoride adsorption using MLC occurred in acidic media at pH values of about 3.0 and at a temperature of 318 K. The defluoridation process using MLC was, however, affected by interferent anions and the anionic interference in fluoride uptake by MLC has been found to be in the order: comprehensive > dihydric phosphate > nitrate > sulphate.

In general, therefore, lignite, charfines and coal have high capacities to sorb fluoride from water. However, fly-ash does not appear to have attractive fluoride adsorption properties desired for easy defluoridation of water. Optimum fluoride removal using carbonaceous adsorbents can be achieved at room temperature in the pH range of 4–12. However, the current global energy needs for coal and lignite supersede the need to use coal-based media for water defluoridation.

2.6 Criteria for selecting soil adsorbents for an adsorption protocol

The choice of a soil adsorbent for water defluoridation is informed, among other factors by: the known adsorption capacities of the mineral for the adsorbate or for related adsorbates, adsorbent availability, cost of procurement, ease of preparation, simplicity of its application, and its user and environmental safety. Based on approximate fluoride adsorption capacities, the minerals that have shown the highest potential for water defluoridation in the most recent studies are: palygorskite (57.97 mg/g), pumice (18.27 mg/g), zeolites (15.65 mg/g), hydroxyapatite (13.27 mg/g), iron-enriched laterites (9.39 mg/g), bauxite (7.53 mg/g) and montmorillonites (4.82 mg/g). The other minerals including kaolinites, ceramics and quartz had mean fluoride adsorption capacities of less than 3.0 mg/g and therefore do not seem to represent very prospective fluoride adsorbents.

Except for fluorspar, gypsum, limestone, some bauxite, bentonites, titania, diatomite, laterites, apatite and a wide variety of alumino-silicate clays, most of Kenyan soil minerals are not well documented. What is more, fluorspar (Fan *et al.*, 2003), gypsum (Thole *et al.*, 2012) and limestone (Fan *et al.*, 2003; Gopal and Elango, 2007) do not represent plausible media for water defluoridation because they have got limited fluoride adsorption capacities. Although significant deposits of both bauxite and bentonites are known to exist in the country (Mutisya *et al.*, 2012), their geological data is scanty and unhelpful in informing exploration of these minerals for use as fluoride adsorbents in Kenya. Titania is localized in Kwale and vast deposits of diatomite have been exploited for decades in the central Rift Valley. It is still unclear,

however, whether this enormous diatomite resource could be utilized to defluoridate drinking water.

The most widely distributed Kenyan minerals with known fluoride adsorption capacities are the laterites, hydroxyapatite and silicate clays. The silicates and laterites are also the easiest to prepare for adsorption and they are environmentally passive making them obvious first choice geomaterials in search of easy-and–safe-to-use fluoride adsorbents for household water defluoridation. Despite its exceptional fluoride adsorption affinities and capacities, natural apatite is hardly an attractive material to procure for easy defluoridation of water. The mineral is among the hardest natural materials (Levy *et al.*, 2008) and considerable energy and efforts are required to pulverize the material to adsorbent-usable form for water defluoridation.

Defluoridation capacities of four locally available geomaterials (LAGs) including: a natural siliceous clay mineral (NSIM), a silicate ferric poly-mineral (FEPM), diatomaceous earth (DIME) and iron-enriched laterites (FELS) from parts of Kenya have been studied in batch simulation tests as a function of adsorption time, adsorbent loading, interferent anions, pH, and temperature. Equilibrium isotherms were used to determine the adsorption capacities and to elucidate the mechanism for fluoride uptake by the LAGs. The batch adsorption results were then verified using high-fluoride water from a natural source from Elementaita-Gilgil, Nakuru County, Kenya. This thesis reports on the findings of these investigations.

2.7 Surface activation of soil adsorbents

Natural soil systems have low ion-exchange capacities because their surfaces are normally saturated with replaceable groups which mask and neutralize intrinsic surface charge to maintain surface stability. The ion-exchange properties of the soil minerals can be enhanced by pre-treatments that dislodge the masking ions from soil surface sites, and unblock the pore in the structure of the soil systems (Girgis, 2005). This is important when the soil surfaces possess net charge that would repel the adsorbate ions that carry similar charge to that of the soil surface groups. For anionic adsorption, surface charge reversal for negatively charged soil adsorbents is achieved by impregnating the soil structure with multivalent cations or by hydrothermal activation in dilute acids among other physicochemical treatments. The latter approach is, however, the more popular because it is simpler and more cost-effective (Falaras *et al.*, 2000; Wu *et al.*, 2006).

Acid activation of soil adsorbents results in partial de-alumination of the clay structure increasing the proportion of silica and density of silanol groups on adsorbent surface. This increases the overall acidity and positive charge of the clay surfaces (Makhoukhi *et al.*, 2009; Frini-Srasra and Srasra, 2010).

Due to a high proportion of electronegative oxygen groups in the soil structure close to the adsorbent surfaces, many soil systems carry a net negative charge, which is unfavourable to fluoride adsorption. In natural systems, this keeps fluoride in the soil solutions making it easily bio-available for easy uptake by plants. So as to enhance the potential of the LAGs for fluoride adsorption, the adsorbent soil samples were pre-

treated in dilute HCl solutions to improve their surface positive charge. The surface charge reversal was then confirmed by determination of the surface pH and the PZNC of the soil adsorbents by alkalimetric titration.

2.8 Influence of solution parameters

Fluoride removal from water by soil adsorbents is influenced by adsorbent dosage and adsorbent particle size, adsorbate concentration, solution pH, temperature, adsorption time, co-existing ions, rate of agitation and activation. The solution parameters exert strongest effects on the adsorption process because of their influence on the surface chemistry of the soil adsorbents and on the transport of solutes through the solution to the adsorbent surface. The effect of adsorbent dosage and particle size, and adsorbate concentration mirror each other. Both adsorbent dosage and adsorbate concentration determine the availability of reacting 'particles' on either side of the adsorption interface. Higher adsorbent dosage and adsorbate concentrations lead to higher rates of adsorption because they intensify solute fluxes by diffusion, migration and convection through solution to the soil surface. The influence of adsorbent dosage and adsorbate concentration on the amount of adsorption are described by adsorption isotherms discussed in section 2.3.

As illustrated in figure 2.4, the pH determines aqueous speciation and reactivity of fluoride in water. It, therefore, controls the availability of adsorbate fluoride particles and how they react with soil surfaces. In the same way, the solution pH controls ionization of reactive groups at the soil colloid surfaces and it determines the nature and intensity of the soil surface charge and the adsorption potential at the soil

surfaces (Zhu *et al.*, 2007). For this reason, the solution pH of maximum fluoride adsorption varies with the type of soil adsorbent. Iron enriched laterites (Sujana *et al.*, 2009; Huang *et al.*, 2011; Maiti *et al.*, 2011); kaolinites (Agarwal *et al.*, 2002; Sugita *et al.*, 2005; Gogoi and Baruah, 2008; Meenakshi *et al.*, 2008; Ibrahim *et al.*, 2010; Wei and Xiang, 2012) and, to a limited extent, certain hydroxyapatites (Gao *et al.*, 2009; Mourabet *et al.*, 2012) have their maximum fluoride adsorption capacities in acidic media; at pH values of 5 or less.

Maximum fluoride adsorption onto montmorillonites (Sujana *et al.*, 1998; Agarwal *et al.*, 2002; Tor, 2006; Ramdani *et al.*, 2010), aluminium oxide minerals (Farrah *et al.*, 1987; Mohapatra *et al.*, 2004; Das *et al.*, 2005; Sujana and Anand, 2010; Jiménez-Becerril *et al.*, 2011; Lavecchia *et al.*, 2012), and calcareous minerals (El-Said and Draz, 2010; Nath and Dutta, 2010) is, however, restricted to pH values of 5-6. Some soil adsorbents, which include: pumice (Malakootian *et al.*, 2011; Asgari *et al.*, 2012); palygorskites (Zhang *et al.*, 2009); and certain ferric oxide minerals such as hematite (Teutli-Sequeira *et al.*, 2011; Mohapatra *et al.*, 2012) sorb high amounts of fluoride over an entire range of pH values form 2 to about 8. Still fluoride adsorption onto zeolites (Xu *et al.*, 2000) and onto certain carbonaceous adsorbents such as lignite (Sivasamy *et al.*, 2001; Pekař, 2008) and coal (Sivasamy *et al.*, 2001; Borah and Dey, 2009) is pH-independent and highest fluoride adsorption using these adsorbents is observed over the entire range of pH values of 4–12.

Differences in pH of maximum fluoride uptake for various soil systems arise principally from the differences in the surface chemistry, which control the affinity of

soil surfaces towards different fluoride species in soils. Soils that have high fluoride adsorptions in strongly acidic media of pH < 5 have higher affinity for molecular HF species, which are dominant in strongly acidic media. The HF particles adsorb by forming continuous hydrogen bonds with electronegative centres in the soil surfaces. Certain soils that preferentially sorb fluoride in media pH values of 5–6 have affinity for F^- species and the mode of fluoride adsorption is mainly complexation with positive centres like Al^{3+}, Fe^{3+}, Si^{4+} among many in the soil lattice structure. It can be assumed that over the entire range of pH values, the soils must then contain surfaces that have mutual attraction to certain fluoride species is solution.

Temperature is another key parameter that controls the thermodynamic adsorption equilibrium of fluoride at soil surfaces. The effect of temperature on fluoride adsorption onto soil surfaces arise from its influence on the adsorption energy balance, kinetics and activation (Biswas *et al.* 2010). Higher temperatures enhance rates of adsorption by influencing faster solute transport through solution towards the adsorbent surfaces. Very high temperatures may, however, counter the adsorption fluxes from solution and reduce the rates and magnitude of uptake of a particular adsorbate by the adsorbent. As for pH, the specific effect of temperature on fluoride adsorption on particular adsorbents is varied. The peak fluoride adsorption by natural montmorillonites (Agarwal *et al.*, 2002; Tor, 2006; Achour and Youcef, 2009; Ramdani *et al.*, 2010), Fe(III)-modified montmorillonite (Bia *et al.*, 2012), pumice (Mahvi *et al.*, 2012), and lignite (Sivasamy *et al.*, 2001; Pekař, 2008), for example, occur at room temperatures of 298 K.

Highest fluoride uptake by both aniline- and pyrole-modified montmorillonites (Karthikeyan *et al.*, 2012) as well as by coal (Sivasamy *et al.*, 2001; Borah and Dey, 2009) are favoured by above-room temperatures of about 303 K. It is found that fluoride exchange reactions of HAps (Fan *et al.*, 2003; Mohapatra *et al.*, 2009; Nie *et al.*, 2012) and of certain ferric oxide minerals such as hematite (Teutli-Sequeira *et al.*, 2011; Mohapatra *et al.*, 2012) occur over a broad range of temperatures from 298 to 323 K. Fluoride adsorption onto Mg^{2+} and Al^{3+} (Zhang *et al.*, 2009), Fe^{3+} (He *et al.*, 2013) and ZrO^{2+} (Zhang *et al.*, 2012) loaded palygorskite; synthetic HAps (Mohapatra *et al.*, 2009; Murutu *et al.*, 2009; Liang *et al.*, 2011); calcareous minerals (Yang *et al.*, 1999); and magnesia-loaded fly ash cenospheres (MLC) is favoured by higher temperatures in the range of 303–323 K. This depicts chemical and endothermic surface reactions. The efficiencies of bauxite to sorb fluoride has, however, been found to decrease with increasing temperature indicating existence of exothermic fluoride immobilization in bauxite surfaces (Sujana *et al.*, 1998; Mohapatra *et al.*, 2004).

The resident time required for attainment of equilibrium in an adsorption process is strongly dependent on the structure of the adsorbent and the nature of surface reactions that occur between the adsorbate and the reactive adsorbent sites. Adsorbents with compact crystalline structures and characteristic exposed surface sites tend to have rapid adsorption rates than porous media with intraparticle surface sites. This is because in the latter case, the adsorbate particles must be transported inside the adsorbent structures by diffusion to access the reactive sites. Thus, fluoride adsorption onto pulverised crystalline calcareous minerals tend to occur rapidly over

the entire mineral surface with surface precipitation of fluorite, CaF_2 (Turner *et al.*, 2005; Sasaki *et al.*, 2013). Water defluoridation using calcareous materials is, therefore, fast as expected for a surface reactions, and the equilibrium time is in the range of 30-60 min (Patel *et al.*, 2009; El-Said and Draz, 2010).

In less compact crystalline adsorbents such as lignite, over 90% adsorption occurs in initial 10 min. However, it takes up to 150 min to saturate the less exposed sites inside the adsorbent (Sivasamy *et al.*, 2001; Pekař, 2008). Such trends have been observed in fluoride adsorption onto coal but with shorter equilibration periods of 60-90 min for the later phase of adsorption (Sivasamy *et al.*, 2001; Borah and Dey, 2009). Coal is, therefore, more crystalline and compact; with less porosity than lignite.

Equilibration periods required for fluoride adsorption onto pumice are in the range of 20-30 min but they have not been associated with the two-phase adsorption phenomenon indicating limited porosity in the mineral (Asgari *et al.*, 2012; Mahvi, 2012). Although some authors have associated fluoride adsorption onto natural montmorillonites with rapid sorption of just 20-30 min (Agarwal *et al.*, 2002; Ramdani *et al.*, 2010), several natural montmorillonites (Tor, 2006; Achour and Youcef, 2009), Fe(III)-modified montmorillonites (Bia *et al.*, 2012), metal-intercalated palygorskites (Zhang *et al.*, 2009) and certain aluminium oxide minerals (Sujana *et al.*, 1998; Mohapatra *et al.*, 2004) appear to have consistent fluoride adsorption equilibrium time intervals in the range of 110–180 min. This indicates that these minerals may possess similarities in structural porosities.

As in fluoride adsorption onto calcareous and carbonaceous soil adsorbents, immobilization of fluoride into adsorbent zeolites (Xu *et al.*, 2000; Díaz-Nava *et al.*, 2002; Samatya *et al.*, 2007), hydroxyapatites (Murutu *et al.*, 2009; Liang *et al.*, 2011; Nie *et al.*, 2012), certain aluminium oxide minerals (Jiménez-Becerril *et al.*, 2011) and iron oxide minerals (Teutli-Sequeira *et al.*, 2011) are characterized by an initial rapid phase of 10–30 min followed by prolongation of fluoride adsorption equilibria to 10–48 h. The later phase of slow equilibration in this case can be ascribed to high structural porosity in case of zeolites and slow valence exchange reactions in case of hydroxyapatite and oxidic aluminium and iron minerals.

Natural water systems contain dissolved species of both organic and inorganic nature. Co-existent ions in water control the adsorption of fluoride by their competitive effect for space in the soil adsorbent surface and in adsorbate flux of ions from the bulk solutions to the adsorbent surface. Co-ions tend to lower the rates and magnitude of adsorption but the extent of these influences largely depends on the chemical and geometric dimensions of the ions, relative concentrations and affinities of the individual ions for the adsorbent surface. The influence of interfering ion, however, varies from adsorbent to adsorbent.

The soil adsorbents whose fluoride uptake is most affected by coexistent anions include iron oxide minerals (Sujana *et al.*, 2009; Huang *et al.*, 2011; Maiti *et al.*, 2011) and certain carbonaceous mineral adsorbents. The suppression of fluoride immobilization onto ferric oxides in presence of common anions follows the order: $PO_4^{3-} > SO_4^{2-} > Cl^- > NO_3^-$ (Huang *et al.*, 2011). Fluoride adsorption onto: zeolites

(Xu *et al.*, 2000), HAps (Mohapatra *et al.*, 2009; Murutu *et al.*, 2009; Liang *et al.*, 2011), bauxite (Sujana *et al.*, 1998; Das *et al.*, 2005) and calcareous mineral adsorbents (Fan *et al.*, 2003; Turner *et al.*, 2005, 2008,2010; Patel *et al.*, 2009; El-Said and Draz, 2010; Nath and Dutta, 2010; Sasaki *et al.*, 2013;) is site-specific and highly selective. It is, therefore, relatively independent of coexisting anions such as Cl^- NO_3^-, SO_4^{2-}, CH_3COO^- and PO_4^{3-} ions.

In general, therefore, the adsorbate concentration, adsorbent dosage, pH, temperature, and the presence of other ions control fluoride sorption processes at the soil surfaces. This influence is ascribed to the effect of these parameters on the: surface chemistry of the adsorbents, mass transfer processes and characteristics of the EDLs close to the adsorbents surfaces. The effect of solution parameters on fluoride adsorption onto LAGs was, therefore, investigated so as to isolate the optimum conditions for fluoride removal from water by adsorption using these minerals. The results are reported in the relevant sections of the current work.

2.9 Analytical methods

2.9.1 Atomic Absorption Spectroscopy (AAS)

AAS is a spectro-analytical method based on the measurement of attenuation of electromagnetic radiations in the visible and the ultraviolet regions of spectrum by atomic absorptions that result from changes in the electronic structures of the atoms. The extent to which the radiation is attenuated by atomic vapours of elements is a function of the length of traverse path of the light through the vapours and of the concentration of the absorbing atoms. For a collimated monochromatic beam of

incident intensity I_o passing through atomic vapours of thickness l, the degree of attenuation can be expressed as:

$$I_v = I_o e^{-k_v l} \qquad 2.30$$

where, I_v is the intensity of transmitted radiation at frequency v and k_v is the corresponding absorption coefficient. The value of the coefficient k_v is related to the concentration of the absorbing atoms by the expression:

$$\int k_v dv = \frac{\pi e^2}{mc} N_v f \qquad 2.31$$

where, m and e are the electronic mass and charge, respectively. The value N_v is the number of atoms per cm^3 volume capable of absorbing radiation at frequency of v and f is the oscillator strength, which is the number of electrons per atom capable of being excited by the incident radiation. For transitions from ground state, the integrated absorption is proportional to N_v, which approximates the concentration of the sample.

The typical AAS instrumentation comprises the source of electromagnetic radiation, flame atomizer, a monochromator, detector and the read-out system (Fifield and Kealey, 2000). The technique is used in chemical resolution of substances (Olajire and Imeokparia, 2001; Oyaro *et al.*, 2007; Ibrahim *et al.*, 2009). In the current work, AAS was employed in elemental analysis of the adsorbent soil materials.

2.9.2 X-Rays Diffraction Analysis (XRD)

X-rays are electromagnetic radiations of wavelengths in the range of 10^{-10} m. They are produced when a metal is bombarded with energetic electrons. Modern use of X-rays in structural elucidation is credited to the work by William Bragg and his son

Lawrence. They came up with an expression called the Bragg's law, which describes the relationship between the X-ray wavelengths, λ, and the diffraction angle $\boldsymbol{\theta}$ at which emergent X-ray beams would interact to provide an analytical tool. This law, which is now known as Bragg's Law, is usually presented as:

$$n\lambda = 2dsin\boldsymbol{\theta} \qquad 2.32$$

where, $\boldsymbol{n}$ is an integral factor representing the $\boldsymbol{n}^{th}$ order of diffraction. To study the X-rays pattern of a solid, a single crystal or powdered X-ray analysis is used (Castellan, 1983; Brittain, 2006s). However, the latter is more popular because it allows for the most precise identification and provides representative data because each measurement represents an average over millions of particles being scanned (S´rodoń, 2006).

XRD is the primary technique for identification of mineral samples. Application of XRD to structural elucidation of soil samples ranges from elemental resolution of the mineral phases, to identifications of the mineral phases (Ford *et al.*, 1997), determination of relative amounts of mineral phases present in mixed mineral systems (Chung, 1974; S´Rodon *et al.*, 2001), and assessment of the degree of crystallinity in the substances (Fey and Dixon, 1981). Phase identification is established when the scattering angles in the powder patterns of the sample and of the reference standard agree to within the calibrated precision of the diffractometer. It is sufficient that the scattering angles of the 10 strongest reflections obtained for a sample agree to within ±0.10 or ±0.20 degrees $2\boldsymbol{\theta}$ (Brittain, 2006).

In the current work, XRD analysis was employed in structural elucidation of the mineral soil adsorbents (S´rodoń, 2006). The X-ray powder diffractometer was employed for rapid determination of soil mineralogy for precise and representative data in identification of soil crystals.

2.9.3 Ion-selective electrodes

Ion-selective electrodes (ISE) represent a subset of potentiometric methods of analysis, which respond to a single species using a membrane that allows the ion of interest to pass through but blocks other ions (Bard and Faulkner, 2001). Activity differences across the selective membrane of the electrode generate a potential difference, which can be used to quantify the concentration of the ion of interest. The mathematical tool, which relates the potential difference, E, across the membrane to the difference in activity of the ion on either side of the membrane, is the Nernst equation, which at 298 K, can be written as:

$$E = E_0 - \frac{0.05916V}{n} \log \frac{a_1^{\,k}}{a_2^{\,q}} \qquad 2.33.$$

In this case, E_0 represents the standard reduction potential in volts, n is the number of electrons in the half reaction, a_i is the activity of species i (and i = 1, 2 …) whereas k and q are the respective charges on electro-active species a_i.

Since ion selective electrodes, deal with a single type of ion on each side of the membrane the values of the coefficients k is equal to that of q, which is unit and equation 2.33 reduces to:

$$E = E_O - \frac{0.05916V}{n}\log[C_i] \qquad 2.34$$

where, C_i is concentration of the analyte. It implies that for every 10-fold change in concentration, a potential difference of 59.16 mV is registered. If the species under investigation is a cation, the slope of the calibration curve is positive; otherwise it will be negative. For direct measurement of the ions of interest, the slope of the calibration curve should be 59.16 mV.

The ISE technique is the most popular method for determination of fluoride. The fluoride ISE consists of a lanthanum fluoride crystal across which a potential is developed by fluoride ions. The cell representation for this electrode is: *Ag/AgCl (0.3), F^-(0.001)LaF_3/test solution/reference electrode*. The chemical activity of fluoride ions in solution is, however, controlled by total ionic strength of the solution, pH, and the potential of fluoride complexation in presence of multivalent cations such as Si^{4+}, Al^{3+} and Fe^{3+}. A buffer called the total ionic strength adjustment buffer (*TiSAB*) is added to the solution to create uniform background ionic strength, adjust solution pH to an optimum value of about 5.5 and release any coordinated fluoride from fluoro-metal complexes present so that the electrode measures the fluoride concentration. The fluoride detection range of fluoride ISE is 0.1–100 mg/L and reproducibility is 3.6–4.8% relative standard deviations.

Potentiometric techniques were, therefore, employed in fluoride determinations and in measurement of surface pH of LAGs. The method is simple, versatile and rapid technique of determination.

2.9.4 Alkalimetric titration

Alkalimetry and acidimetry (syn. acidometry) are volumetric techniques of analysis based on neutralization reactions. Alkalimetry is used in determination of alkaline concentrations whereas acidometry is the parallel concept for determination of acid levels in substances. Application of alkalimetric titration to determine surface acidity of soil samples is comparable to titration of a weak acid versus a strong base. The amount of acidity (change in pH) at any point along the course of titration varies with the amount of base added according to the expression:

$$\phi = \frac{C_b V_b}{C_a V_a} = \frac{\alpha_{A^-} - \frac{[H^+]-[OH^-]}{C_a}}{1 + \frac{[H^+]-[OH^-]}{C_b}} \qquad 2.35$$

Where, □ is fraction of acid consumed by the base; C_a and C_b are the initial acid and base concentrations, respectively; V_a and V_b are the reacted acid and base volumes, respectively; α_{A^-} is the degree of dissociation of the acid and K_a is the acid dissociation constant.

The titration graphs, based on this equation and which are also obtainable by plotting the pH of the titre mixture against volume of the base, are typical sigmoid curves of the form depicted in figure 2.5. The equivalence point of the titration process coincides with the point of inflection on the titration curves.

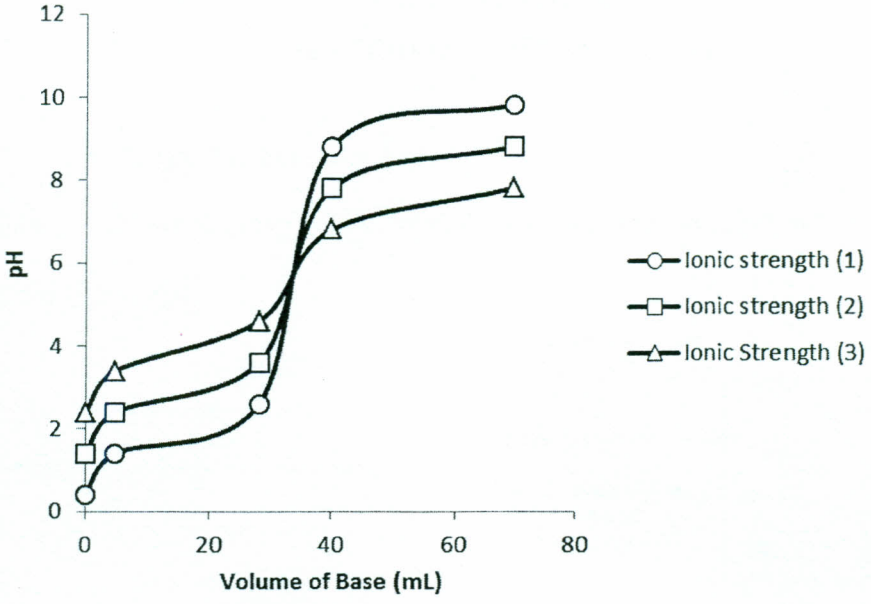

Figure 2.5: Alkalimetric curves showing technique for estimation of PZNC of soil adsorbents

In case of soil solutions, this point corresponds to the PZNC at which the amount of H^+ ions sorbed at the soil surfaces is equal to the amount of surface sorbed OH^- ions.

The PZNC is an intrinsic parameter of a particular soil type. Both the surface charge and surface potentials of soils are controlled by solution parameters but the PZNC of the soil depends on the chemical composition and soil mineralogy only. This means that if alkalimetric titration using soil samples is carried out at varying ionic strengths, the different titration curves intersect at the PZNC of the soil (figure 2.5). It is because at this point the adsorption of PDIs is independent of the ionic strengths of the solution. Alkalimetric titration, therefore, offers an inexpensive option for estimating the PZNC of soil samples (Weng *et al.*, 2007).

CHAPTER THREE
MATERIALS AND METHODS

3.1 The Gilgil-Elementaita Area

Figure 3.1 shows the map of the Gilgil-Elementaita area in relation to maps of Africa (a) and Kenya (b).

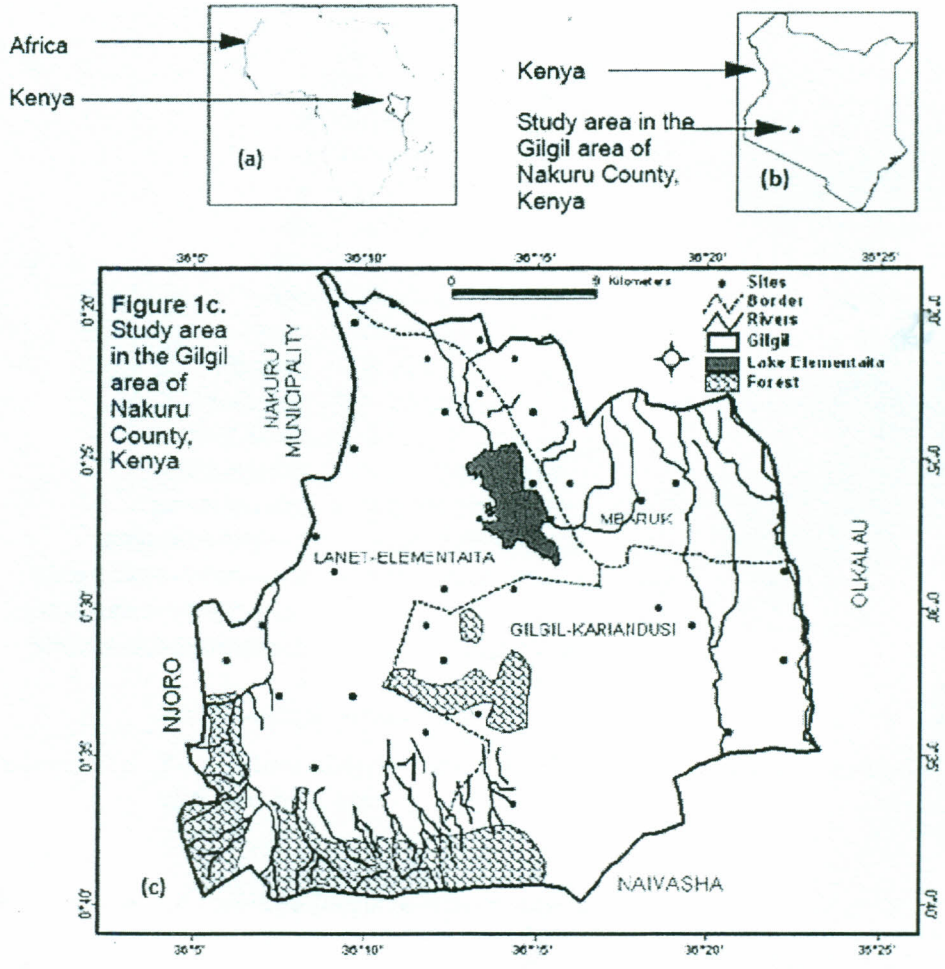

Figure 3.1: Map of the study sampling sites in Gilgil-Elementaita region, Nakuru County, Kenya

The area is about 1100 km^2 in size and it had a population of 130,000 people, which was distributed by gender and age brackets as depicted in figure. 3.2 (Kenya National

Bureaou of Statistics, 2010). Majority of the inhabitants used borehole water; piped water was limited to peri-urban areas but the primary sources of all piped water were boreholes, streams or rivers. At the household level, the inhabitants who used piped water collected and stored it in plastic tanks to ensure continuous availability. As illustrated in figure. 3.2, children under age 9, who are most vulnerable to the toxic effects of excessive fluoride in water, comprised 29% of the entire population.

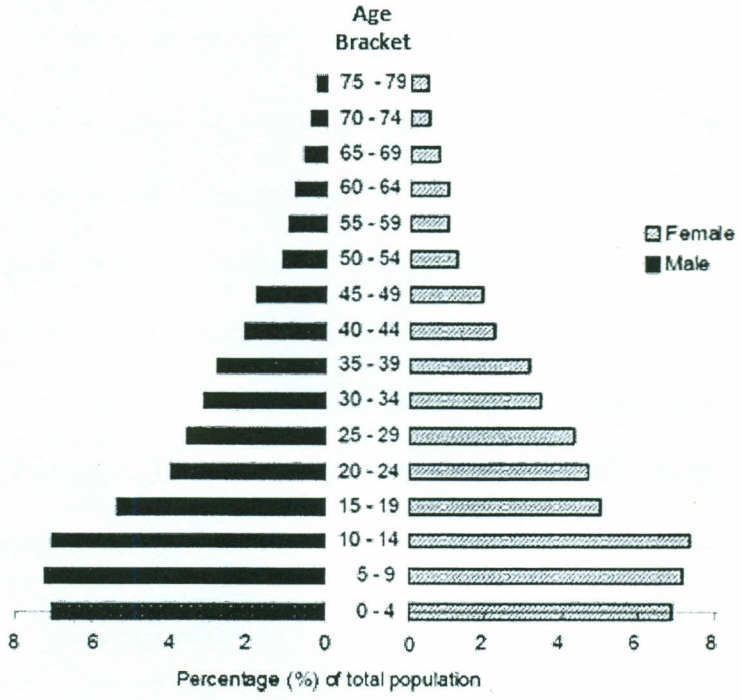

Figure 3.2: Population distribution in the Gilgil-Elementaita area by gender and age-bracket

3.2 Survey of fluoride levels in water sources

A total of 37 water samples were collected from different water sources, which were randomly selected from the study area by type of water source as summarized in table 3.1.

Table 3.1: Water samples collected from the study area for fluoride analysis

Sampling region	Piped water	Stream or river	Borehole (wells)	Storage Tank	Lake Water	Total
Mbaruk	2	2	5	0	0	8
Lanet-Elementaita	6	2	10	0	2	19
Gilgil-Kariandusi	0	3	3	1	0	10
Total (*n*)	**8**	**7**	**19**	**1**	**2**	**37**

Water samples were collected directly into clean 60-mL plastic containers and stored frozen at 263 K before analysis. The fluoride content of the water was determined using *Tx EDT Model 3221 direct fluoride ISE* by addition of appropriate volume of TiSAB II (Gikunju *et al.*, 1995). For ISE meter calibration, standard solutions containing 0.1, 1.0, 10.0 and 100.0 mg/L fluoride prepared by serial dilution of a 1000-mg/L fluoride stock solution with doubly de-ionized water (DDW) were employed.

3.3 Adsorbent Materials (LAGs)

Four different types of LAGs, namely; a natural siliceous mineral (NSIM) from Matili in Bungoma County, [00°44.98′N, 34°43.70′E; elevation 1638 m], a ferric poly-mineral (FEPM) also from Matili, [00°45.03′N, 34°43.61′E; elevation 1635 m], a diatomaceous earth (DIME) from Kariandusi in Nakuru County, [00°25.00′S, 36°17.60′E; elevation 2201 m]), and ferric laterites (FELS) from Mianga in Bungoma County, [00°34.67′N, 34°23.71′E; Elevation 1263 m]), were identified and randomly sampled for study.

Each of the soil samples was air-dried and ground to pass through < 2 mm mesh. The ground samples were dispersed by repeated mechanical treatment and sedimentation in doubly de-ionized water (DDW) to isolate < 1.0-μm fractions. Different portions of known mass of the adsorbent minerals were then placed in 0.1 M HCl at 0.2 g/mL sorbent-water ratio (S/W) and magnetically stirred for different time intervals between 30 and 420 min. The mixture was then filtered via suction through 0.5-μm Whatman No. 1 membranes, washed with excess DDW and oven-dried at 382 K overnight.

The capacities of the samples to sorb fluoride from water were then assessed using 1000-mg/L fluoride solution at 293 K, and 0.1 g/mL adsorbent dosage as described in section 3.5 and the results compared with those of the respective untreated minerals. The sample with highest fluoride adsorption for each mineral was then retained for the subsequent tests.

3.4. Reagents

Analytical grade reagents provided by *Aldrich Chemical Company Ltd* were used in all analysis throughout this work.

3.5 Characterizations of adsorbent materials

3.5.1 Determination of surface pH and the PZNC

Acid-treated adsorbent samples were pre-soaked in 1 M KCl at 10 g per 25 mL ratio and the mixture allowed to stand for 1 hour to equilibrate (Wambu *et al.*, 2009). At the end of this period, the pH of equilibrated suspension was measured using a *Hanna*

Instruments pH-211-microprocessor pH meter. The pH of zero net charge (PZNC) for each of the acid-treated adsorbent samples was determined by fast alkalimetric titration method, which is described elsewhere in the relevant literature (Weng, 2004).

3.5.2 Chemical and mineralogical analyses

The mineralogical analysis of LAGs was conducted by powder XRD using a *P-Analytical X'pert PRO PW-3040/60 X-Ray Diffractometer* equipped with a Cu-Kα radiation at 1.2° per min scan speed over a range of 5–70°. The chemical compositions of the adsorbents were then determined by AAS using a *Varian Spectra Model 10 Spectrophotometer* and the results recorded in terms of percent oxide content. Loss on ignition (LOI) was determined by ashing the sample at 1273 K.

3.6 Fluoride sorption tests

Batch adsorption tests unless otherwise specified were conducted at specific temperature and pH conditions as follows: exact mass of acidified adsorbent was mixed with 20 mL of solution of known concentration of fluoride. The mixture was then agitated on a *DKZ Model 1 Shaking Water-Bath* at 293 K for pre-selected time intervals. At the end of the agitation, the mixture was centrifuged and the supernatant fluoride concentration measured using fluoride ISE as described in section 3.2. The equilibrium amount, q_e (mg/g) and the percentage adsorption ($\%q_e$) were calculated from the respective expressions presented in equation 2.10 and equation 2.11, respectively

Conversely, fluoride adsorption from natural high-fluoride water using the LAGs was conducted in batch and column experiments using high-fluoride water from Gilgil area in Nakuru County, Kenya. The adsorbent regeneration tests were then conducted by agitating fluoride-laden adsorbent samples in aqueous Na_2CO_3 and NaCl as previously described by Rao (2003).

3.7 Data analysis and presentation

All tests were performed in triplicate. The data were analyzed by descriptive statistics by calculating the range, mean and standard deviation on replicate results. Causative relationships were then analyzed by graphical regression of the variables and determination of correlation coefficients.

CHAPTER FOUR
RESULTS AND DISCUSSION

4.1 Fluoride levels in water sources from the study area

Fluoride levels in 37 water samples that were studied showed the values reported in tables 4.1 and 4.2, respectively.

Table 4.1: Fluoride levels in water samples

Source	Number of samples	Range of F content (mg/L)	Mean F (mg/L)	Std Dev.
Tap (piped)	8 (21.6%)	0.001–32.80	7.69	11.9
Streams/rivers	7 (18.9%)	0.002–5.79	2.32	2.54
Boreholes	19 (51.4%)	0.026–21.50	6.57	6.07
Storage tank	1 (2.7%)	–	5.13	–
Total (*n*)	**37 (100%)**	**–**	**5.01**	**36.6**

Table 4.2: Proportion of water samples with fluoride levels exceeding the maximum permissible level of 1.5 mg/L

Source Type	Number of samples with fluoride>1.5 (%)	Mean fluoride concentration (mg/L)	Standard deviation
Stream	1 (14.3%)	5.79	–
Borehole	16(84.2%)	7.34	5.96
Storage tank	1(100%)	5.79	–
Tap (piped)	4(50%)	12.3	13.3
Total (*n*)	**26(70.2%)**	**5.85**	**7.34**

All types of the water sources had mean fluoride levels above the prescribed maximum permissible standards of 1.5 ppm (World Health Organization, 2011).

Among the seven stream and river water samples, only one sample collected from River Mbaruk contained fluoride above the maximum permissible limits. In fact, with the exception of the one sample, stream/river water samples in this study had lower mean fluoride levels (< 0.1 mg/L) compared to those in Kenyan river water samples, which had previously been reported elsewhere in the literature (Gikunju *et al.*, 1995).

As depicted in table 2, a total of 16 (or 84.2%) out of the 19 water samples that were collected from boreholes had fluoride contaminations above the WHO allowable limits. The severity of fluoride contamination in borehole waters in this region increased with proximity of the sources to the salty lakes in the region and with the increasing depth of the boreholes. This was consistent with previous surveys by Williamson (1953), which showed that most severe fluoride levels in the underground water sources were associated high fluoride lakes. The fluoride levels recorded in the present study were, however, lower compared to those reported by Kahama and colleagues (1997). The range of fluoride levels of borehole water in other parts of Nakuru County have been reported to be in the range 7.75–8.51 mg/L (Moturi, 2004), which is also higher than the 7.34 mg/L reported in the current study. The higher levels of fluoride in the deep boreholes close to Lake Elementaita could be ascribed to fluoride-rich underground feeder streams that drain into the lake.

Half of the eight samples of piped (tap) water whose primary sources were borehole water had mean fluoride levels of 12.3 mg/L, which was well above the 7.34 mg/L mean fluoride levels for the borehole water. This suggests that regardless of the primary sources of water, long storage hours used in traditional water handling

(Pasteur, 2000) could increase the levels of fluoride in the treated water through constant evaporation on the stored water. This could then explain the high fluoride levels of 5.1 ppm found in water samples drawn from one of the storage tanks at the diatomite mining industries at Kariandusi. There is, however, a general paucity in data on fluoride levels in tap water in the current study area to compare with.

High mean fluoride levels (162.5 mg/L) that were found in lake water could be attributed to leaching of fluoride from the fluoride-rich volcanic rock systems around the lake, which enrich underground drainage into the lake with labile fluoride (Kahama *et al.*, 1997). The high tropical temperatures in the region cause extensive evaporation from the lake increasing concentration of fluoride in its water. Given that the lake does not have any overland outlets, it has formed a natural reservoir for dissolved salts that lead to high accumulation of fluoride in its waters. Some authors have indicated that during certain months of the year the levels of fluoride in the lake water in this region rise to as high as 3000 mg/L (Nair *et al.*, 1984).

4.2 Chemical and Mineralogical Characterization of LAGs

To understand the nature of interactions that occur between the reactive surface sites in the LAGs and fluoride ions in water, the mineralogy and the corresponding elemental composition of the soil adsorbents was analyzed by X-rays diffraction (XRD) and atomic absorption spectrophotometry (AAS), respectively. The results for the XRD and AAS analyses are depicted in figure 4.1 and in table 4.3, respectively. As can be seen from figure 4.1 (a) NSIM consisted of quartz, potassium tecto-aluminotrisilicates and albite minerals (S´Rodon *et al.*, 2001).

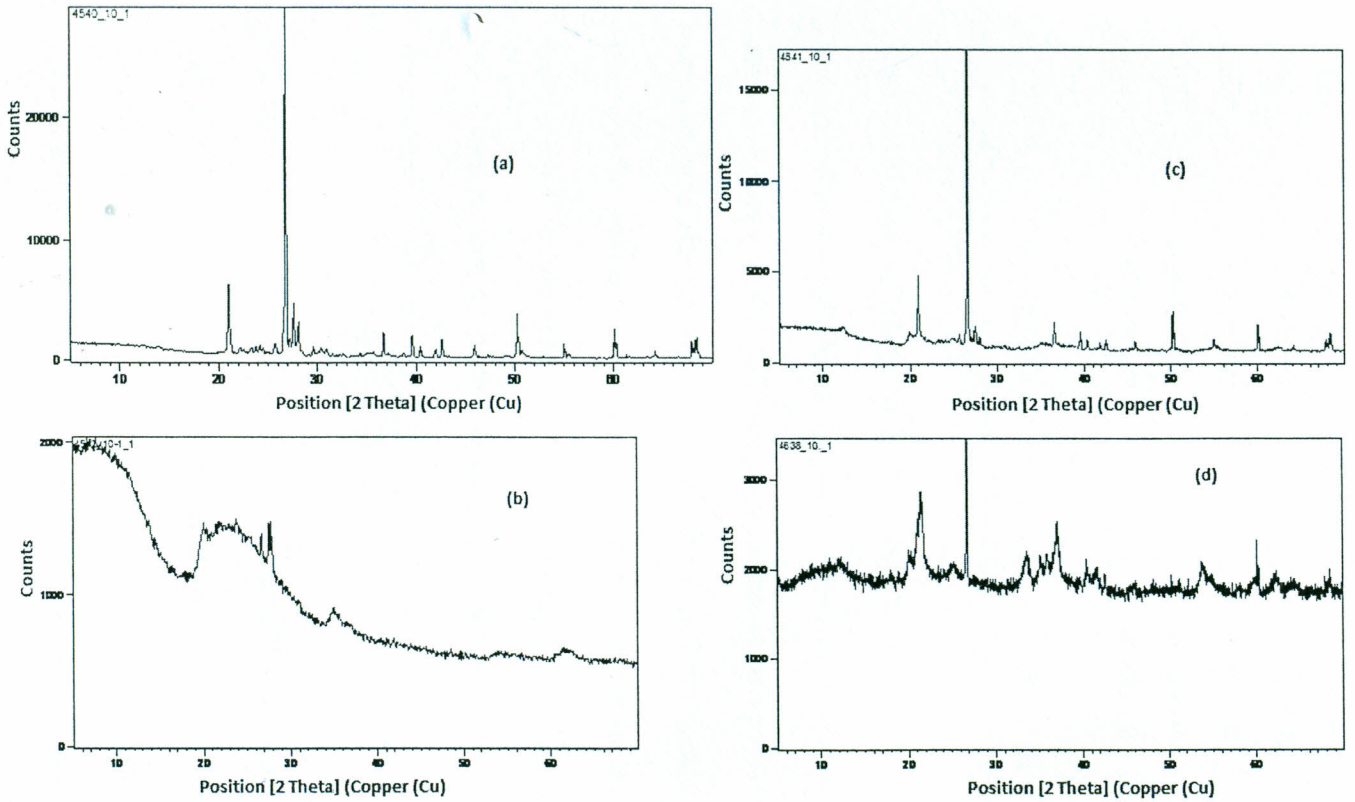

Figure 4.1: XRD spectra for (a) NSIM, (b) DIME, (c) FEPM and (d) FELS

Table 4.3: Main chemical characteristic of mineral adsorbent materials

Property (%)	NSIM	DIME	FEPM	FELS
SiO_2	80.75±4.01	70.40±2.71	68.19±2.14	28.2±1.40
Al_2O_3	10.73±0.82	9.29±0.41	13.00±0.71	18.8±0.88
K_2O	3.93±0.11	2.36±0.02	2.10±0.54	0.36±0.02
Na_2O	1.52±0.03	1.00±0.01	0.59±0.11	–
Fe_2O_3	0.89±0.01	3.76±0.15	5.89±0.23	37.2±1.65
CaO	0.81±0.01	0.77±0.02	0.39±0.01	–
TiO_2	0.40±0.00	0.61±0.01	0.50±0.12	0.77±0.03
MgO	0.33±0.01	–	0.19±0.01	0.24±0.02
MnO	–	–	–	3.00±0.43
LOI*	1.91±0.08	–	10.19±0.68	13.9±0.65

* Loss on ignition

The results also correlated with AAS results in table 43, which confirmed that the alumino-silicate clays were the main chemical constituents in the material. The mineral surfaces would, therefore, assume net negative surface charge due to the high proportion of electronegative oxygen atoms in its structure. The negative surface of the material would be unfavourable for fluoride uptake from water using this clay necessitating for its activation using acid media as described in section 3.3. This would then reverse the surface charge and enhance the fluoride adsorption potential of the mineral.

The mineralogy and geochemistry of diatomite is well documented (Miretzky *et al.*, 2011). The XRD spectra of DIME, which is depicted in figure 4.1 (b), demonstrated that the principal mineral component of DIME was silica, SiO_2. The XRD pattern showed that diatomite was poorly crystallized. According to Sheng *et al.* (2012) the amorphous band may be attributed to the glass formation by SiO_2 in DIME. The

peaks at 19°, 21°, 26° and 35° are typical of diatomite. The results of AAS analysis depicted in table 4.3 also showed the natural DIME such as used in this study are, as expected, contaminated to varying degrees with alumino-silicates (>9.29±0.41%), ferric materials (3.96±0.15%) and exchangeable salts (4.13±0.05%) as also reported elsewhere in the literature (Shawabkeh, 2003).

Both the XRD spectrum of FEPM, which is depicted in figure 4.3 (c) and the results of the spectrophotometric analysis shown in table 4.3 indicated that the ferric-polymineral, FEPM, was an alumino-(13.00%)-silicates (68.19%) mineral enriched in iron oxyhydroxides up to 5.89%. It comprised 10.19% combustibles and 2.73 % exchangeable alkalis. The mineral was expected to have high affinity for fluoride ions due to its high proportion of ferric- and alumino- minerals (Coetzee *et al.*, 2006).

As in the analysis of FEPM, the spectrophotometric (table 4.3) and X-ray diffraction (figure 4.3 (d)) results showed that the main mineral constituents of FELS were: haematite, goethite, quartz and crystobalite. The material was low in exchangeable cations and was, therefore, expected to exhibit heterogeneous surface chemistry comprising of low-affinity alumino-silicates (47.0%) and high-affinity iron and manganese oxide (40.2%) surfaces. High fluoride adsorption capacity based on mixed fluoride adsorption mechanisms involving the two principal surfaces was, therefore, anticipated of this material (Chen *et al.*, 2010b).

4.3 Effect of acid pre-treatment of LAGs

The effects of acid-activation of LAGs on their fluoride adsorption are represented in figure 4.2.

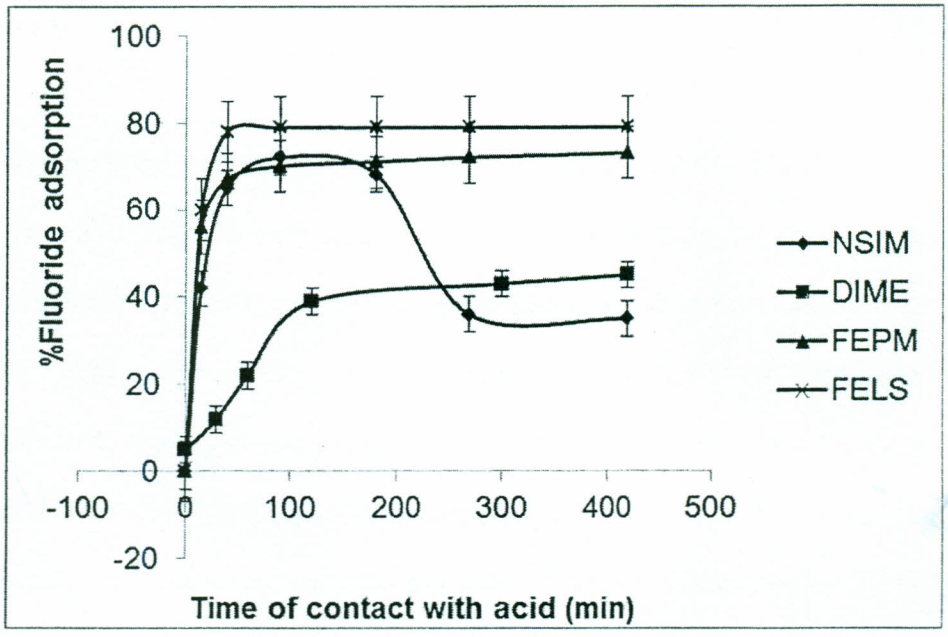

Figure 4.2: Effect of acid-activation of adsorbents on their fluoride adsorption capacities (Experimental conditions: initial fluoride concentration, C_0 = 1000 mg/L; temperature, T = 293 K; Adsorbent dosage = 0.1 g/mL)

The efficiency of fluoride adsorption onto the siliceous mineral, NSIM, increased from approximately 55% for untreated samples to more than 70% when the material was pre-treated in dilute HCl for 30 min. Further prolonged exposure of the material to the acid did not result in significant change in the efficacy of the mineral to sorb fluoride. Instead, the fluoride adsorption efficiency of the material dropped and remained constant at about 30% when the activation time was increased to 270 min.

It showed that prolonged exposure of the adsorbent to the acid caused the acid media to attack and damage the adsorptive surface of the soil. Such acid degradation of soil adsorbents have also been reported for certain adsorbents in the literature (

Makhoukhi *et al.*, 2009; Alagumuthu *et al.*, 2010). A 30-min acid-activation interval was adequate to produce a high fluoride adsorption surface in NSIM. This contact time was then maintained for subsequent activations of this mineral in the rest of the tests.

Starting from just about 24% for untreated samples the fluoride adsorption capacity of diatomaceous earth (DIME) rapidly increased with increasing time of contact with the acid media and remained constant at 40% after about 60 min. Unlike in the activation of NSIM, however, there was no eventual degradation in the adsorption capacity of DIME at prolonged periods of exposure to the acid under the conditions of these tests. It showed that when DIME is immersed in acid, the adsorbent surface of the material rapidly got protonated generating additional surface silanol groups (Si–OH). This led to increased overall positive charge in the mineral surface, which enhanced the fluoride adsorption capacity of the mineral (Tsai *et al.*, 2005; Miretzky *et al.*, 2011). Even though the fluoride adsorption capacity of DIME did not remarkably increase with acid-pre-treatment, the material depicted a stable adsorbent surface indicating that it could be used to sorb fluoride from water over wide spectrum water conditions. A 60-min contact time was sufficient to produce optimum fluoride adsorption onto DIME. This time interval was, therefore, maintained in the subsequent activation of DIME in current work.

The acid activation of FEPM and FELS using 0.1 M HCl showed trends that were analogous. The activation of FELS, however, depicted fluoride removal capacities that were superior to that of FEPM. As for NSIM, the fluoride adsorption onto FEPM

increased with increasing contact time with the acid media from about 40% for the untreated samples to 70% of fluoride removal when the contact time with the acid was increased to 60 min and remained constant thereon. A 60-min contact time was sufficient and, therefore, adopted for acid-activation of FEPM in subsequent tests. On the other hand, fluoride adsorption onto FELS increased from 20% for the raw untreated materials and reached 80% as time of acid-treatment was increased from 0 to 30 min. The 30-min interval was then utilized in all subsequent activation of the FELS mineral samples.

In general, therefore, the ferric poly mineral, FEPM, and the siliceous mineral, NSIM, had comparable sorption capacities when treated with 0.1 M HCl solutions. However, the capacity of NSIM to sorb fluoride deteriorated at prolonged exposure of the adsorbent to acid. Under the experimental conditions employed in the current work, diatomaceous earth, DIME, was least responsive to acid-treatment. The adsorbent depicted a stable mineral surface and was not strongly affected by the acidic media. The best activation was shown by the lateritic adsorbent, FELS, because its capacity to sorb fluoride was most enhanced on exposure to acid and the adsorbent did not deteriorate at prolonged acid treatment. Differences in activation characteristics of adsorbents, such as reported in the current work, are due in part to differences in the mineralogy; chemistry and surface properties of the minerals but the solution parameters can also influence the activation efficacy of the media.

4.4 Surface pH and PZNC of the LAGs

To elucidate the net surface charge of the LAGs, the pH of the acidified samples was determined and the PZNC estimated by fast alkalimetric titration as described elsewhere in the literature (Weng *et al.*, 2007). The results of these tests are recorded in figure 4.3. The surface pH of the LAGs ranged from values of 1–3 and the PZNC were in the range of 1.5–3.8. In all cases the adsorbent surface pH was lower than the respective PZNC and the adsorbent surfaces were, therefore, positively charged as desired for anionic fluoride adsorption. It could be assumed that when the soil adsorbents were immersed in the acid, the oxygen centres in the clay systems got protonated and increased the soil surface acidity resulting into net positive surface charge of the materials (Martı *et al.*, 1998).

Although the adsorbent characteristics of soils is dependent on the mineralogy and structural chemistry of the soil minerals, surface physicochemical characteristics of soil adsorbents is related to the soil solution parameters including the pH, contact time, ionic strength, dissolved ligands, temperature and sorbent-to-water ratio. These parameters control ionizations at the soil surface groups and hence the magnitude of the surface adsorption potentials (Zhu *et al.*, 2007). The transfer of chemical groups across the soil-solutions interface is, therefore, a function of ambient solution conditions.

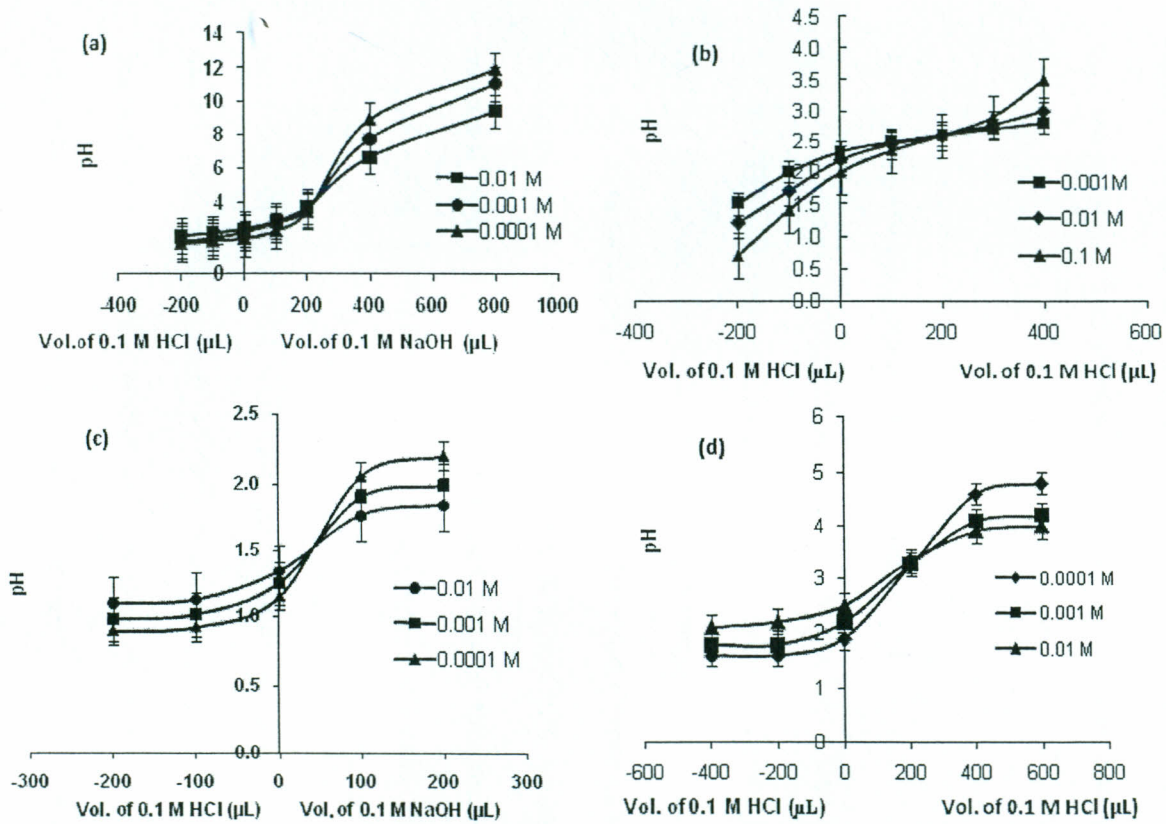

Figure 4.3: Net alkalimetric titration curves for (a) NSIM, (b) DIME, (c) FEPM and (d) FELS at various concentrations of aqueous $KClO_3$

So as to understand the physicochemical changes that occur in the adsorbent surfaces of LAGs when the soils are contacted with electrolyte solutions containing fluoride ions, batch adsorption tests were undertaken to assess fluoride uptake by LAGs as a function of the solution pH, contact time, fluoride concentration, presence of co-ions and temperature. The results of these tests are now discussed in the subsequent sections.

4.5 Effect of change in fluoride solution pH

The effect of pH on fluoride adsorption onto the LAGs was studied at pH values of 3.2–7.4. The adsorbate pH was adjusted by addition of small amounts of 1 M NaOH or 1 M HCl using 50-µL pipettes. The percentage of fluoride adsorption was plotted as a function of initial solution pH and the results presented in figure 4.3. Fluoride adsorption onto NSIM decreased from 80% to 20% when the solution pH was increased from 3.4 to 4.7 and it remained constant thereon. This shows that highest fluoride uptake by NSIM occurs in acidic media at pH values less than 3.4.

According to figure 2.4, molecular HF particles dominate fluoride speciation in the water in acid media at such pH (Stumm and Morgan, 1996). It could be assumed that fluoride adsorption onto NSIM surfaces was, therefore, dominated by electrostatic type interactions involving bridging hydrogen bonds between protonated mineral surfaces of acidified NSIM and molecular HF particles in solution. It means that as the solution pH increased NSIM surface sites deprotonated and the overall positive charge density on the adsorbent surface decreased.

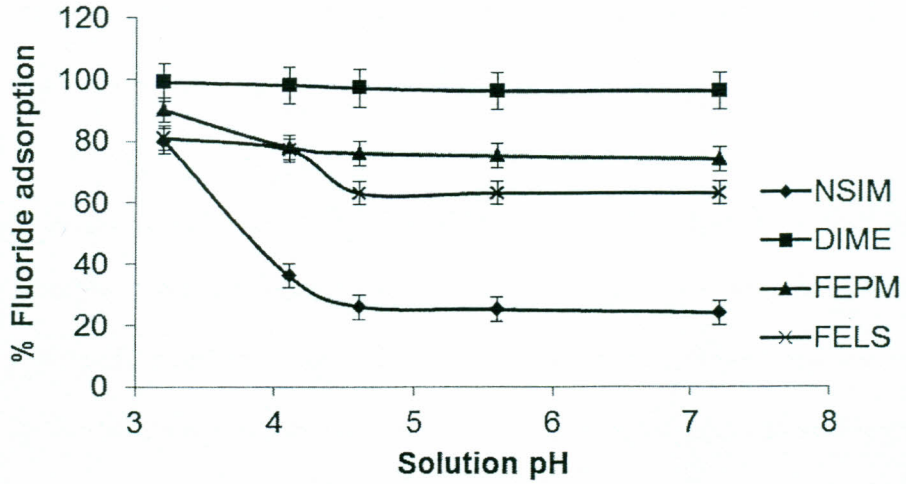

Figure 4.4: Effect of change in solution pH on fluoride uptake by LAGs [Experimental conditions: Fluoride concentration, c = 1000 mg/L; time, t = 120 min, Temperature, T= 303 K, and adsorbent batch dosage, m = 0.5 g/mL]

Above the PZNC, which was at pH value of about 3.8, NSIM surfaces developed a net negative charge; the adsorbent surfaces lost their affinity for fluoride. This led to coulombic repulsion against adsorbing fluoride particles to increase, which led to decrease in fluoride immobilization into the NSIM adsorbent surface.

Again figure 2.4 shows that the concentration of F^- ions in the solution increases under pH values of 4–5. It can be assumed that this is accompanied by ionization decomposition hydrogen-bond-assisted adsorption complexes from NSIM surfaces leading to reduced fluoride adsorption in this range of pH values (Stumm and Morgan, 1996). At this point the adsorbent surface gets appreciably hydroxylated and the overall fluoride uptake is then suppressed from a lofty 80% at pH value of 3.4 to just below 20% in the pH range of 4–7. It shows that it becomes increasingly difficult

for negatively charged fluoride ions, F^-, to sorb at negatively charged NSIM surfaces at elevate values of pH.

Related findings have been reported for fluoride adsorption onto other adsorbents. For example, while investing fluoride uptake by granular ferric hydroxide, Tang *et al.* (2009) observed decreased fluoride adsorption, when the pH was less than 3, caused by the formation of HF species, which is considered less adsorbable than F^-. While studying fluoride retention by certain Tunisian clay soils, Hamdi and Srasra (2007) indicated that the fluoride adsorption capacities of the soils decreased by a magnitude of 50% when the solution pH was raised from 3 to about 6.5.

It can be assumed that interlinking hydrogen bonds are the primary interactions in fluoride immobilization onto NSIM at pH values below PZNC. However, ion-exchange reactions involving surface hydroxyl groups and inner sphere complexation mechanisms involving positive centres in the clay systems of NSIM become the primary modes of fluoride immobilisation onto NSIM surfaces in more alkaline media. The current results indicated that the differential partitioning of fluoride between the sorbed and solution phases under different pH values of the media showed that the ratio of electrostatic adsorption to ion-exchange adsorption in NSIM was about 75% to 25%.

In contrast to fluoride adsorption onto NSIM, changes in solution pH did not strongly control fluoride uptake by acidified diatomaceous earth, DIME. Fluoride uptake by DIME decreased marginally from 98.8% to just below 98.0% when the solution pH

was increased from 1.56 to 6.89. It showed that acid-treatment did not induce pH-dependent adsorptive surface in DIME. The process of acid-activation of DIME was, therefore, a surface phenomenon but rather a structural one involving the unlocking of the mesoporous siliceous structure of DIME. It shows that fluoride adsorption onto DIME was based on mixed surface reactions based upon protonated silanol groups in DIME surfaces and on intraparticle diffusion of fluoride particles into the mesoporous structure of the adsorbent. The synergy between the two processes meant that fluoride adsorption onto DIME is independent of the solution pH. It shows that DIME could be used to sorb fluoride from water at all pH conditions.

The trends in fluoride adsorptions onto iron-enriched FEPM and FELS adsorbents were similar. The percentage fluoride adsorption onto the two adsorbents decreased with increasing solution pH and remained constant at pH value of 5.24 thereon. The fluoride adsorption efficiency of FEPM was, however, slightly better.

In general, the effect of change in pH on fluoride adsorption onto LAGs mirrored the results of acid-activation of the adsorbents. Diatomaceous earth, DIME, which was inert in regard to the acid, showed fluoride uptake trends that were not strongly affected by the changes in the pH of the solution. The pH-dependent fluoride uptake by the other LAGs showed pH-induced degradation in the mineral structures of the adsorbents to varying degrees. The decline in fluoride adsorption onto the LAGs at high pH value followed the order: NSIM > FELS > FEPM > DIME. In all cases, however, fluoride uptake by LAGs attained highest equilibrium value in a media of pH values of about 4.7 and remained constant thereon.

4.6 Effect of change in adsorption contact time

The kinetic effect of solution pH on fluoride adsorption onto NSIM, DIME and FEPM is depicted in figure 4.5. Figure 4.5(a) shows that at pH value of 3.24, fluoride adsorption onto NSIM was rapid and 90% fluoride adsorption could be achieved in about 120 min. However, fluoride adsorption onto NSIM was slower at pH values greater than 5.24 as expected for ion-exchange reactions, which have been postulated in section 4.5. Highest fluoride adsorption onto NSIM occurred in acidic media and diffuse interlinking by hydrogen bonds involving protonated sites in the adsorbent surface was the principal mode of fluoride uptake by NSIM. Approximately 20% fluoride adsorption onto NSIM occurred by ion-exchange reactions at pH values greater than 3.24. However, the time required for attainment of equilibrium increased with increasing solution pH from 120 min at pH value of 3.24 to 240 min at pH 6.78. This showed that superficial physisorption diminished as ion-exchange reactions become increasingly significant at more alkaline pH values of solution.

The pH-dependent kinetics of fluoride adsorption onto DIME is illustrated in figure 4.5 (b). Fluoride adsorption onto DIME was almost instantaneous and 96–99% fluoride removal from water could be attained in the first 10 min for all pH values from 3.24 to 6.89. This was followed by a phase of continuous gradual increase in fluoride uptake by the material. Like it was for NSIM, highest fluoride removal by DIME was achieved in pH values of about 3.24. Unlike for NSIM, however, the trends in fluoride adsorption onto DIME were similar at all pH values.

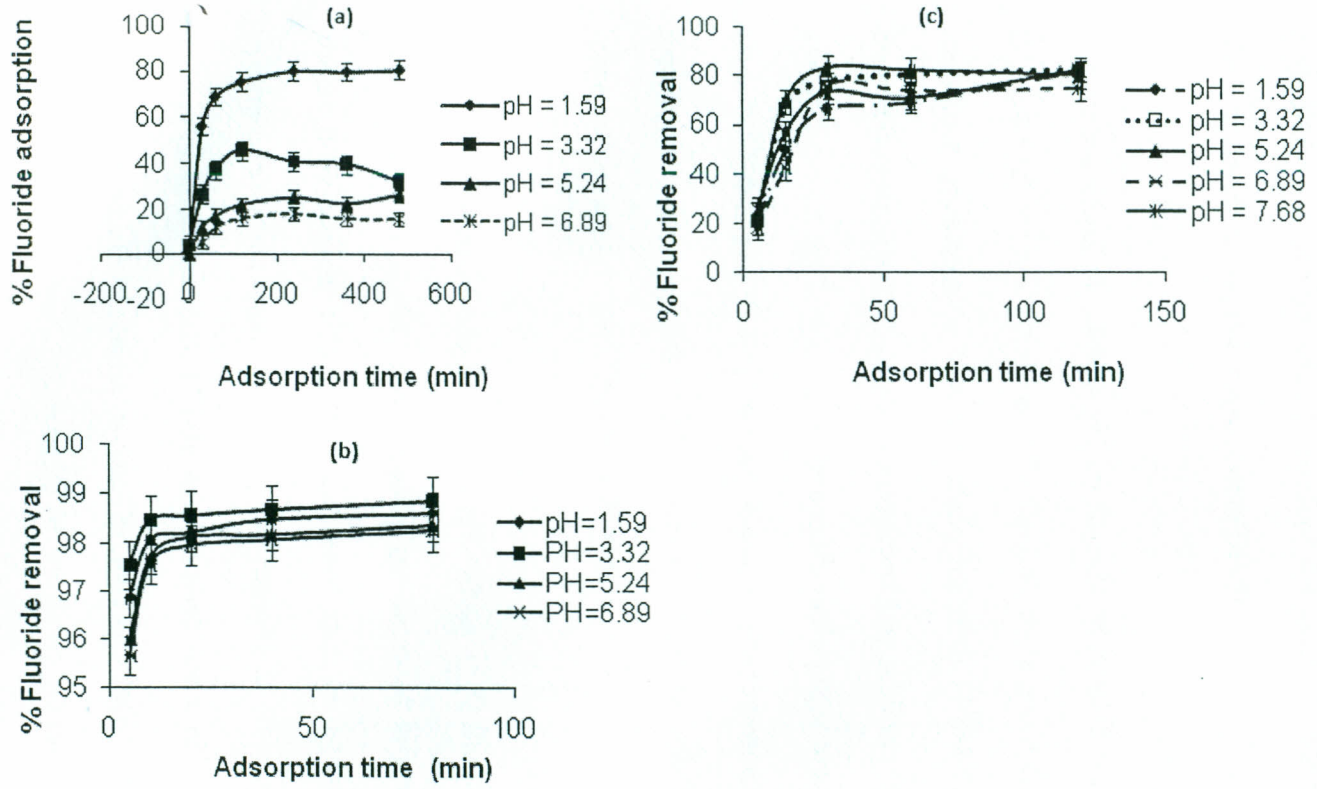

Figure 4.5: **Effect of initial adsorbate pH and time of contact on fluoride adsorption onto (a) NSIM, (b) DIME, (c) FEPM and [Experimental conditions: Fluoride concentration, C_0 = 1000 mg/L; Temperature, T= 303 K; and 0.5 g/mL adsorbent batch dosage,]**

It showed, as also postulated in sections 4.3 and 4.5, that the pH did not strongly control fluoride adsorption kinetics onto DIME.

The kinetic effect of solution pH on fluoride adsorption onto FEPM is presented in figure 4.5 (c). At low pH values of 1.59–3.24, there was a distinct two-phase fluoride adsorption phenomenon. Fluoride adsorption onto FEPM increased with increasing time of contact and 60% pseudo-maxima could be achieved in just 15 min. The rate of adsorption then slowed down before another rapid phase to a maximum of about 75% after about 60 min. The two-phase adsorption phenomenon was, however, absent at higher pH values greater than 5, where maximum adsorption of 70–80% was achieved in a shorter time interval of 30 min.

It could be assumed that at acidic pH values < 3, fluoride adsorption occurs at exposed sites in FEPM, which rapidly get saturated in just about 30 min. This is followed by gradual filling of less exposed sites in the adsorbent structure as the system approaches maximum adsorption capacity at 60 min. Subsequent increase in adsorption after the initial 15 min was not observed at pH values > 5. It showed that as the solution pH increased, excess OH^- ions in solution filled the microporous sites in FEPM making them inaccessible to adsorbing fluoride ions. Thus, both surface reactions and diffusion of fluoride into the microporous sites in the adsorbent controlled fluoride adsorption onto FEPM in acidic media of pH value < 3.24. It, therefore, required longer equilibration time (60 min) leading to greater adsorption capacity of about 90% at these range of pH values. At higher pH values (5.24–7.68),

however, only surface adsorption dominated resulting in lower capacity of the adsorbent to sorb fluoride (85%) and shorter equilibration time of just 30 min.

In general, high fluoride adsorption (□70%) could be achieved using FEPM over the entire pH range of 1.59–7.68. It showed that the adsorbent had stable sorptive surfaces and could, therefore, be used to sorb fluoride from water under wide range of pH conditions (Teutli-Sequeira *et al.*, 2011; Mohapatra *et al.*, 2012).

4.7 Effect of change in mass of adsorbent

The mass of adsorbent in a batch adsorption system determines the amount of the reactive adsorbent surface available to the adsorbing electrolyte particles in the solution. For most inorganic reactions, the amount of available sorptive surface and the amount of fluoride adsorbed increase in proportion to mass of adsorbent. The effect of change in mass of LAGs on their fluoride uptake from water was, therefore, studied under conditions of constant adsorbate volume, adsorbate concentration (1000 mg/L), temperature (298 K), pH value (3.24) and time of contact (120 min). The results are presented in figure 4.6.

Figure 4.6 (a) shows that fluoride uptake by NSIM increased from just about 40% to 50% when the mass of NSIM was increased from 5 g to 15 g. The percentage of fluoride adsorption onto NSIM then further increased to about 80% when the adsorbent mass was further increased to 20 g before it approached complete fluoride removal from solution at 35 g NSIM dosage. It showed that at very low adsorbent doses NSIM surfaces were rapidly saturated by excess fluoride in solution.

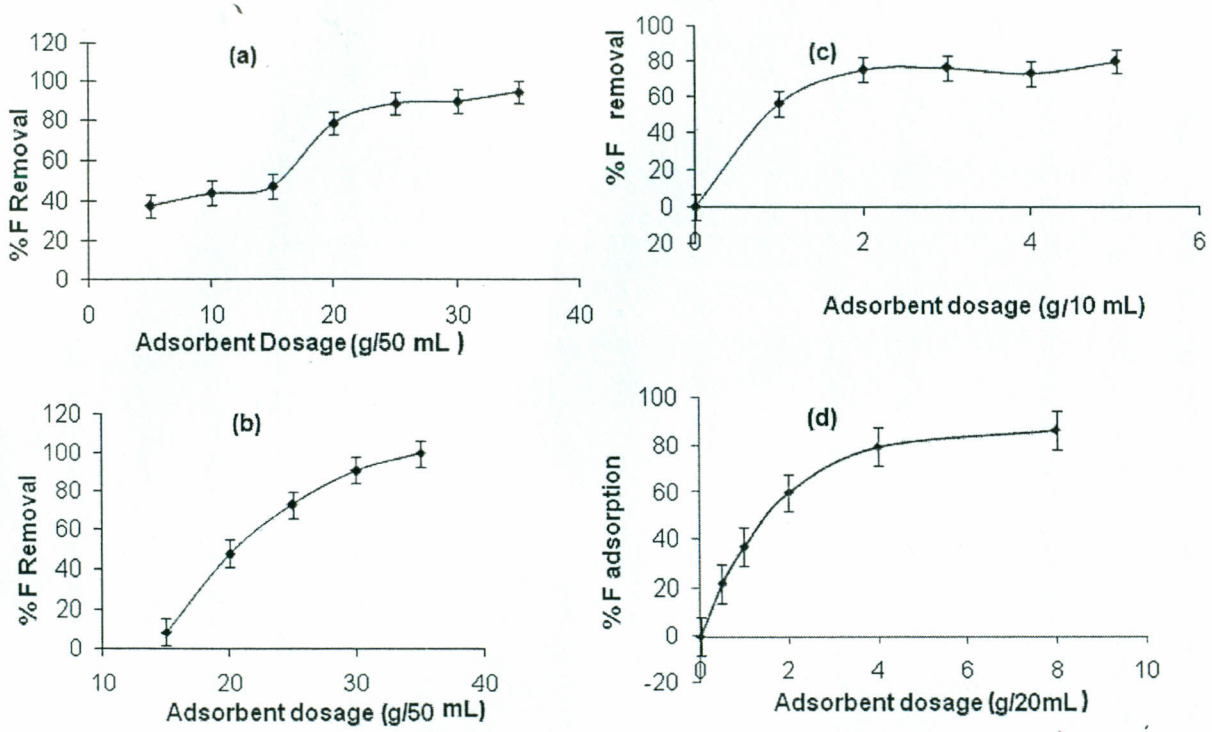

Figure 4.6: **Effect of change in adsorbent dosage on fluoride adsorption onto: (a) NSIM, (b) DIME, (c) FEPM and (d) FELS [Experimental conditions: 1000 mg/L fluoride concentration, 120-min contact time, and pH value of 3.32 at 293 K]**

It, however, became increasingly difficult for the incoming fluoride particles to find vacant sites in the adsorbent due to repulsive effects of adsorbed fluoride groups in the adsorbent surface. It indicates that HF molecules, which are the dominant adsorbate particles at low pH values of aqueous fluoride solutions (Stumm and Morgan, 1996), adsorbed at NSIM surfaces head-on with repulsive like-charges oriented into the solution and repulsing incoming HF particles from solution.

These redirecting effects of sorbed HF particles on the adsorbent surface stop when the free surface becomes excess and a sudden increase in percent fluoride adsorption is observed. Close to 100% removal of fluoride from solution was achieved using NSIM doses of 0.5 g/mL but higher doses were not feasible because the adsorption mixture became too thick to agitate effectively. Adsorbent doses of 0.5 g/mL were, therefore, adopted in all subsequent fluoride uptake tests using NSIM.

Figure 4.6 (b) shows, on the other hand, that fluoride adsorption onto DIME increased with increasing mass of adsorbent and 90% fluoride removal from solution could be achieved at 0.6 g/mL doses. This indicated that DIME particles dispersed in water and did not get aggregated as the amount of adsorbent in the batch system was increased. As in the case of NSIM, DIME doses greater than 0.6 g/mL were not feasible because the slurry became too thick to agitate. The DIME adsorbent dosage ratio of 0.5 g/mL, which was maintained in all the subsequent tests, was adequate for 80% fluoride adsorption from water under the conditions of these tests. This showed that DIME could be used as a low-cost media in water defluoridation as it has also been demonstrated elsewhere in the literature (Mohan and Pittman, 2007).

The effect of change in the mass of FEPM on its efficiency to sorb fluoride ions from water is illustrated in figure 4.6 (c). The percentage fluoride adsorption onto FEPM increased with increasing mass of FEPM up to 80% when the mass of adsorbent was increased to 2 g per 10 mL fluoride and remained constant thereon. This was consistent with results obtained by Sujana *et al.* (2009), who observed that fluoride removal from water increased with increase in sorbent mass. They ascribed it to the fact that a greater amount of sorbent implies a greater amount of available binding sites. Further increase in the mass of the adsorbent did not, however, produce equivalent increase in percent fluoride uptake by the material. It showed that FEPM particles aggregated at greater adsorbent doses diminishing the active surface sites available to incoming fluoride ions. As a result, the percentage fluoride removal approached a limiting value of about 80% when the adsorbent doses reached 2 g per 10 mL of adsorbate solution.

Like for FEPM, fluoride adsorption onto FELS increased with increasing adsorbent doses and remained constant at 80% when the adsorbent mass was increased to 2 g/10 mL of solution. At lower adsorbent dosage the number of available adsorbent sites increased with increasing mass of FELS. At certain critical values, however, increasing FELS dosage into the batch system increasingly diminished the available surface of the adsorbent. This suggested that the colloid particles of FELS got aggregated and lessened the number of sorbent sites available to adsorbing fluoride particles from solution. Such observations have also been reported by Asgari *et al.* (2012) while investigating fluoride adsorption onto functionalize pumice stone.

It can be assumed that at high adsorbent doses the protonated sites in the acid activated FEPM and FELS interlink through hydrogen bonds between the mineral colloids. These interlinking bonds result in coagulation and aggregation of colloid soil particles in the adsorption mixture, which reduce the capacity of the adsorbent to sorb more fluoride ions. Nonetheless, FELS had superior fluoride adsorption capacity to that of FEPM. The adsorbent could be used to adsorb fluoride from water.

4.8 Effect of change in solution temperature

The effect of adsorption temperature on the thermodynamic equilibrium of fluoride adsorption onto soil adsorbents arise from the influence of temperature on the adsorption energy balance of the system. Adsorption temperature also relate to the adsorption kinetics because of its influence on activation energies of reaction (Biswas *et al.* 2010). The effect of temperature on the adsorption of fluoride on LAGs was, therefore, investigated over temperatures of 298-333 K while maintaining the other adsorption parameters constant. The results of these tests are presented in figure 4.7 and figure 4.8.

Figure 4.7 (a) and (b) show that, while using adsorbate solutions containing 200 mg/L fluoride, the percent fluoride adsorption onto NSIM increased with increasing solution temperature from 98.5% to about 100% when solution temperature was increased from 293 K to 308 K. However, the fluoride adsorption efficiency of the material decreased to 97% when the temperatures were further increased to 323 K. Such trends were also observed while using initial fluoride adsorbate concentrations of 400 mg/L.

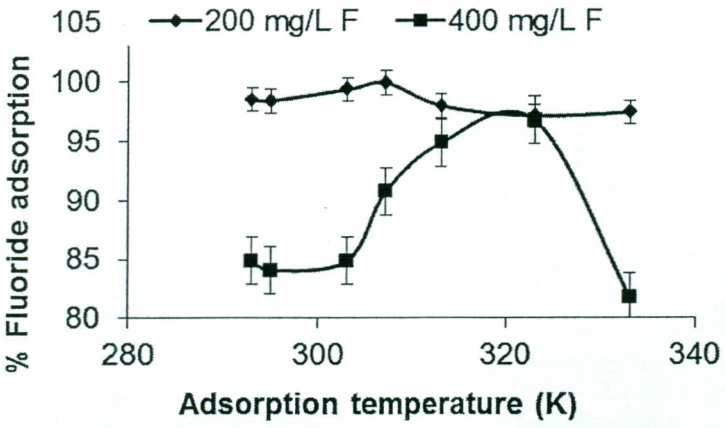

Figure 4.7: Effect of temperature on NSIM adsorption capacity of fluoride ions at pH 3.4 and adsorbent dosage of 0.5 g/mL

In the latter case, however, the peak fluoride adsorption, which was lower, as expected for higher adsorbate concentrations, occurred at higher temperatures of 313-323 K. It showed that at higher temperatures more adsorbate particles could to attain the requisite adsorption energies more easily resulting in higher percentage adsorptions than at lower temperatures.

Above a certain range of temperatures, however, excessive heat in the system decomposed the adsorption complexes at the adsorbent surface. At this point, further increase in temperature led to decrease in the capacity of the adsorbent to sorb the adsorbate particles as also reported by Ramdani and colleagues (2010) while studying removal of excess fluoride ions from Saharan brackish water using certain natural materials.

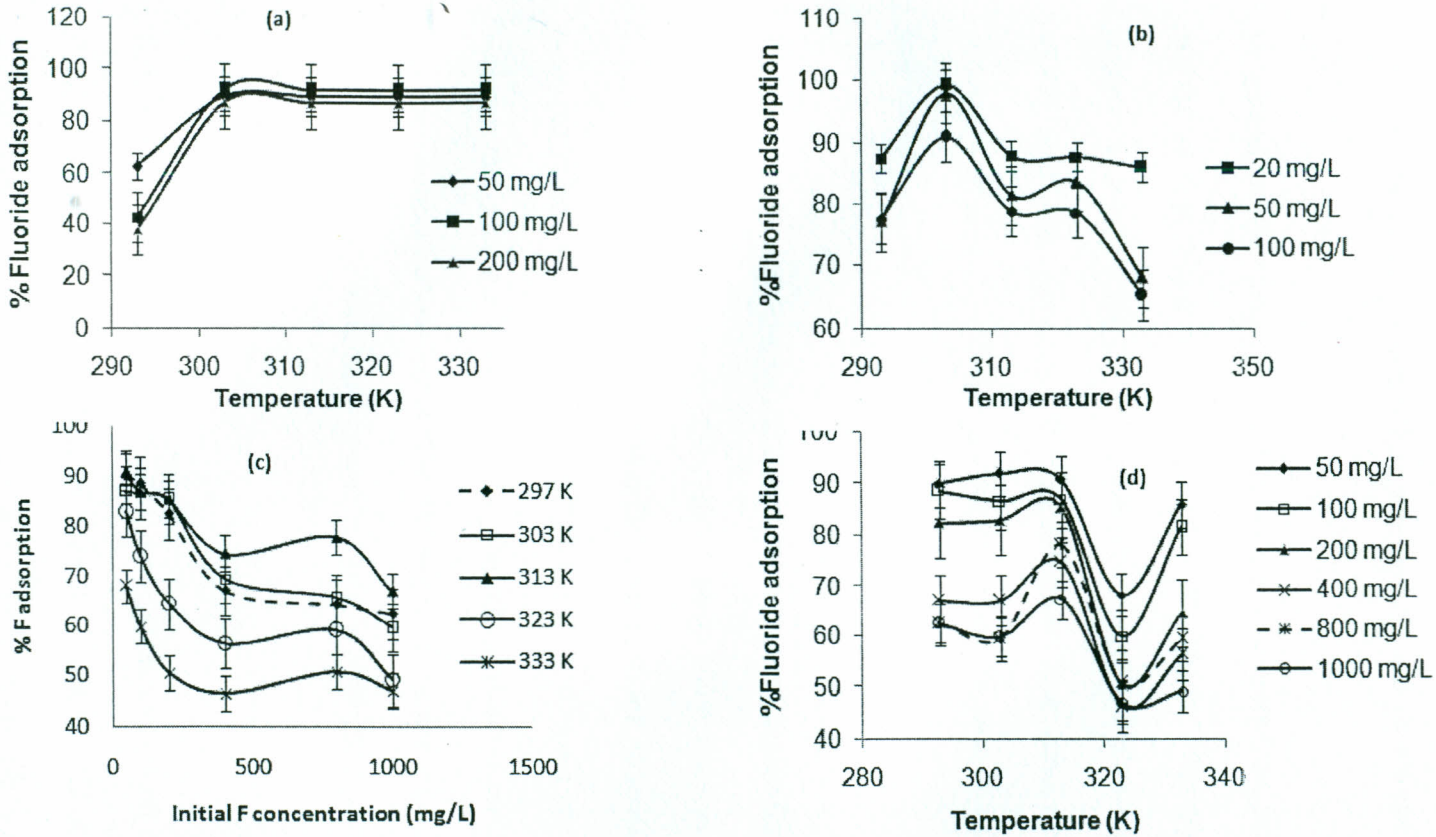

Figure 4.8: **Effect of change in temperature on fluoride adsorption onto (a) DIME, (b) FEPM and (c & d) FELS [Experimental conditions: pH 3.4; 0.5 g/mL adsorbent dosage and 1000 mg/L initial fluoride concentration]**

The eventual decline in percentage fluoride adsorption onto NSIM when the adsorption temperatures were increased above 323 K suggested that fluoride adsorption onto NSIM was a diffuse, non-specific and physisorption reaction.

In general, while using 200 mg/L adsorbate concentrations, most efficient fluoride adsorption onto NSIM occurred at 303 K but higher temperatures of 323 K were required to produce similar adsorption percentages at higher fluoride concentrations of 400 mg/L. All subsequent fluoride adsorption tests using NSIM were, therefore, conducted at 303 K, which was advantageous because it approximates ambient tropical temperatures.

The effect of solution temperature on fluoride immobilization into DIME is presented in figure 4.8 (a). The results show that close to 100% fluoride adsorption could be achieved at all initial adsorbate fluoride concentrations up to 400 mg/L. The results were the same over temperatures of 293-333 K. It was not possible to discriminate between the effects of temperature on fluoride adsorption onto DIME using initial adsorbate concentrations lower than 400 mg/L. Even at high fluoride concentrations of 1000 mg/L only marginal increase in fluoride adsorption between 323 and 333 K could be observed.

Unlike fluoride adsorption onto NSIM, however, there was no decline in percentage fluoride adsorption onto DIME at high temperatures. It showed that fluoride adsorption onto DIME was an endothermic chemical process, which resulted in more stable surface complexes than fluoride-NSIM complexes. Optimum fluoride

adsorption onto DIME occurred in the temperature range akin to the ambient tropical temperature of 298–313 K. This showed that DIME could be utilized to sorb fluoride at ordinary tropical temperatures, which is desired for easy defluoridation of water in Kenya.

The temperature-dependence of fluoride adsorption onto FEPM was then studied at fluoride adsorbate concentrations of 20 to 100 mg/L over a range of temperatures from 293-303 K and the results represented in figure 4.8 (b). The percentage fluoride adsorption onto FEPM increased with increasing temperature to complete fluoride removal from solution at 303 K and declined thereon. The reaction was, however, reversible at low temperatures, which showed that most of the adsorbate particles could not attain necessary activation to sorb at the active sites in FEPM at such temperatures. It also showed, as in the case of fluoride adsorption by DIME, that fluoride uptake by FEPM was a chemical phenomenon. The eventual decline in percentage fluoride adsorption at temperature greater than 303 K showed that the escaping tendency of the fluoride particles from FEPM surface increased with increasing temperature. The current results, therefore, showed that fluoride adsorption onto ferric geomaterials is typically an exothermic process as also postulated elsewhere in the literature (Sujana *et al.*, 2009).

Figure 4.8 (c) and (d) showed that fluoride adsorption onto FELS increased from 70 to 75% when the adsorption temperature was increased from 297 to 313 K. It then decreased to 50% when the solution temperature was further increases to 333 K. This could be ascribed to increase in the energy of the adsorbate particles with increasing

temperature. It meant that at higher temperatures more adsorbate particles were able to attain requisite activation energy to adsorb at FELS surface per unit time than at lower temperatures. As in the fluoride adsorption onto FEPM, however, above a certain critical temperature the percentage fluoride adsorption declined as a result of thermo-degradation of sorptive sites in the adsorbent as also observed in the literature (Bhaumik *et al.*, 2012). The highest fluoride adsorption onto FELS was recorded at a temperature of 313 K, which was then maintained in the subsequent fluoride adsorption experiments using this adsorbent.

4.9 Effect of competing inorganic anions

Natural water systems contain other anions that could interact and compete with fluoride for sites on soil mineral surfaces. Such co-ions impact on the hydrogeochemistry of fluoride and affect fluoride immobilization onto soil aggregates (Tang *et al.*, 2009; Chen *et al.*, 2010a). The effect of Cl^-, NO_3^-, SO_4^{2-} and $H_2PO_4^-$ ions on fluoride adsorption onto LAGs was, therefore, studied and the results depicted in figure 4.9.

The removal of fluoride from solution by adsorption using NSIM decreased in presence of the anions in the order: $Cl^- > NO_3^- > SO_4^{2-} > H_2PO_4^-$. The order of the effect of individual ions was consistent with increasing steric effects of the anions. Smaller anions with less steric effects reduced fluoride adsorption onto NSIM more strongly than the larger and more sterically hindered anions. This showed that the smaller ions penetrated the adsorbate solution bulk more easily and sorbed at the adsorbent structure more strongly than the large anions.

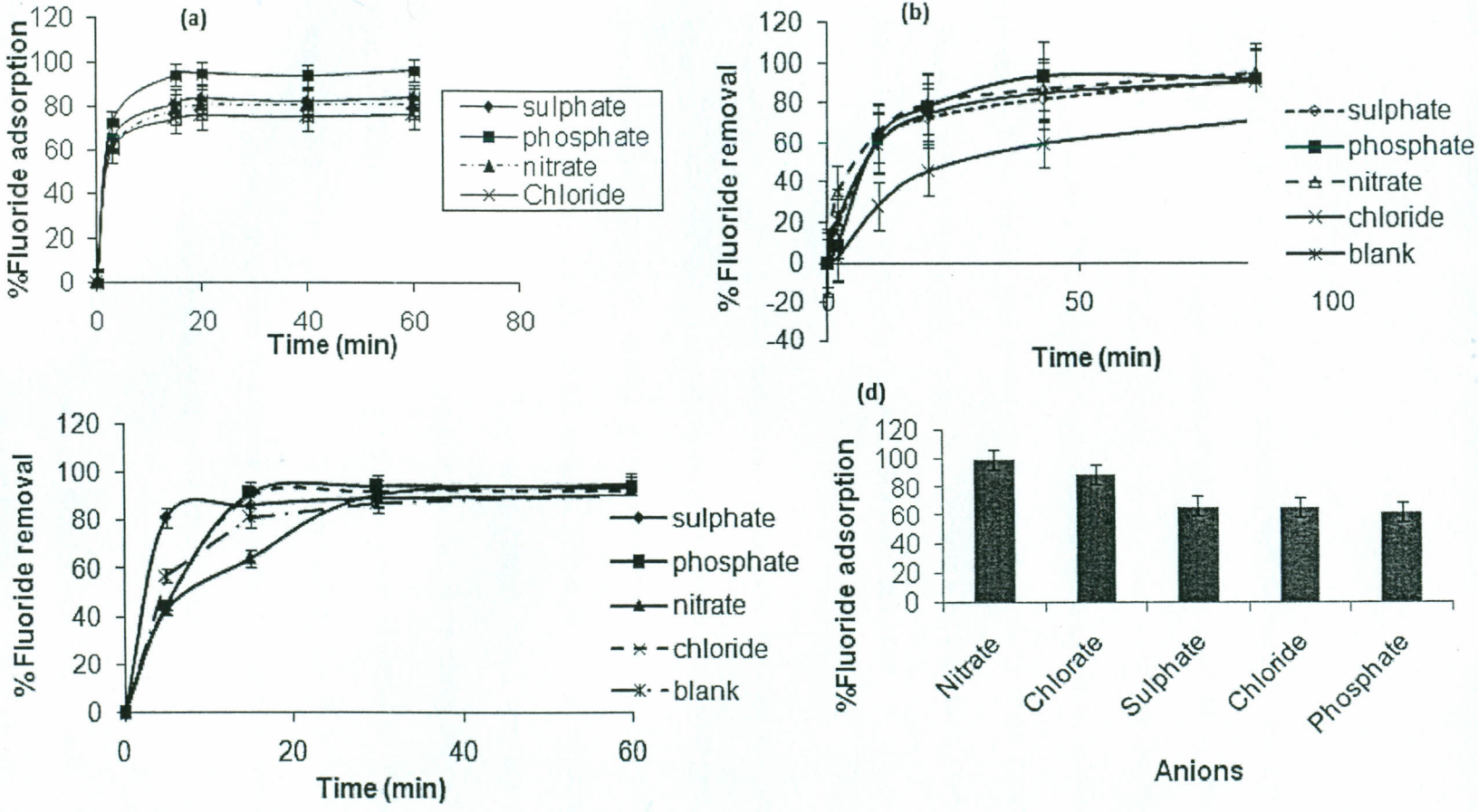

Figure 4.9: **Effect of selected co-ions on the adsorption of fluoride onto: (a)NSIM, (b) DIME, (c) FEPM, (d) FELS [Experimental conditions:1000 mg/L initial fluoride concentration; 303 K; pH 3.4 and adsorbent dosage of 0.5 g/mL]**

The small anions could, therefore, compete with fluoride for reactive sites in NSIM more effectively than larger anions. This differential impact of anions on fluoride uptake by NSIM could also be linked to the degree of the shared charge in the polyatomic anions. The sulphate with a more electronegative sulphur centre draws electrons from the oxygen atoms more strongly making them poorer Lewis acids (electron donors) than in the nitrate. The sulphate was, therefore, a weaker competitor for positive centres in the adsorbent surface than the nitrate.

As expected, however, the dihydrogen phosphate ion did not suppress fluoride adsorption onto NSIM because the hydrogen atoms in the dihydrogen phosphate ions lessen the overall negative charge of the anion and reduce its potential to sorb at the positive centres in acidified NSIM surfaces. Nonetheless, the current results appeared to contradict earlier findings by Tang et al. (2009). While studying effect of co-ions on fluoride uptake by granular ferric hydroxide, the authors showed that at solution pH of 6.7 fluoride adsorption onto GFH decreased in presence of the co-ions in the order: $H_2PO_4^- > HCO_3^- > SO_4^{2-} > Cl^-$. They indicate that both PO_4^{3-} and Cl^- adsorb onto soil mineral adsorbents by forming outer-sphere surface complexes but the SO_4^{2-} ions forms both outer- and inner-sphere surface complexes.

As indicated in figure 2.4, dominant fluoride speciation under the experimental conditions of the cited work and those in the current work were at variance. Thus, the nature of interactions between fluoride and the adsorbent surfaces, hence, the mode and the degree of adsorption in the refferred work and the current work were expected to be at odds with each other as well.

Figure 4.9 (b) showed that anions investigated, except the Cl^-, did not affect fluoride adsorption onto DIME. The adsorption of fluoride ions onto DIME increased in presence of the phosphate ions. Selective adsorption of fluoride onto DIME surfaces in presence of the anions indicated that fluoride sorbed at reactive sites in DIME that were inert (or inaccessible) to the other anions. Due to close similarity in physicochemical properties of fluoride and chloride ions the latter ion significantly interfered in fluoride adsorption onto DIME. On the whole, however, the current results demonstrated that fluoride ions could be removed from solution by adsorption using DIME as also reported by other authors for similar adsorbents in the literature (Zhu *et al.*, 2007).

It can be seen from figure 4.9 (c) that percentage fluoride adsorption onto FEPM increased in presence of potassium salts of the co-ions. The magnitude of fluoride removal in presence of the anions decreased in the order: $NO_3^- > PO_4^{3-} > Cl^- > SO_4^{2-}$. The anions did not, therefore, strongly interfere with fluoride adsorption onto FEPM. It was revealed that high levels of fluoride ions could be removed from solution using this adsorbent even at high concentrations of the co-ions.

As for the fluoride adsorption onto FEPM, figure 4.9 (d) shows that, fluoride adsorption onto FELS also increased in the presence of NO_3^- and ClO_4^- but it decreased in presence of SO_4^{2-}, Cl^- and PO_4^{3-}. Trends such as revealed here have been reported in the literature by several other researchers. Chen *et al.* (2010a), for instance, observed increased fluoride adsorption onto a ceramic adsorbent in the presence of Cl^- and NO_3^-. The authors showed that the fluoride adsorption onto the

material was, however, strongly suppressed in the presence of the SO_4^{2-}, CO_3^{2-} and PO_4^{3-} ions. They postulated that increased fluoride uptake in presence of certain co-ions could be attributed to the effect of the anions on the ionic strength of the adsorbate solution and to surface disruption of fluoride-fluoride repulsive interactions on the adsorbent surface.

In summary, therefore, the presence of other anions decreased fluoride adsorption onto NSIM. The fluoride uptake by DIME was, however, not affected by the presence of most of the co-ions but certain anions could enhance fluoride uptake by both FEPM and FELS. The nature and extent of the effect of the anions on fluoride adsorption onto LAGs varied with adsorbent type. Both the SO_4^{2-} and Cl^- ions, generally, lowered fluoride uptake by the LAGs. The NO_3^- was the least interfering whereas the PO_4^{3-} was, generally, the strongest interferent in fluoride uptake by LAGs.

Differences in the fluoride adsorption characteristics of LAGs in presence of competing anions could be attributed in part to differences in the properties of the adsorbents such as variation in mineralogy, chemistry and surface properties of the materials. However, the solution matrices may also amplify or diminish certain properties of the anions like ionic mobility through solution and the EDL close to the adsorbent surface as well as their affinities for adsorbent sites and the degree of coulombic repulsions, which impact on the adsorption process.

4.10 Effect of adsorbate concentration

The adsorbate concentration is the primary driving force that controls the partition of solutes between the solution and the sorbed phases. Adsorption equilibrium tests are, for this reason, useful in elucidating the adsorption mechanism and they provide invaluable insight into the adsorbate behaviour and the surface chemistry of the adsorbents (Giles *et al.*, 1960). The degree of adsorbent surface coverage by adsorbate ions can be described in terms of adsorption isotherms. The plots of adsorbent surface coverage by adsorbate ions, q_e, versus the equilibrium solute concentration, C_e, can be used to predict and compare performances of adsorbents (Vijayaraghavan *et al.*, 2006).

The effect of change in fluoride concentration on its removal from water using the LAGs was studied under conditions of constant temperature (303 K), solution pH (3.4), adsorbent dosage (0.5 mg/mL) and contact time (120 min) and the results presented in figures 4.10 and 4.11. From figure 4.10(a), the results show that complete removal of fluoride from solution using NSIM could be achieved at all initial fluoride concentrations up to 200 mg/L. The percentage adsorption of fluoride onto NSIM then decreased and remained constant at about 86% when the adsorbate concentration was further increased to 400 mg/L. It showed that saturation of adsorbent sites in NSIM did not occur under the conditions of the current tests and that increasingly more fluoride was sorbed onto NSIM with increasing initial adsorbate concentration. It can be assumed that when NSIM is contacted with fluoride-containing water, the fluoride ions initially sorb on exposed surface sites in the adsorbent.

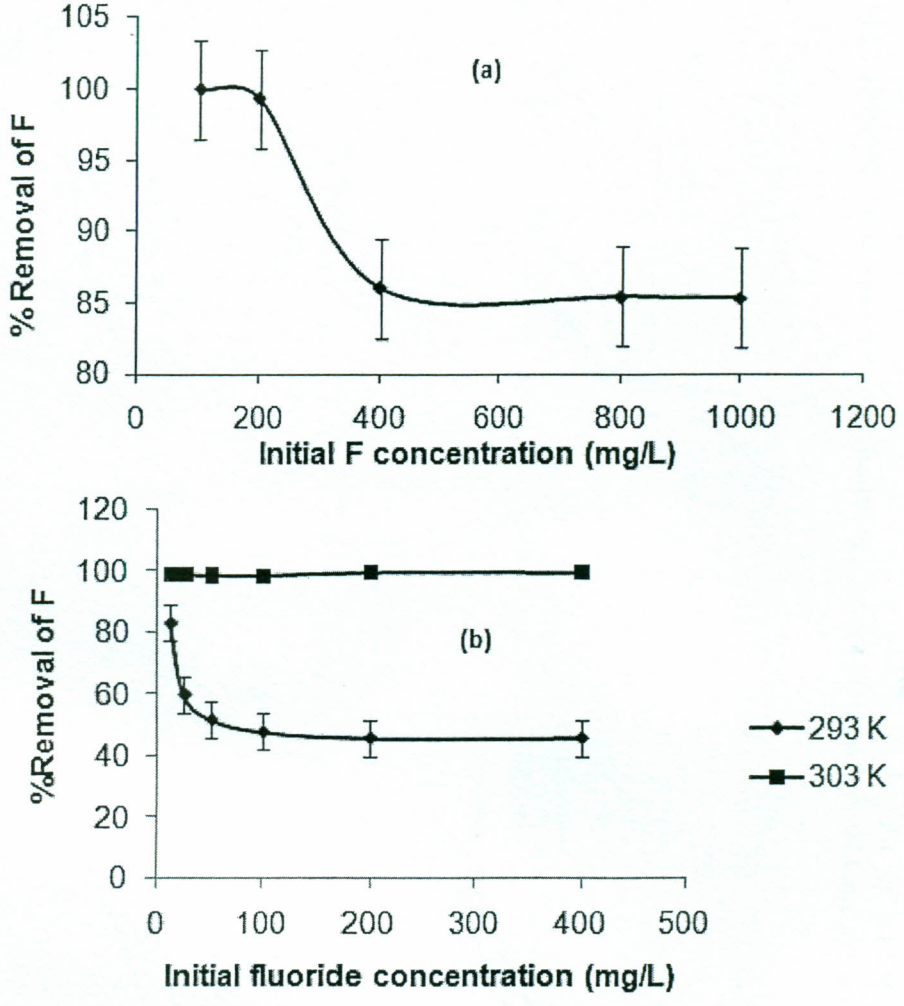

Figure 4.10: Effect of change in initial adsorbate concentration on fluoride adsorption onto (a) NSIM, (b) DIME.

However, as the monolayer adsorbent surface sites get exhausted more fluoride particles penetrate and sorb onto inner core sites in clay structure of NSIM.

The constant increase in the amount of fluoride adsorption with increasing adsorbate concentration showed that the inner sorptive sites in NSIM were relatively inaccessible to competing species from the solution.

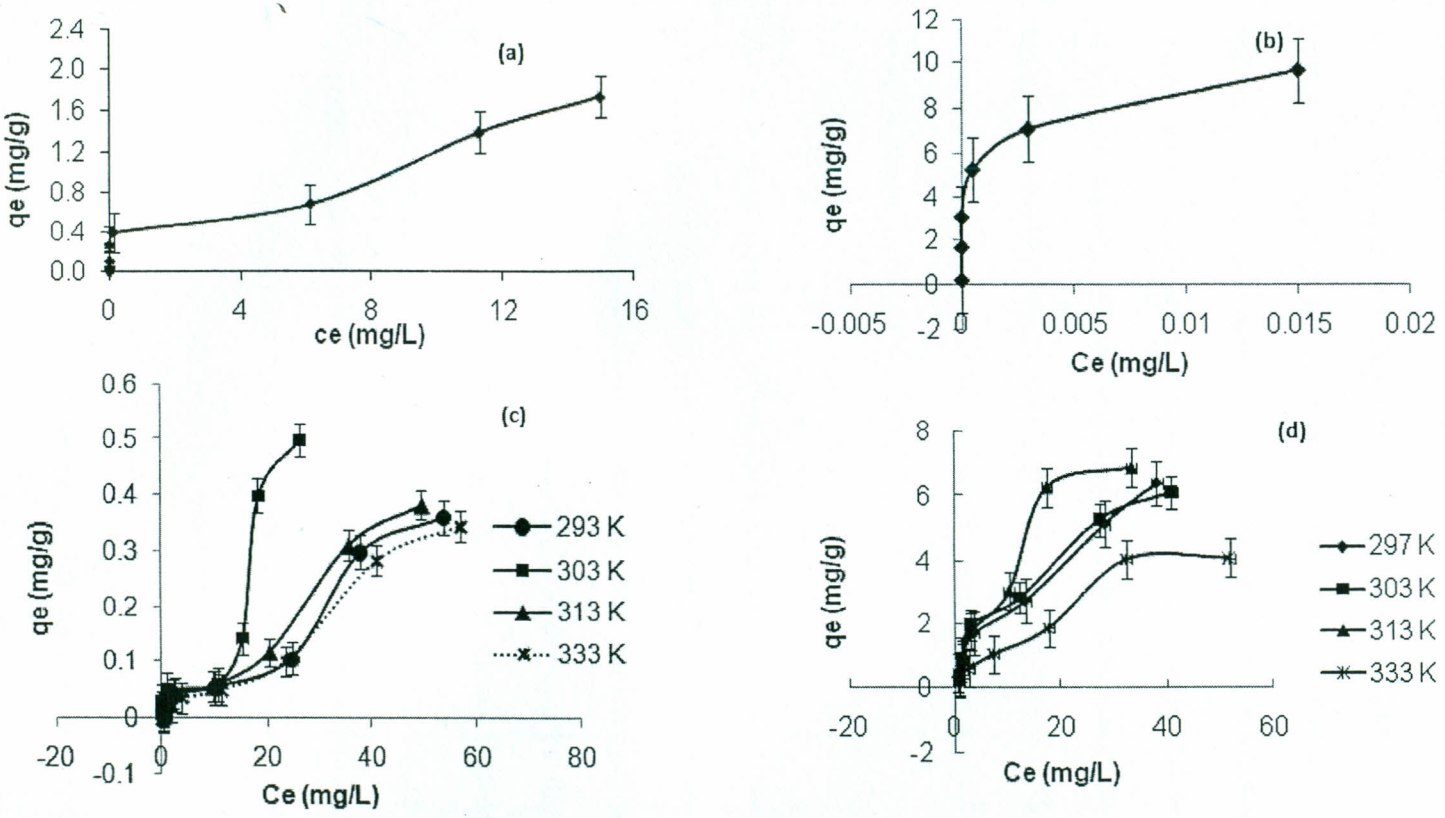

Figure 4.11: General adsorption isotherms for the removal of fluoride ions from aqueous solution using (a) NSIM, (b) DIME, (c) FEPM and (d) FELS at 303 K and pH 3.4.

The degree and extent of intraparticle diffusion of fluoride into NSIM structure was, therefore, concentration-dependent. This led to constant partition of the adsorbate between the aqueous and the sorbed phases of fluoride at concentrations greater than 400 mg/L. Giles and co-workers (1960) indicated that constant adsorbate partition results when the adsorbate ions sorb onto the adsorbent surfaces in successive layers so that the initially adsorbed particles form secondary sites on the adsorbent surface upon which subsequent adsorption occurs. The adsorption isotherm depicted in figure 4.11(a) for fluoride uptake by NSIM, was as expected, an high-affinity type-three or an H3 isotherm (Giles *et al.*, 1960).

The initial vertical portion of the curve confirmed that at concentrations less than 200 mg/L, all fluoride is removed from solution. The later linear portion of the curve corresponds to the penetration of the adsorbate particles into inner core sites in the structure of the clay or to the multilayer adsorption of fluoride on high-affinity heterogeneous adsorbent surfaces in NSIM. It shows that ion-exchange reactions involving substitution of low-affinity ions in NSIM surface dominated fluoride adsorption onto NSIM at low adsorbate concentrations (Attahiru *et al.*, 2012). However, physisorption reactions were more significant in the later stages of immobilization of the anion onto the adsorbent surface.

The effect of adsorbate concentration on fluoride adsorption onto DIME was temperature–dependent. As illustrated figure 4.10 (b), complete fluoride removal from solution using DIME could be achieved at all fluoride concentration up to 400 mg/L when the experiments were conducted at 303 K. At lower temperatures of 298 K, only about 84% fluoride adsorption was achieved and complete fluoride removal could not

be achieved using this adsorbent even at very low fluoride concentrations. The percentage fluoride adsorption declined to just about 40% when the fluoride concentration was increased to 50 mg/L. All subsequent fluoride adsorption tests using DIME was, for this reason, conducted at optimized temperature of 303 K.

A plot of the amount of fluoride adsorbed onto DIME, q_e (mg/g), versus the equilibrium concentration, C_e (mg/L) is illustrated in figure 4.11 (b). It was revealed that immobilization of fluoride into DIME surfaces increased with increasing initial fluoride concentration to a limiting value. The resulting isotherm was a Langmuir type-two (L2) isotherm based on Gile's classifications of adsorption isotherms (Giles *et al.*, 1960). This was consistent with earlier postulates in section 4.5 that fluoride adsorption onto DIME was a chemical process based on ion-exchange mechanisms involving lower-affinity sites in DIME surfaces. The initial fluoride concentration and the free adsorbent surfaces controlled fluoride adsorption onto DIME. Findings such as have been reported in the current work have also been published by other authors in the literature. Zhang *et al.* (2009), for example, while studying the removal of fluoride ions from aqueous solution using modified attapulgite adsorbent, showed that fluoride adsorption was accompanied by changes in hydroxyl ion concentration indicating that anion exchange reactions controlled the adsorption process.

The adsorption isotherm for fluoride adsorption onto FEPM is illustrated in figure 4.11 (c). The fluoride adsorption isotherm for FEPM was, therefore, a Langmuir type four or an L4 isotherm plot (Giles *et al.*, 1960). The stepwise shape of the curve indicates that FEPM consisted of heterogeneous surfaces, which filled up with adsorbate fluoride particles in succession. The initial curvature of the isotherm

indicated that as more sites in FEPM were filled-up, the sorptive surfaces in FEPM approached saturation at some point. It indicated that fluoride adsorption onto FEPM was more specific compared to the fluoride adsorption onto both NSIM and DIME. The conformation of the adsorption process to L4 isotherm showed that the adsorbate particles did not experience significant competition for the adsorbent surfaces from other species in solution. Additionally, it showed that once adsorbed the adsorbate particles did not interact with each other at the adsorbent surface.

As for fluoride adsorption onto FEPM, figure 4.11 (d) shows that the adsorption isotherm for fluoride uptake by FELS was also an L4 type isotherm with two adsorption plateaus. This indicated heterogeneity in sorptive surfaces of FELS. The shape of the curve shows that upon saturation of exposed surface sites in FELS, the fluoride uptake by the mineral increased with increasing aqueous fluoride concentration as fluoride particles migrated into the inner sites in the mesoporous structure of the adsorbent. The second plateau, associated with the filling-up of the inner sorptive sites, was clearer at higher temperatures indicating a relaxation-type endothermic and diffusion-controlled process. In line with Gile's postulates, the increase in fluoride adsorption stopped when the inner sites in the structure of FELS got used up (Giles *et al.*, 1960).

It could be concluded that surface reactions of fluoride with adsorptive surfaces in NSIM were diffuse and multi-layer, which led to continuous constant partition of fluoride between the solution and the adsorbed phases at high fluoride concentration. The mechanism of fluoride reactions with DIME surfaces were temperature-controlled with diffuse surface reactions taking place at lower temperatures and more

specific chemical reactions being favoured by higher temperatures. Both FEPM and FELS depicted heterogeneous surfaces sustaining fluoride adsorption that was characterized by initial rapid chemisorption onto exposed high affinity sites in the adsorbents followed in the later stages by temperature-controlled diffusion of fluoride into less exposed sites in the mesoporous structure of the adsorbents.

4.11 Adsorption isotherms

The Langmuir isotherm, and the Freundlich isotherm are commonly used to describe the adsorption equilibrium of the uptake of inorganic solutes onto clay minerals in aqueous systems (Babarinde *et al.*, 2006; Gueu *et al.*, 2007; Hamdi and Srasra, 2009). The respective linear plots of Langmuir and Freundlich isotherms for fluoride adsorption onto the LAGs were constructed from the relevant equilibrium data and presented in figure 4.12 and in figure 4.13, respectively. The resulting equilibrium constants were then computed and presented in table 4.4. figure 4.12 (a) and (b) show that the data for fluoride adsorption onto NSIM could simultaneously be fitted by both the Langmuir and the Freundlich isotherms, respectively. The equilibrium data for fluoride adsorption onto NSIM was fitted by both the Langmuir and Freundlich isotherms with R^2 values of 0.9991 and 0.9934, respectively. The values of the Freundlich affinity coefficient, K_f (0.0807) and intensity parameter, n (1.062), as well as those of the Langmuir constants, q_m (12.25 mg/g) and b (0.00637 L/mg), indicated efficient fluoride binding onto NSIM surfaces.

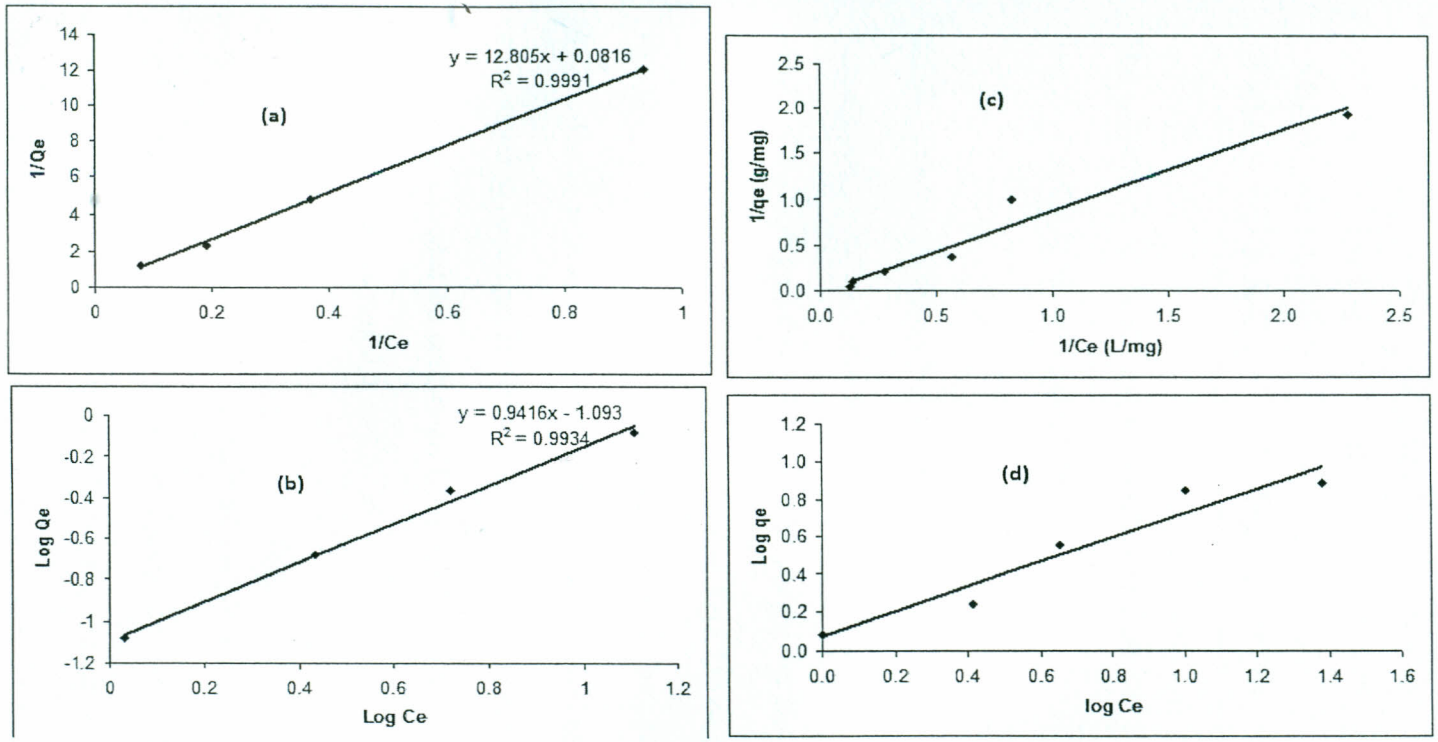

Figure 4.12 **Langmuir isotherm plots and Freundlich Isotherm plots for the adsorption of fluoride onto NSIM, (a) and (b); and onto DIME, (c) and (d), respectively**

Table 4.4 Langmuir and Freundlich isotherm constants for the adsorption of fluoride onto LAGs

Adsorbent &Source	Langmuir		Freundlich	
	pH, Temp (K)	q_m (mg/g)	b (L/mg)	K_f	n
NSIM	3.4, 303	12.25	0.00637	0.0807	1.062
DIME	3.4, 303	51.81	0.0223	1.185	0.6524
FEPM	3.4, 303	12.7	1.38	4.73	0.37
FELS	3.4, 303	10.4792	0.0524	0.6322	1.6526

The value of r_L for fluoride adsorption onto NSIM was 0.006 showing that the system was favourable for fluoride adsorption.

As illustrated in figure 4.12 (c) and (d), fluoride adsorption onto DIME could also be described by both the Langmuir and the Freundlich isotherms. The corresponding R^2 values were 0.97 and 0.93, respectively. As for the fluoride adsorption onto NSIM, values of the Freundlich affinity coefficient K_f (1.185 mg/g) and intensity parameter n (0.6524) were consistent with effective binding of fluoride particles by DIME.
The value of n was, however, less than unity indicating that the adsorption was not monolayer in coverage. It showed that the mineral surface did not have homogeneous surfaces as can also be confirmed from XRD and AAS mineralogical data presented in table 4.3 under section 4.2.

The equilibrium analysis of fluoride adsorption onto FEPM using the Langmuir and the Freundlich isotherms is shown in figure 13 (a) and (b), respectively. The data fit for both Langmuir and Freundlich isotherms had linear plots with R^2 values greater than 0.92. Again, as for fluoride adsorption onto DIME, the data fit for the Langmuir model was better than for the Freundlich model.

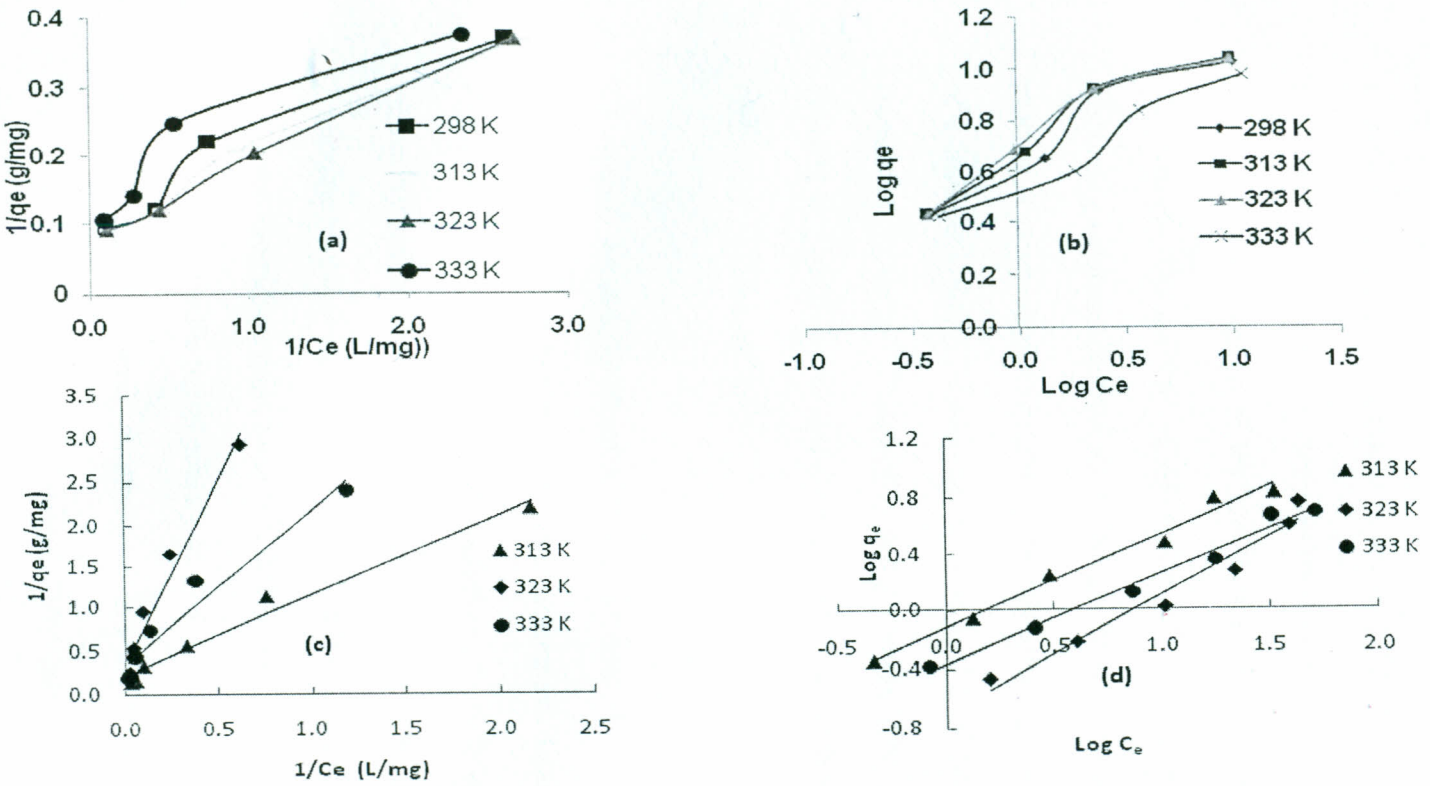

Figure 4.13: Langmuir plots (a & c) and Freundlich Isotherm plots (b &d) for the adsorption of fluoride onto FEPM and onto FELS, respectively

The simultaneous correlation of the adsorption data to Langmuir and Freundlich models indicated that fluoride sorption onto FEPM was based on mixed adsorption mechanisms involving surface chemisorption of adsorbate fluoride particles and absorptive physisorption of the ions in the mesoporous structure of the adsorbent. Nonetheless, the number of adsorptive sites in FEPM appeared to increase with increasing solution temperature showing that chemisorption was the more dominant process. The monolayer capacity of the adsorbent, q_m, averaged 10.8 mg/g and values of b indicated higher affinity for fluoride by FEPM sites at temperatures of 323 K compared to those at the other temperatures. The Langmuir constant, b, and Freundlich constants, K_f and n, were consistent with effective binding of fluoride particles by FEPM surfaces.

To validate the data for fluoride adsorption onto FELS, the Langmuir and Freundlich isotherms were applied to the fluoride adsorption data and the results presented in figure 4.13 (c) and (d). The data correlated to both the Langmuir and Freundlich isotherms and the respective correlation coefficients, R^2, averaged 0.9514 for the Langmuir isotherm and 0.9658 for the Freundlich isotherm. This showed that the data fit for the Freundlich model was better. The high correlation coefficients in both cases were consistent with heterogeneity in FELS surfaces as also revealed by XRD and AAS compositional analyses presented in table 4.3 in section 4.2. The trends in R^2 values showed that more Freundlich surfaces became available at higher fluoride concentrations and at elevated temperatures.

In general, therefore, fluoride adsorption onto FELS followed mixed adsorption mechanism. However, physisorption by intra-particle diffusion of fluoride into

mesoporous sites of FELS became increasingly significant at higher concentrations and at higher temperatures whereas exchange reactions with surface OH^- dominated at lower surface coverage in alkaline media. These findings were also consistent with thermodynamic analysis presented in section 4.14 in which indicated the corresponding values of both ΔG^0 and ΔH^0 suggested a spontaneous endothermic physisorption processes for fluoride uptake by FELS. However, the q_m values computed from the Langmuir isotherm compared well with obtained experimental values indicating that the fluoride uptake by FELS could also be described by Langmuir isotherm.

4.12 Comparison with other low-cost adsorbents

The equilibrium adsorption constants of LAGs based on the Langmuir and Freundlich adsorption isotherms were compared with those of the other low-cost adsorbents that have recently been reported in the literature. Except for modified hematite, 116.75, (Teutli-Sequeira *et al.*, 2011); certain palygorskitic clay, 93.45, (Hamdi and Srasra, 2009); smectic clay, 84.03, (Hamdi and Srasra, 2009); Chitin/cellulose composite, 83.75, Glutaraldehyde cross-linked calcium alginate, 75.5, (Vijaya *et al.*, 2011); and certain illito-kaolinitic clay, 69.44, (Hamdi and Srasra, 2009), DIME, which had the highest fluoride uptake capacity among the LAGs, also had higher fluoride adsorption capacity (51.81 mg/g) than most of the other low-cost adsorbents reported in literature.

It was observed that both activated silica and ion-exchange resins had fluoride adsorption capacities well above that of NSIM. However, besides bone char and certain carbonaceous adsorbents the fluoride adsorption capacity of NSIM was greater

than those of most the biosorbents, carbonaceous adsorbents and aluminium-based adsorbents that have recently been considered for fluoride removal and reported in the literature.

Similarly, it was found that even though modified hematite, tourmaline, palygorskite, smectic clay, illito-kaolinites, and kaolinite-ferrihydrite associates had higher fluoride sorption capacities than those of NSIM (12.25 mg/g), FEPM (12.7 mg/g) and FELS (10.48 mg/g), the fluoride adsorption capacities of the LAGs was higher than mean adsorption capacities of lignite, 6.9 mg/g (Pekař, 2008); hydroxyapatite, 4.54 mg/g (Fan *et al.*, 2003); Boehmite, 2.057 mg/g (Jiménez-Becerril *et al.*, 2011); fluorspar, 1.79 mg/g (Fan *et al.*, 2003); Chinese red soil, 0.8545 mg/g (Zhu *et al.*, 2007); calcite,0.39 mg/g (Fan *et al.*, 2003) pumice, 0.97 mg/g (Malakootian *et al.*, 2011); quartz, 0.19 mg/g (Fan *et al.*, 2003); activated kaolinite, 0.045 (Gogoi and Baruah, 2008); montmorillonites, 1.5–1.9 mg/g (Alagumuthu, 2005); certain activated carbons, 4.6 mg/g (Alagumuthu *et al.*, 2010); and some activated alumina, 7.7 mg/g (Wu *et al.*, 2010).

In summary, the fluoride adsorption data for LAGs compared well with those of other inexpensive fluoride adsorbents reported in the literature. Differences in fluoride adsorption properties of adsorbents arise from differences in the chemical, structural and surface properties of adsorbents. The adsorption parameters including: concentration, pH, temperature, ionic strength, counter ions, co-ions, rate of agitation, speciation and time of contact employed may also affect the performance of an adsorbent towards particular adsorbate ions (Weng *et al.*, 2007). The remarkable fluoride adsorption characteristics depicted by the LAGs in this work show that the

minerals adsorbents could be used as alternate media in the removal of fluoride from high-fluoride water. Furthermore, they can be obtained cheaply and abundantly from their natural resources for easy and safe use.

4.13 Adsorption Kinetics

Fluoride adsorption onto soil surfaces consist of the transfer of adsorbate fluoride particles from the bulk adsorbate solution to the surface of the adsorbent. The adsorbate particles then interact with reactive sites in the adsorbent surface or penetrate into the inner adsorbent sites in the crystalline lattice of the soil adsorbents. Lagergren's pseudo-first order rate law (equation 2.22) was applied to test the influence of external diffusions on fluoride adsorption onto LAGs. In addition, so as to investigate the nature of interactions between fluoride particles and the soil surface sites, Ho's pseudo-second order equation (equation 2.24) was then applied to the adsorption data. Nonetheless, besides adsorption onto the outer surface sites in the adsorbents, the adsorbent ions from solution may get transported by diffusion into the inner core pores of the adsorbents. In order to assess existence of intraparticle diffusion of fluoride into inner pores of the LAGs, the amount of fluoride sorbed per unit mass of adsorbents (q_t) at time, t, was plotted as a function of square root of time, $t^{0.5}$, in accordance with the Weber-Moris kinetics depicted in equation 2.28. The respective linear plots for the three rate laws were constructed and the derived kinetics constants presented in table 4.5.

The time-dependence of fluoride removal from water using NSIM is depicted in figure 4.14. Fluoride adsorption onto NSIM was rapid and the adsorption equilibrium could be established in just about 20 min as depicted in figure 4.14 (a). The maximum

percentage fluoride removal was about 80%. Figure 4.14 (b and c), on the other hand, indicate that the adsorption process could be correlated to both the pseudo-first order kinetics (R^2 = 0.9882) and to the pseudo-second order kinetics (R^2 = 0.999). The data fit to the latter model was, however, better. It showed that the rate of fluoride adsorption onto NSIM was controlled more strongly by surface reactions between NSIM sites and adsorbate fluoride particles than by external transfer processes. The values of second order rate constant, $k_{2,ad}$, (5.9416 g/mg min^{-1}), equilibrium adsorption capacity, q_e, (1.6722 mg/g) and the initial rate of adsorption, h_o, (9.4340 g/mg min^{-1}), were such as reported in the literature for similar systems (Bouguerra *et al.*, 2007; Sulaiman *et al.*, 2009; Onyango *et al.*, 2010).

Figure 4.14 (d) shows clearly that the intra-particle diffusion equation did not fit the NSIM fluoride adsorption data (R = 0.597). It showed that intraparticle diffusion did not play a significant role in fluoride adsorption onto NSIM. The graph was curved in the initial portions depicting film diffusion effects. This showed that film diffusion and surface reactions could have controlled the rate of fluoride adsorption onto NSIM.

The corresponding kinetic plots and the respective kinetic constants for fluoride adsorption onto DIME are shown in figure 4.15 and in table 4.5, respectively. As shown in figure 4.15 (a), fluoride adsorption onto DIME was rapid and more than 40% fluoride adsorption occurred within the first minute of reaction. The process then assumed a gradual approach to the equilibrium at about 90 min. Like for NSIM, fluoride adsorption onto DIME could be fitted by both the pseudo-first order and pseudo-second order kinetics models with R^2 values of 0.996 and 0.997, respectively.

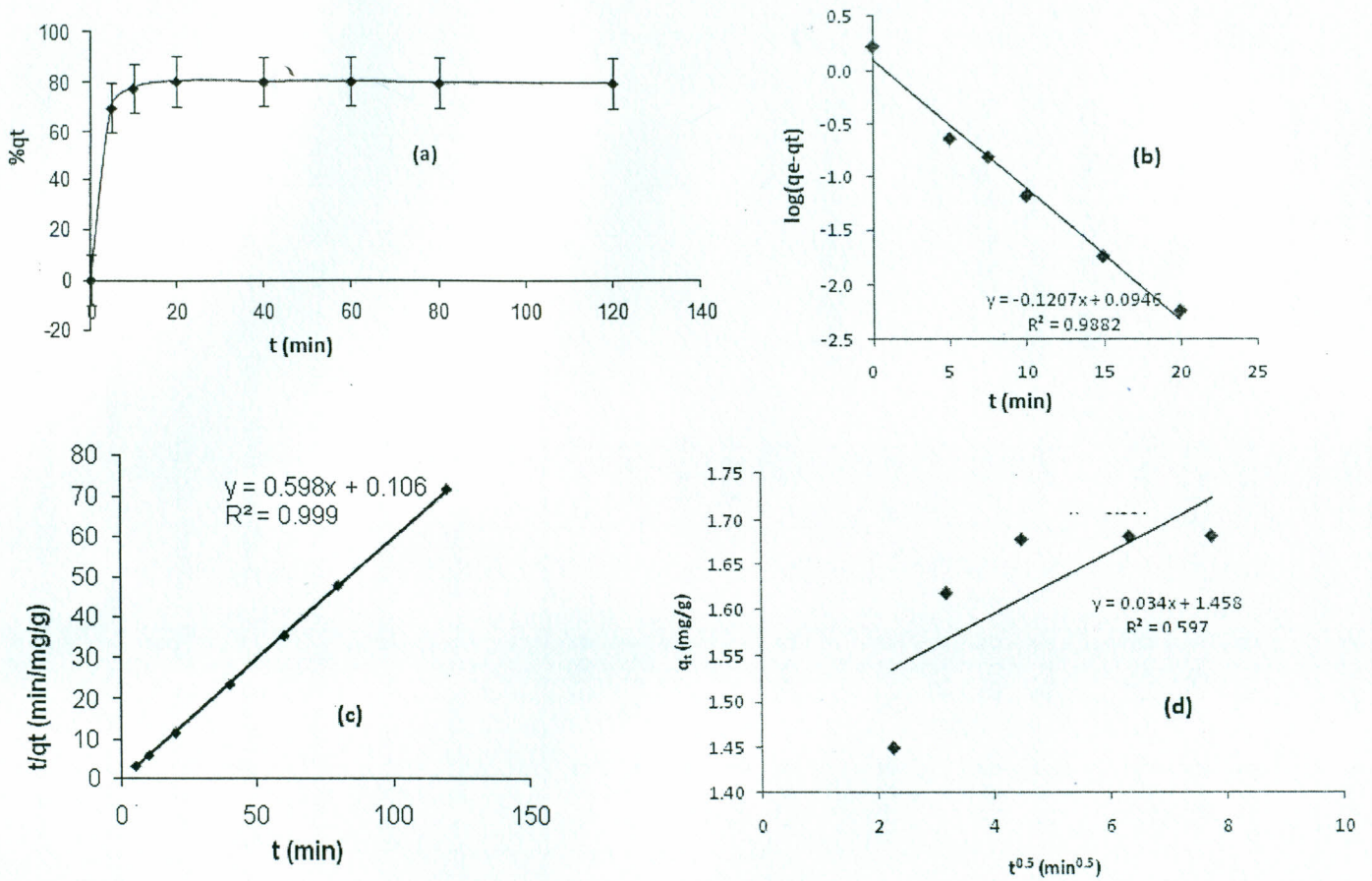

Figure 4.14: **Time profile for fluoride adsorption onto NSIM showing (a) the effect of change in adsorption time, (b) Lagergren pseudo-first order plot , (c) Pseudo-second order plot and (d) Intra-particle diffusion kinetics plots [Experimental conditions: T (K): 303; C0 (mg/L): 1000; pH 3.4; M (g/100 mL): 40].**

Table 4.5: Kinetics constants for fluoride adsorption onto LAGs [T (K): 303; C_0 (mg/L): 1000; pH: 3.4; M (g/100 mL): 293-40].

Adsorbent	NSIM	DIME	FEPM	FELS
Pseudo-first order				
$K_{1,ads}$ (min^{-1})	0.277	0.039	0.0967	0.0046
q_e (mg/g)	5.621×10^{-11}	5.082	0.3597	4.5709
R^2	0.986	0.996	0.971	0.583
Pseudo-second order				
$h_o=k_{2,ads}q_e^2$ (mg/g/min)	9.434	1.778	0.001	13.5135
$k_{2,ads}$ (g/mg/min)	5.642	0.190	0.048	2.51351
q_e (mg/g)	1.672	9.363		5.3763
R^2	0.9980	0.9970	0.9810	0.9981
Intra-particle diffusion				
k_p(mg/g/min^2)	0.34	0.548	0.025	0.4720
$K_{w,1}$	0.098	-	0.072	0.7170
$K_{w,2}$	0.001	-	0.003	0.2220
C	1.458	4.0120	0.129	3.4010
R^2	0.5970	0.983	0.579	0.9300

The rates of external transfer of fluoride were, therefore, comparable to the surface reactions rates in controlling the overall rate of fluoride adsorption onto DIME. It showed that the overall rate of adsorption was controlled by the concentration of fluoride particles in the DIME surface. These findings were consistent with earlier postulates in section 4.5, which showed that fluoride adsorption onto DIME was controlled by mixed surface reactions based upon protonated silanol groups in DIME surfaces with significant intraparticle diffusion of the adsorbate particles into the mesoporous structure of the adsorbent. Thus, in agreement with expected behaviour of intra-particle diffusion, figure 4.15 (d) shows high linearization of data fit to the Weber-Morris intraparticle diffusion kinetics (R^2 = 0.983) over the entire period of reaction.

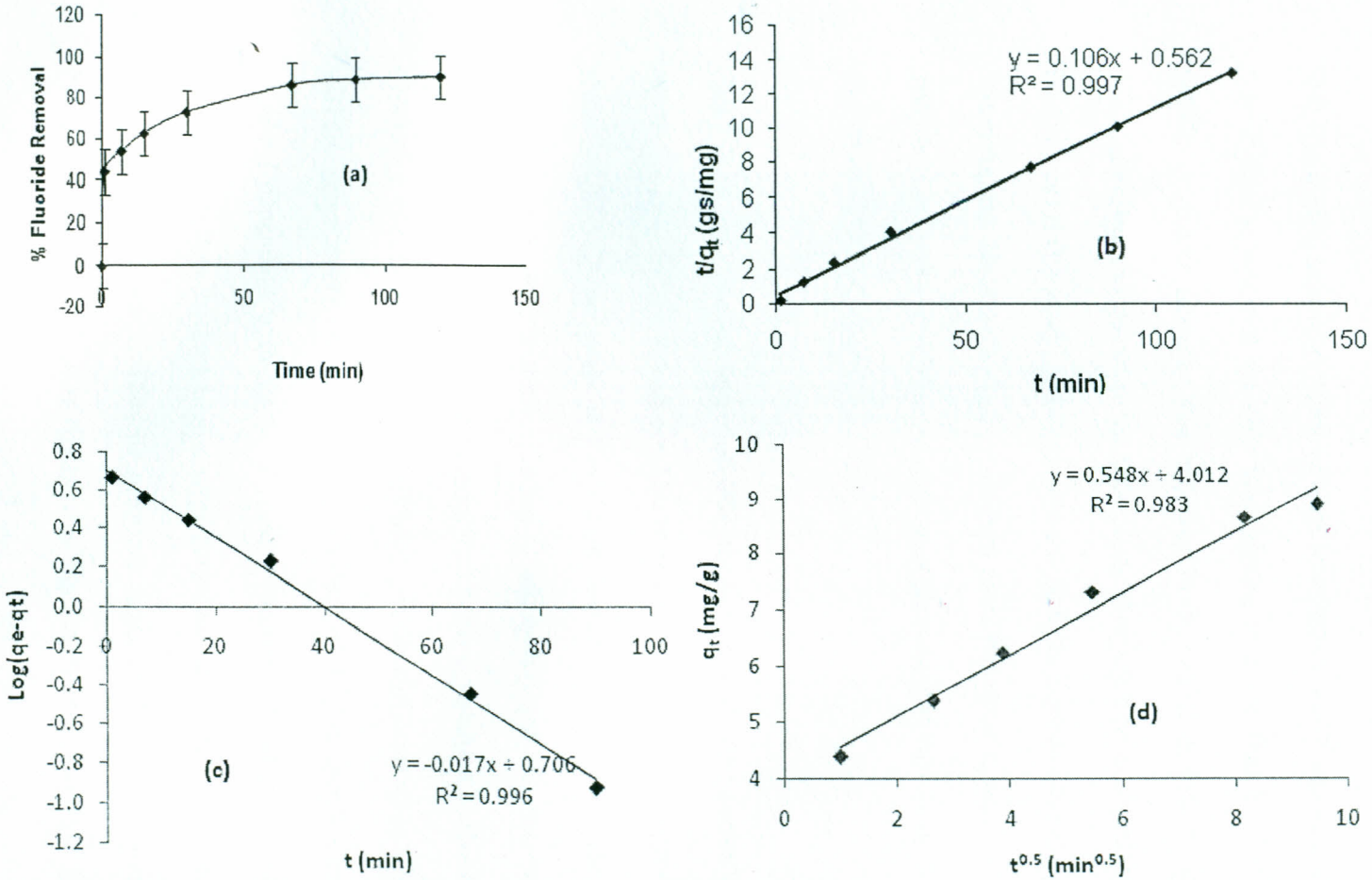

Figure 4.15 **Adsorption kinetic of fluoride adsorption onto DIME showing: (a) Effect of agitation time; (b) Lagergren pseudo-first order, (c) Pseudo-second order and (d) Intra-particle diffusion plots [Conditions: T (K): 303; C0 (mg/L): 1000; pH 3.4; M (g/100 mL): 40].**

The linear plot, however, had a vertical intercept of 4.012 showing, as expected, that pore diffusion was not the sole rate-limiting step for fluoride immobilization into DIME. A greater linearity was observed in the initial periods as also observed by other authors in the literature for similar adsorbents (Chen *et al.*, 2010b; Goswami and Purkait, 2011; Bia *et al.*, 2012). Due to the high porosity and the amorphous nature of diatomite, the adsorption data conformed to all the three kinetics models. It showed that fluoride uptake by DIME is a complex phenomenon that could not be ascribed to one mode of reaction kinetics.

The kinetic plots for adsorption of fluoride onto FEPM were constructed for fluoride adsorption at different pH values. The time-dependent data and representative kinetics plots for pH 5.24 are presented in figure 4.16. The rate of fluoride adsorption onto FEPM was very fast at the beginning of adsorption and the adsorption equilibrium could be attained in just about 30 min. The mean correlation coefficients for pseudo-first order, pseudo-second-order, and intra-particle diffusion were 0.971, 0.9810, and 0.5790, respectively. As expected, the values of R^2 for pseudo-first order kinetics were pH dependent with higher R^2 values occurring at higher pH values. It showed that, perhaps due to their high charge-to-radius ratio, the diffusion of free F^- ions, which dominate aqueous fluoride solutions at high pH values, as illustrated in figure 2.4, is slower than molecular HF species that dominate the aqueous fluoride media in strongly acidic media. This indicated that the influence of bulk diffusion on fluoride adsorption onto FEPM was enhanced in less acidic media due to the dissociation of HF species into more labile F^- ions in mid acid pH values.

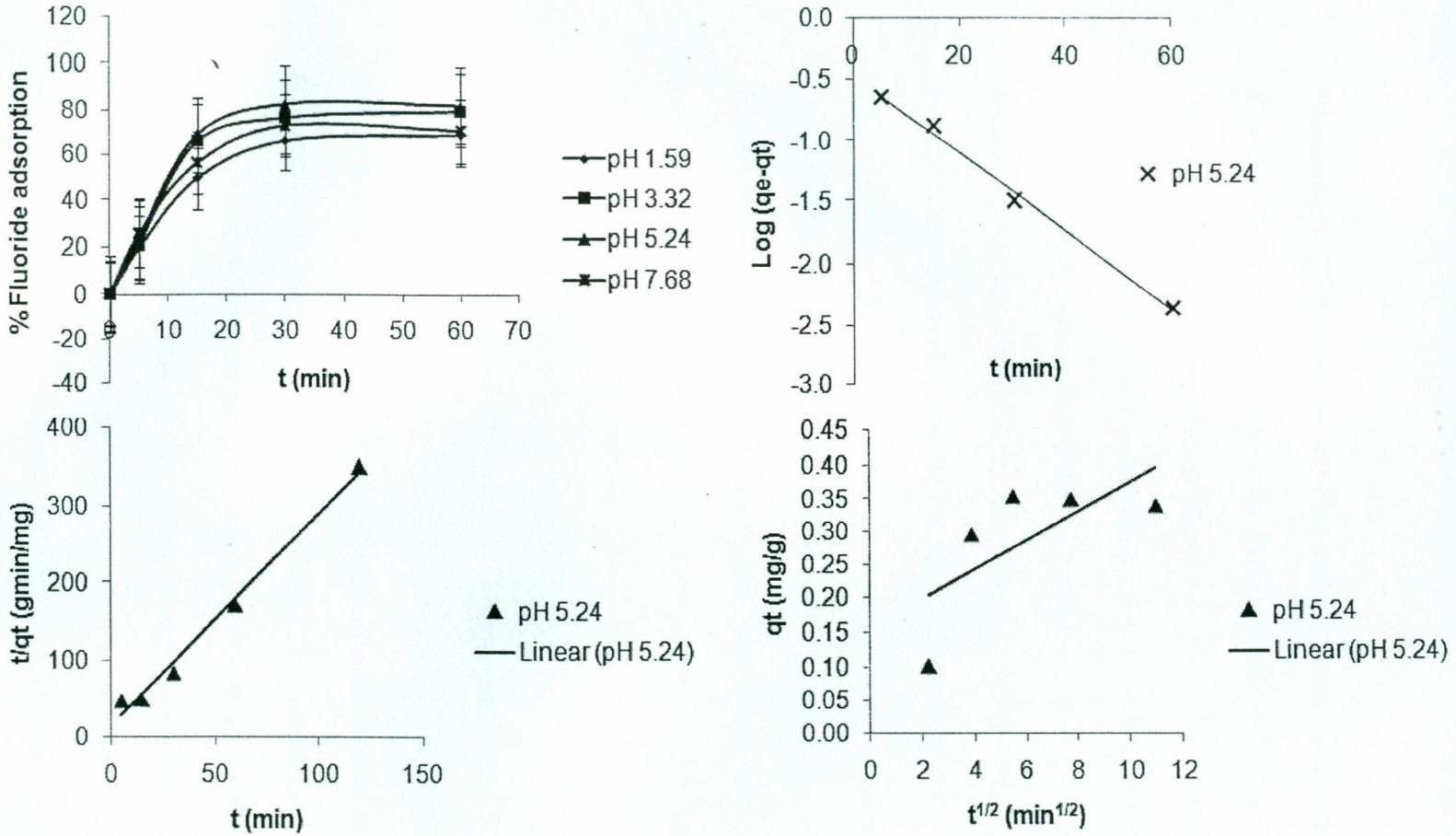

Figure 4.16: Kinetics of fluoride adsorption onto FEPM: (a) adsorption time-profile (b) Pseudo-first-order kinetics, (c) Pseudo-second-order kinetics, (d) Weber-Morris plot (intra-particle diffusion kinetic model) [Experimental conditions: pH = 5.24, FEPM Dosage = 0.2 g/50 mL, Initial conc. = 25–200 mg/L, Temp. = 303 K].

High linearity of the plots showed the validity of the pseudo-first order kinetics for fluoride adsorption onto FEPM. The pseudo-second-order kinetics plot for fluoride adsorption onto FEPM is shown in figure 4.16 (c). The sorption reactions were better approximated by the pseudo-second-order kinetics model under strongly acidic media. It indicated that whereas bulk diffusion became increasingly important in controlling the rate of fluoride adsorption at high pH values, surface reactions appears to be the principal rate determining step for the adsorption process under acidic conditions. It also showed that F^- ions had higher surface affinity for reactive sites in FEPM that HF. This led to less rapid fluoride uptake in lower pH media, which was dominated by HF species. However, the simultaneous correlation of the adsorption data to pseudo-first order and pseudo-second order kinetic models indicated existence of mixed fluoride adsorption mechanism onto FEPM.

Figure 4.16 (d) shows that there were two separate sections in Weber-Morris plot for intra-particle diffusion kinetics of fluoride adsorption onto FEPM. These were, the initial portion (0-30 min) attributed to bulk diffusion kinetics and the linear portion (30-120 min) relating to intra-particle diffusion. The values of intra-particle diffusion rate constants for the two parts, $k_{w,1}$ and $k_{w,2}$, respectively, were separately computed and are presented in table 4.5. The results showed that intra-particle diffusion became increasingly insignificant with increasing pH of the solution. Increased concentration of OH^- ions, therefore, interfered with microporous diffusion of fluoride into the adsorbent pores reducing feasibility of intra-particle reactions in alkaline pH media.

In general, the pseudo-second-order model gave the best fit for the fluoride adsorption data using FEPM adsorbent. The surface reaction step was, therefore, the slowest and

the rate determining step in fluoride adsorption onto FEPM. Again, it was observed that both film and pore diffusions were effective in controlling fluoride removal from water using this adsorbent to different degrees. Macro-pore diffusion was larger than the micro-pore diffusion rate.

The time-dependent fluoride adsorption onto FELS and the results of the corresponding kinetic analysis of fluoride removal from water using this adsorbent are reported in figure 4.17. As can be seen from figure 17 (a), the rate of fluoride uptake by FELS was rapid in the first 10 min and proceeded more steadily after 40 min.

Figure 4.17 (b), on the other hand, shows that the first order correlation coefficient for fluoride adsorption onto FELS was low (R^2 = 0.583). The kinetics of fluoride adsorption onto FELS did not, therefore, show good applicability of pseudo-first-order regression to the adsorption data. The kinetics data were, therefore, further analyzed using the pseudo-second-order and intraparticle diffusion kinetics. The linear plots of Ho's pseudo-second order kinetics model showed good agreement between experimental data and the calculated q_e values. The resulting correlation coefficient (R^2) for the second-order kinetics model was close to unity indicating applicability of this kinetics equation to the adsorption of fluoride onto FELS. Surface reactions between fluoride particles and reactive sites in FELS were, therefore, chemical and rate-controlling. Such findings have also been reported for fluoride adsorption from water onto a ceramic adsorbent (Chen *et al.*, 2010a), modified montmorillonite adsorbent (Bia *et al.*, 2012), and graphene (Li *et al.*, 2011).

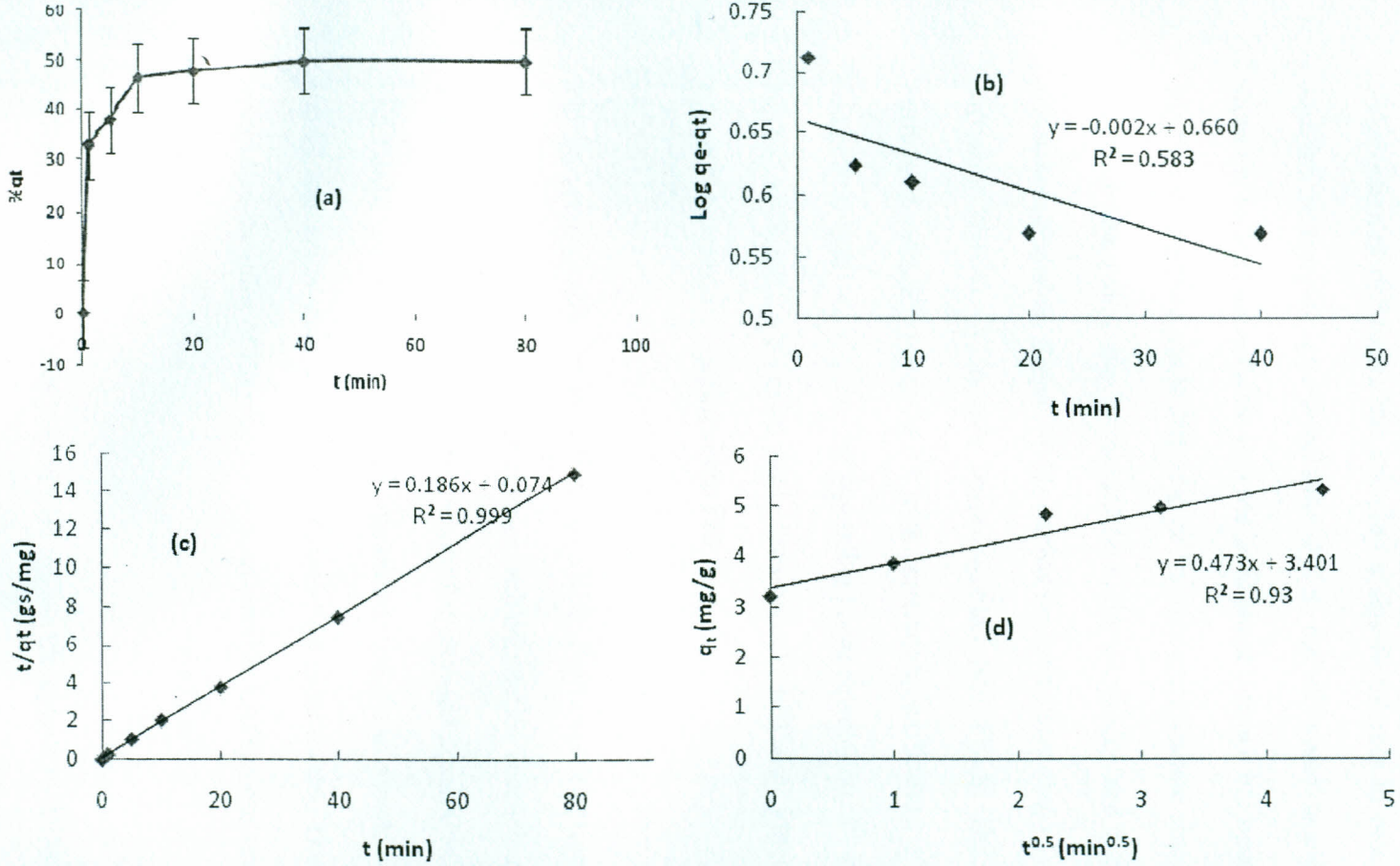

Figure 4.17: Adsorption kinetics of the adsorption of fluoride onto FELS showing: (a) Effect of time of contact, (b) Pseudo-first order kinetics plots, (c) Pseudo-second order kinetics plots and (d) Intra-particle diffusion plots [Experimental conditions = 313 K, Co = 200 mg/L, adsorbent = 1 g, V = 0.2 L].

Since external diffusions did not play a significant role in determining the rate of reaction in fluoride adsorption onto FELS, the adsorbate species were transported from the bulk of the solution into the solid phase through intra-particle diffusion. The likelihood of intra-particle diffusion of fluoride particles into structural pores in FELs was assessed using the intra-particle diffusion model and the intra-particle rate constants calculated. Figure 17 (d) depicts the linear plot of q_t vs. $t^{0.5}$ for intra-particle diffusion kinetics of fluoride immobilization into FELS. The values of q_t were correlated with the values of $t^{0.5}$ with correlation coefficients, R^2 in excess of 0.93. The values of k_p, C, and the corresponding linear correlation, R^2, showed applicability of this model to adsorption data. Intra-particle diffusion kinetics, therefore, also controlled fluoride adsorption onto FELS.

On the whole, with the exception for FELS, fluoride adsorption data for all LAGs correlated to pseudo-first order kinetics with correlation coefficients greater than 0.97. It indicated that external diffusion controlled fluoride adsorption onto NSIM, FEPM and DIME. In all cases, however, the kinetic data-fit to pseudo-second order kinetic model was better than that for the pseudo-first order model. Thus, surface reactions controlled the rates of fluoride adsorption onto the LAGs more strongly than the other processes.

The intra-particle kinetics played part in fluoride uptake by DIME and FELS, which was consistent with the porous mineral structures of these adsorbents. The graphs for fluoride adsorption onto DIME and onto FELS did not, however, have the greatest coefficient of determination for intraparticle model. Furthermore, the linear regression

curves did not extrapolate through the origin. This showed that intra-particle diffusion was not the sole rate determining steps in either case.

4.14 Adsorption Thermodynamics

The Gibb's free energy change, ΔG^0, is the fundamental criterion for assessment of the spontaneity of a chemical process. A more negative value of ΔG^0 indicates a more feasible process. The ΔG for fluoride uptake by the LAGs was examined based on the Langmuir thermodynamic equilibrium constant, b according to equation 2.16. The enthalpy change (ΔH^0) and entropy change (ΔS^0) were then determined based on equation 2.17. The corresponding van't Hoff's plots as well as the values of ΔG^0, ΔH^0 and ΔS, which were computed from the respective plots, are presented in figure 4.18 and in table 4.6, respectively. The values of ΔG^0 decreased with increasing temperature of fluoride adsorption onto NSIM. The positive value of ΔS^0 and the negative value of ΔG^0 confirmed feasibility of fluoride adsorption onto NSIM. It showed that spontaneity of fluoride adsorption onto NSIM increased with increasing temperature of reaction. The values of the adsorption enthalpy, ΔH^0, for fluoride adsorption onto NSIM were negative, as expected for an exothermic process as also postulated in section 4.8. The corresponding ΔG^0, ΔH^0, and ΔS^0 values for fluoride adsorption onto DIME were derived from relevant plots in figure 4.18 (b) and presented in table 4.6. The values of ΔG^0 (-150.2 to -160.7 kJ/mol) and those of ΔH^0, (-73.065 kJ/mol) were both large and negative indicating a spontaneous exothermic adsorption process. The ΔS^0 value (+0.2632 kJ/mol/K), on the other hand was positive reflecting the affinity of the adsorbate fluoride particles for acidified DIME surfaces.

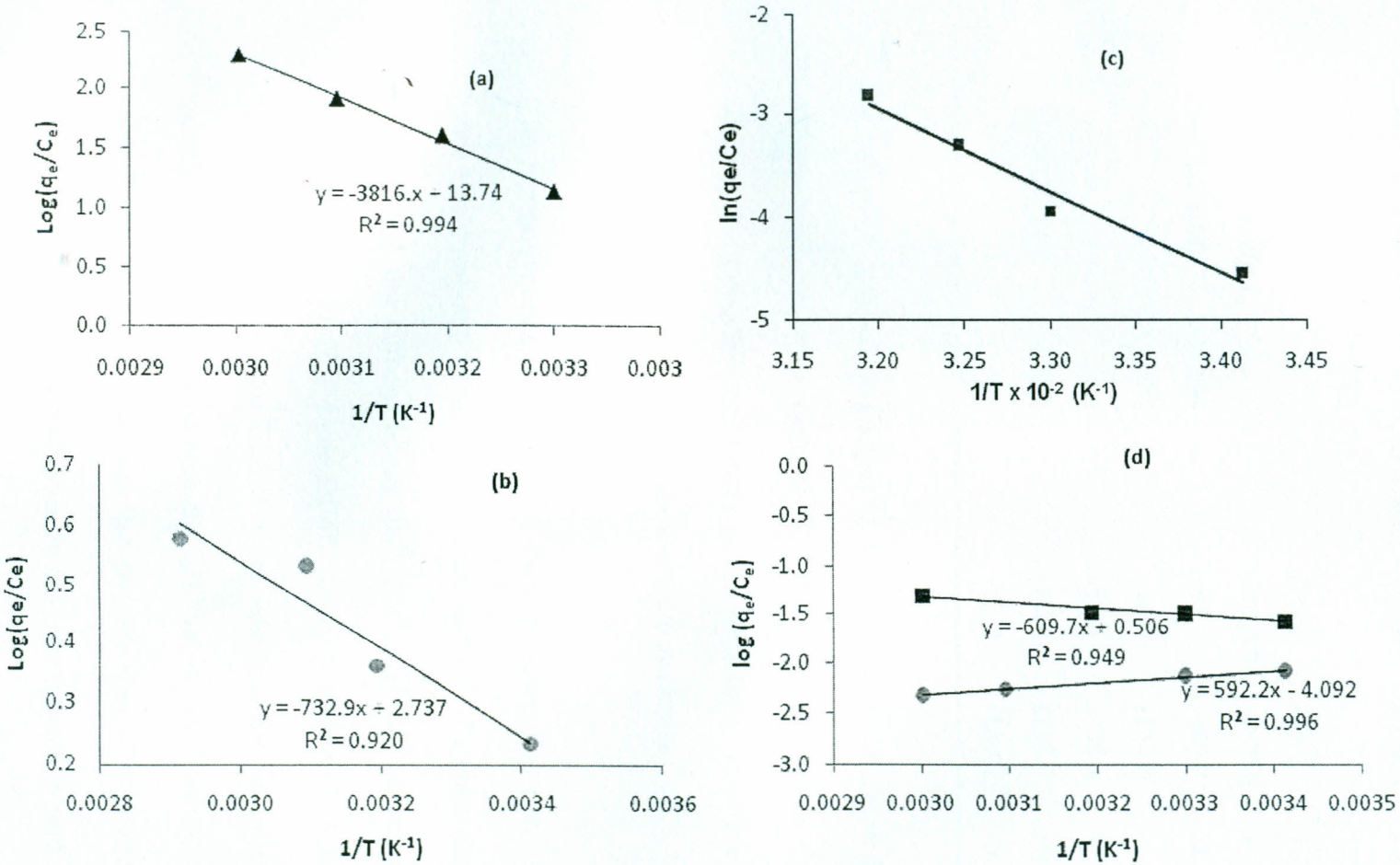

Figure 4.18: Regressions of van't Hoff's plot for fluoride adsorption on (a) NSIM, (b) DIME, (c) FEPM and (d) FELS[Experimental conditions: T (K): 303; C_0 (mg/L): 100 and 400; pH 3.4; M (g/100 mL): 40]

Table 4.6: Thermodynamic parameters for the uptake of fluoride by LAGs

Thermodynamic quantity	Temperature (K)	NSIM	DIME	FEPM	FELS
ΔH^0(kJ/mol)	-	0.066	-73.1	+3004.187	-72.897
ΔS^0 (kJ/mol/K)	-	+0.187	+0.263	+26.251	+0.246
ΔG^0 kJ/mol)	298	-55.7	-150.2	-4.819	-7.211
	303	-56.6	-152.8	-4.950	-3.951
	313	-58.5	-155.4	-5.212	-7.195
	323	-60.4	-158.1	-5.475	-8.845
	333	-62.2	-160.7	-5.737	-6.344

It suggested structural changes at the adsorption interface between the adsorbate solution and adsorbent surfaces. It could be assumed that these structural changes resulted in increased randomness at the solid/liquid interface during the adsorption process contributing to a more positive entropy change.

The thermodynamic parameters of fluoride adsorption onto FEPM and onto FELS were also computed from the respective van't Hoff's plots shown in figures 4.18 (c) and (d) and the corresponding ΔG^0, ΔH^0, and ΔS^0 values presented in table 4.6 alongside those for NSIM and DIME. As for NSIM and DIME, the values of ΔG^0 for fluoride adsorption onto FEPM were negative for feasible spontaneous fluoride adsorption processes. However, the ΔH^0 values for fluoride adsorption onto FEPM were large and positive showing that fluoride uptake by FEPM was endothermic and that favourable adsorption of fluoride onto the mineral would occur at more elevated temperatures.

The estimated values of ΔG^0 for fluoride adsorption onto FELS were in the range of -3.9–-8.85 kJ/mol, and the ΔH^0 and ΔS^0 of fluoride adsorption were -72.89 kJ/mol and +0.2463 J/mol/K, respectively. Both the values of ΔG^0 and ΔH^0 for fluoride adsorption onto FELS suggested a spontaneous exothermic physisorption process. This was consistent with experimental observations which showed that fluoride adsorption onto FELS was favoured by close to ambient tropical temperatures as also postulated in section 4.11. The positive value of ΔS for this process indicated the affinity of the adsorbent for fluoride.

4.15 Fluoride removal from natural high-fluoride water

4.15.1 Batch tests

To verify the applicability of LAGs in practical defluoridation of water, batch adsorption experiments were then conducted on water samples from a high-fluoride natural source from Gilgil, Nakuru County, Kenya and the results presented in figure 4.19. As depicted in figure 4.19 (a & b), after an initial rapid increase in fluoride adsorption to about 25% in case of NSIM and up to 15% for DIME, the percentage fluoride adsorption from the water using the two adsorbents declined to less than 15% and 5% for the two adsorbents, respectively. The build-up adsorption took place in 30 min for NSIM and 5 min for DIME and the corresponding decomposition lasting 120 and 30 min, respectively. It showed that after initial fluoride adsorption, adsorbed fluoride was desorbed from the adsorbent surface back into the water. It can be assumed that the water contained components that were able to solubilise sorbed fluoride particles from the adsorbent surfaces and keep it in solution.

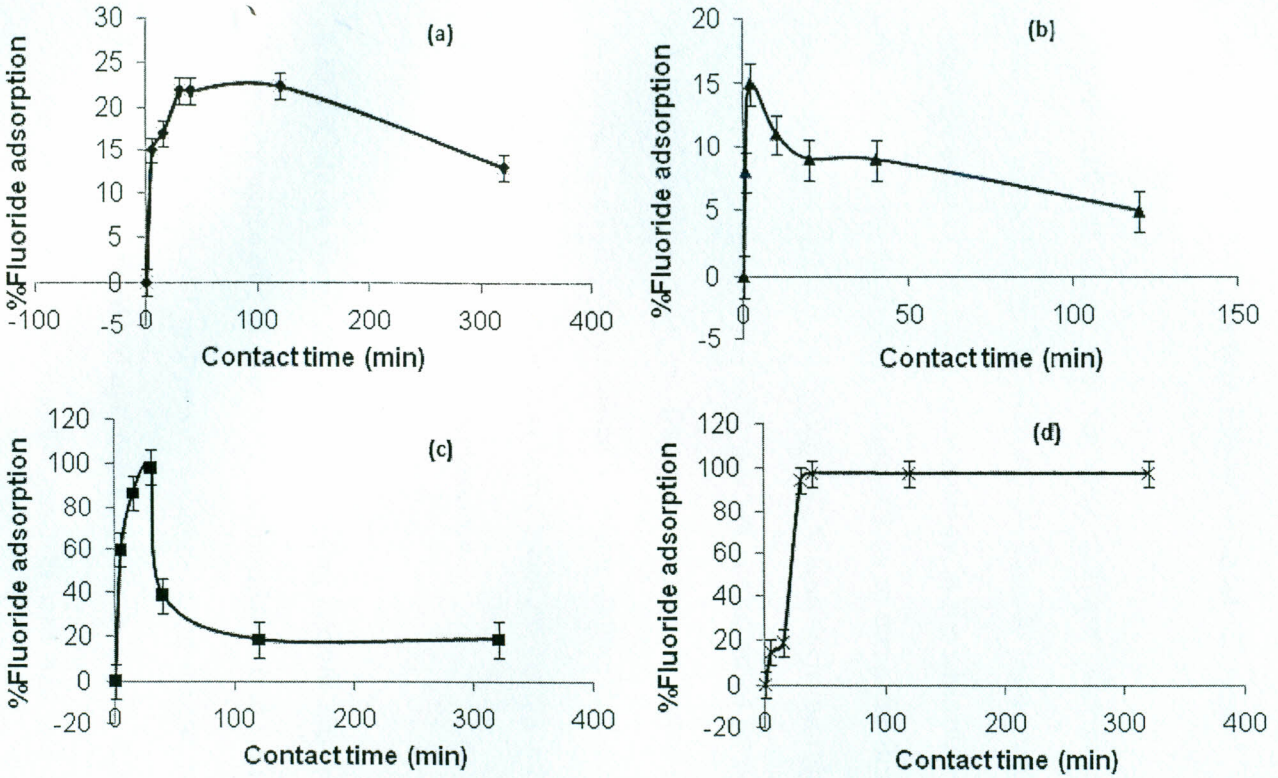

Figure 4.19: Fluoride removals from natural high-fluoride water using (a) NSIM, (b) DIME, (c) FEPM and (d) FELS. [Experimental conditions: Fluoride concentration = 50 mg/L, pH = 5.3, T = 299 K, adsorbent dosage = 0.1 g/mL].

Figure 19 (c) shows that similar trends occurred in fluoride adsorption onto FEPM with almost 100% instantaneous fluoride adsorption being desorbed back into the solution to just 20% in a time interval of about 120 min.

Figure 4.19 (d) shows that the most efficient fluoride removal from water was achieved using FELS. The removal of fluoride from water using FELS depicted a stepwise process indicating heterogeneity in the adsorptive surface of FELS as also discussed in the preceding sections. Close to complete fluoride removal from water could be achieved by contacting FELS with high-fluoride water for 60 min. The adsorption process, in this case, was not accompanied by concordant resolubilization of solute fluoride from the adsorbent surface. It demonstrated the plausibility of convenient use of this adsorbent in water defluoridation. Column adsorption tests using natural high-fluoride water were, therefore, conducted for this adsorbent and the results discussed in the subsequent section.

4.15.2 Column water defluoridation using lateritic adsorbent FELS

The performance of FELS in water defluoridation was studied in up-flow adsorption experiments mounted in Pyrex™ columns using natural water containing 21 mg/L fluoride and the breakthrough curve shown in figure 4.20. At a flow rate of 1.2 mL/min, more than 90% fluoride removal was achieved in the initial stages. The effluent fluoride concentration then increased and remained constant at 20.9 mg/L after about 80 mL of effluent volume. The fluoride adsorption data based on the column experiments were analyzed using the Thomas model (equation 2.13) and the results presented in figure 4.21. The Thomas rate constant (K_{Th}), and adsorption

capacity (q_{Th}), were then computed from the slope and intercept of linear plots of $log\left[\frac{C_0}{C_v} - 1\right]$ versus V. The Thomas model fitted the adsorption data with $R^2 = 0.964$ at bed height (m) of 4 g and effluent flow rates (Q) of 1.1538 mL/min.

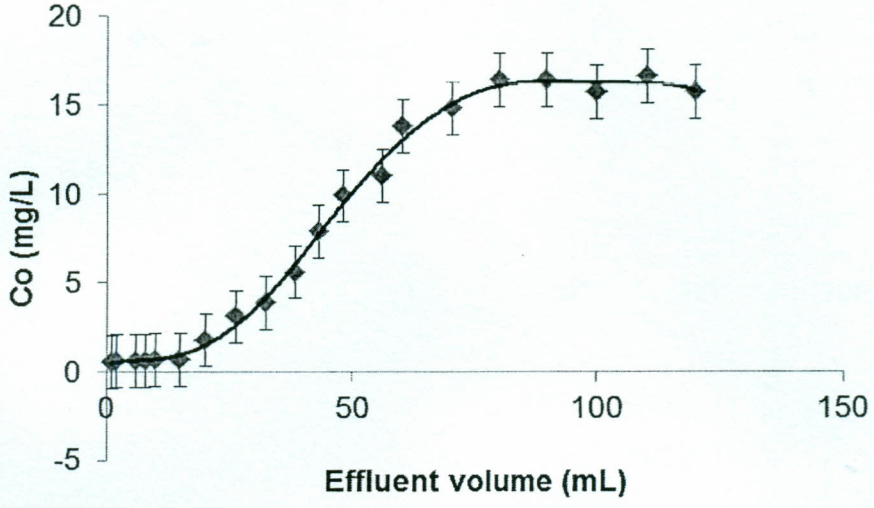

Figure 4.20: Breakthrough curves at a dose of 4.0 g of FELS and at 90 mg/L effluent fluoride concentrations at a flow rate of 9.9 mL/min.

The Thomas rate constant, K_{Th}, (0.0121 L/mg/min) and maximum adsorption capacity, q_{Th}, values showed efficient fluoride removal from water using these materials. The values of q_{Th} predicted by the Thomas model were consistent with the Langmuir adsorption capacity predicted in section 4.11.This showed that column fluoride sorption onto FELS could be described by this model. However, Thomas adsorption capacity was three times better showing that fluoride removal using FELS was more strongly removed using FELS in stationary upward flow mode than in continuous agitation in batch system. Findings such as reported in the current work have also been reported for Kanuma mud (Sulaiman *et al.*, 2009), alumina cement granules (Chen *et al.*, 2011) and magnesia-loaded fly ash cenospheres (Xu *et al.*, 2011). High adsorption capacity of FELS showed that the adsorbent is not affected by

the complex aqueous matrix of the water. This showed that FELS could be used to scavenge fluoride from natural water room temperature.

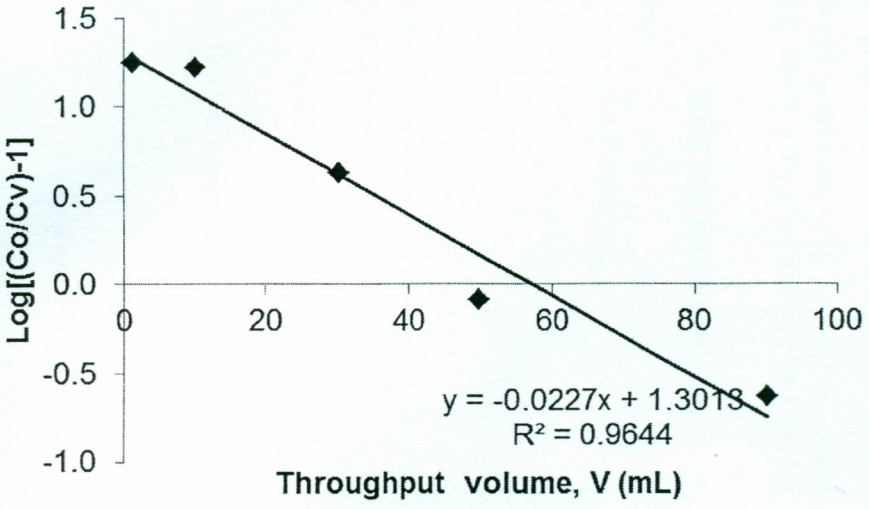

Figure 4.21: Thomas plots for fluoride removal from water using FELS [Experimental conditions: Co = 21 mg/L, T = 298 K, m = 4.0 g, Q = 0.1538 mL/min]

4.16 Desorption studies

Batch desorption studies were then conducted to test the reversibility of fluoride adsorption onto the LAGs. Two desorbing reagents, 0.1 M NaOH and 0.1 M Na_2CO_3, were used independently and in combination. The amount of desorption was computed based on the saturation capacities of the adsorbents and the results presented in figure 4.22. The trends in fluoride desorption from NSIM, which are presented in figure 4.22 (a) and in fluoride solubilisation from DIME presented in figure 4.22 (b) were similar. In both cases, fluoride desorption from the adsorbents using the desorbing agents was rapid but desorption of fluoride from DIME was slower.

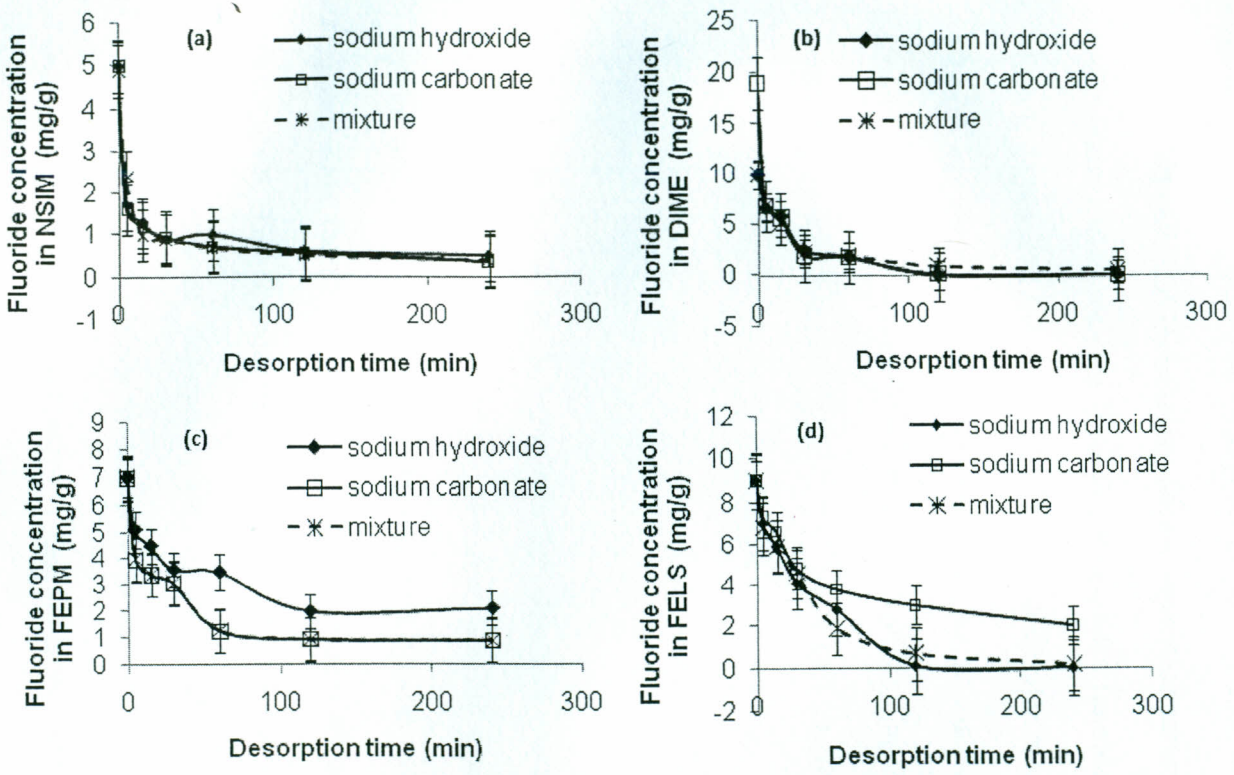

Figure 4.22: Fluoride desorption from LAGs: (a) NSIM, (b) DIME, (c) FEPM and (d) FELS using 0.1 M NaOH and 0.1 M Na_2CO_3 [Experimental conditions: T = 299 K, Batch dosage = 0.1 g/mL, Shaking rate = 120 rpm]

The desorption from the latter adsorbent attained lower residual concentration closer to zero than in NSIM, where a residual concentration of 1.0 mg/g was recorded instantaneously. Differential desorption of fluoride ions from FEPM was observed using NaOH and Na_2CO_3 solutions but the desorption using the carbonate on its own and in combination with the base was better. Like fluoride desorption from FEPM, which is depicted in figure 4.22 (c), fluoride desorption from FELS shown in figure. 4.22 (d) exhibited differential behaviour for the two desorbing agents. NaOH was however, the better desorbing agent in this case attaining zero residual fluoride in a period of 120 min. The capacity of NaOH and Na_2CO_3 to desorb fluoride from FELS was complementary because the mixture of the two desorbing solutions had desorption efficiency that averaged the sum of their individual removal capacities.

The removal of adsorbate ions from the adsorbent surfaces reflects their uptake properties (Wambu *et al.*, 2009). Whereas fluoride desorption from NSIM was uniform and almost instantaneous showing that fluoride adsorbed on uniform surface exposed sites, the desorption trends in the other three adsorbents were both stepwise and gradual. The stepwise fluoride desorption indicates mixed surface sites while differential rates of desorption are indicative of heterogeneity in adsorption mechanism. Longer periods of desorption of fluoride from ferric adsorbents, FEPM and FELS, indicate stronger binding of fluoride in the mineral lattice than is in NSIM and DIME. It showed that the mode of fluoride binding in the siliceous minerals, NSIM and DIME, was physisorption but the fluoride binding in FEPM and FELS was based on chemisorption.

CHAPTER FIVE
CONCLUSSIONS AND RECOMMENDATIONS

5.1 Conclusions

From the foregoing discussions, it could be found that all water sources in the Gilgil-Elementaita area of Nakuru County of Kenya had mean fluoride levels above WHO maximum permissible levels (1.5 mg/L) for drinking water. Prevalence of excessive fluoride in potable water sources increased by the type of water source in the order: streams and rivers < piped water < boreholes < lake water.

Most of the inhabitants in the area used borehole water, which contains high levels of F. Although a significant proportion of the population uses stream and river water that is low in F and safer. However, the streams and rivers were few, with long walking distances in between them. Rain, which would be an alternative source of water, is sparse and sporadic. Defluoridation of existing waters was, therefore, the only plausible alternative to assist the resident communities' access reliable safer household water.

The fluoride adsorption capacities of LAGs were greatly improved by acid activation in 0.1 M HCL and the time required for effective activation was 30–60 min. Under these conditions, FEPM and NSIM had comparable fluoride adsorption capacities but the efficiency of NSIM to sorb fluoride deteriorated at prolonged exposure of the adsorbent to the acidic media. DIME was least responsive to acid-treatment and it depicted stable surface that were not strongly affected by the acidic media. The best

activation was shown by FELS because it showed highest capacity to sorb fluoride and it did not depreciate under acid treatment.

Based on batch simulation tests, DIME showed the highest maximum fluoride adsorption capacities of 51.1 mg/g. The rest of the LAGs had fluoride adsorption capacities in the range of 10–13 mg/g, which was quite high when compared to those of most other low-cost adsorbents that have been reported in the literature, especially in the most recent past.

The fluoride adsorption capacities of the LAGs were, however, strongly controlled by solution parameters including the pH, temperature, adsorbent mass, contact time and co-ions in the solution. Optimum fluoride adsorption by the LAGs would best be conducted in low acidic pH of 4-6 at temperatures of 303 K in absence of the competing anions including SO_4^{2-} , Cl^- , NO_3^- and the PO_4^{3-}

The fluoride adsorption equilibrium data for the LAGs were fitted by both the Langmuir and the Freundlich isotherms. Fluoride adsorption onto the LAGs was therefore based on mixed reactions. Additionally, the fluoride adsorption data for both NSIM and FEPM were simultaneously correlated to pseudo-first order and pseudo-second order kinetic models. The fluoride adsorption onto DIME was, however, described by Weber-Moris intraparticle diffusion model. Unlike NSIM and FEPM, however, the fluoride adsorption kinetics of FELS did not correlate to pseudo-first order kinetics but it had a high R^2 value for Ho's second order kinetics showing that

chemical reactions at the sorbent surfaces in FELS controlled the rate of fluoride uptake by the mineral.

NSIM, FEPM and DIME could not efficiently be employed in the removal of fluoride from natural water sources. The adsorption build-up on these adsorbents decayed at prolonged periods of contact time. FELS could, however, efficiently be used to remove fluoride from natural water in both batch and column experiments and fluoride removal from water using FELS was better in the fixed-bed experiments than in the stirred batch experiments, which is desired for easy defluoridation of water using this material.

5.2 Recommendations

From the foregoing conclusions the following recommendations are made that:

i. Industrial scale-up using FELS for water defluoridation to harness this abundant and cheap resources for high-fluoride water treatment so as to reduce human exposure to excessive fluoride through water and lessen its concomitant toxic effects to the communities in the affected area in the country.

ii. Further studies to decide the safe distances from high-fluoride lakes of the Rift Valley and the safe depth to which domestic and industrial water boreholes should be sunk

iii. Further studies in pre-treatment of natural water to reduce chemical interferents that poison the adsorbent media derived form NSIM, FEPM and

DIME so as to improve usability of these adsorbents for practical defluoridation of high-fluoride water.

iv. Further studies such as described in the current work based on other low-cost materials and minerals in the country, using other and improved pre-treatment procedures could be intensified to develop more efficient water defluoridation protocols.

REFERENCES

Achour, S. and Youcef, L. (2009). Defluoridation of the Algerian north Sahara waters by adsorption onto local bentonites. *Int. J. Environ. Stud.* 66, 151–165.

Adelana, S.M., Bi, A.E., Hycinth, S.F.A., Cletus, S.B.A., Woincham, L.N., Uehara, A.Y., Zhang, A.J., Fantong, W.Y., Satake, H., Ayonghe, S.N., Suh, E.C., Fantong, E.B.S., Banseka, H.S., Gwanfogbe, C.D., Uehara, Y. and Zhang, J. (2010). Geochemical provenance and spatial distribution of fluoride in groundwater of Mayo Tsanaga River Basin, Far North Region, Cameroon: implications for incidence of fluorosis and optimal consumption dose. *Environ. Geochem. Health* 32, 147–63.

Agarwal, M., Rai, K., Shrivastav, R. and Dass, S. (2002). Fluoride speciation in aqueous suspensions of montmorillonite and kaolinite. *Toxicol. Environ. Chem.* 82, 11–21.

Alagumuthu, G. (2005). Fluoride adsorption studies of montmorillonite clay. *Indian J .Chem.* 12, 263–272.

Alagumuthu, G., Veeraputhiran, V. and Venkataraman, R. (2010). Adsorption isotherms on fluoride removal□: batch techniques. *Arch. Appl. Sci. Res.* 2, 170–185.

Aoba, T. (1997). The effect of fluoride on apatite structure and growth. *Crit. Rev. Oral Biol. Med.* 8, 136–153.

Arveti, N., Sarma, M.R.S., Aitkenhead-Peterson, J.A., Sunil, K., Sarma, N.A.M.R.S. and Sunil, J.A.A.K. (2011). Fluoride incidence in groundwater: a case study from Talupula, Andhra Pradesh, India. *Environ. Monit. Assess.* 172, 427–43.

Asgari, G., Roshani, B. and Ghanizadeh, G. (2012). The investigation of kinetic and isotherm of fluoride adsorption onto functionalize pumice stone. *J. Hazard. Mater.* 217-218, 123–32.

Attahiru, S., Shiundu, P.M. and Wambu, E.W. (2012). Removal of Cr(III) from aqueous solutions using a micaceous poly–mineral from Kenya. *Int. J. Phys. Sci.* 7, 1198–1204.

Ayoob, S. and Gupta, K. (2006). Fluoride in drinking water: a review on the status and stress effects. *Crit. Rev. Environ. Sci. Technol.* 36, 433–487.

Babarinde, N.A.A., Babalola, J.O. and Sanni, R.A. (2006). Biosorption of lead ions from aqueous solution by maize leaf. *Int. J. Phys. Sci.* 1, 23–26.

Bagotsky, V.S. (2006). Faundamentals of electrochemistry, 2nd ed. John Wiley & Sons, Inc., New Jersey.

Bard, A.J. and Faulkner, L.R. (2001). Electrochemical methods: fundamentals and applications, 2nd ed. John Wiley & Sons, Inc., New York.

Bardsen, A. and Bjorvatn, K. (1996). Fluoride sorption isotherm in fired clay, in: Dahi, E., and Bregnhøj, H. (Eds.), 1st International Workshop on Fluorosis Prevention and Defluoridation of Water. International Society of Fluoride Research, Bergen, Norway, pp. 56 59.

Bhatnagar, A., Kumar, E. and Sillanpää, M. (2011). Fluoride removal from water by adsorption—A review. *Chem. Eng. J.* 171, 811–840.

Bhaumik, R., Mondal, N.K., Das, B., Roy, P., Pal, K.C., Das, C., Baneerjee, A. and Datta, J.K. (2012). Eggshell powder as an adsorbent for removal of fluoride from aqueous solution: equilibrium, kinetic and thermodynamic studies. *E-Journal Chem.* 9, 1457–1480.

Bia, G., De Pauli, C.P. and Borgnino, L. (2012). The role of Fe(III) modified montmorillonite on fluoride mobility: adsorption experiments and competition with phosphate. *J. Environ. Manage.* 100, 1–9.

Biswas, K., Debnath, S. and Ghosh, U.C. (2010). Physicochemical aspects on fluoride adsorption for removal from water by synthetic hydrous iron(III)–chromium(III) mixed oxide. *Sep. Sci. Technol.* 45, 472–485.

Boldaji, M.R., Mahvi, A.H., Dobaradaran, S. and Hosseini, S.S. (2009). Evaluating the effectiveness of a hybrid sorbent resin in removing fluoride from water. *Int. J. Environ. Sci. Technol.* 6, 629–632.

Borah, L. and Dey, N.C. (2009). Removal of fluoride from low TDS water using low grade coal. *Indian J. Chem. Technol.* 16, 361–363.

Borgnino, L., Garcia, M.G., Bia, G., Stupar, Y. V, Le Coustumer, P. and Depetris, P.J. (2013). Mechanisms of fluoride release in sediments of Argentina's central region. *Sci. Total Environ.* 443, 245–55.

Bouguerra, W., Sik, M. Ben, Hamrouni, B. and Dhahbi, M. (2007). Equilibrium and kinetic studies of adsorption of silica onto activated alumina. *Desalination* 206, 141–146.

Brittain, H.G. (2006). X-ray diffraction and x-ray fluorescence, in: Ahuja, S., Jespersen, N. (Eds.), Comprehensive analytical chemistry. Elsevier B.V., Amsterdam, pp. 177–226.

Burt, B.A. (1992). The changing patterns of systemic fluoride intake. *J. Dent. Res.* 71, 1228–1237.

Castellan, G.W. (1983). Physical chemistry, 3rd ed. Addison-Wesley Publishing Co, Menlo Park, California.

Centre for Disease Control and Prevention (2005). Private well water and fluoride [WWW Document]. Priv. well water fluoride. URL http://www.cdc.gov/fluoridation/fact_sheets/wellwater.htm (accessed 3.5.14).

Chen, N., Zhang, Z., Feng, C., Li, M., Chen, R. and Sugiura, N. (2011). Investigations on the batch and fixed-bed column performance of fluoride adsorption by Kanuma mud. *Desalination* 268, 76–82.

Chen, N., Zhang, Z., Feng, C., Li, M., Zhu, D., Chen, R. and Sugiura, N. (2010a). An excellent fluoride sorption behavior of ceramic adsorbent. *J. Hazard. Mater.* 183, 460–465.

Chen, N., Zhang, Z., Feng, C., Sugiura, N., Li, M. and Chen, R. (2010b). Fluoride removal from water by granular ceramic adsorption. *J. Colloid Interface Sci.* 348, 579–584.

Chibole, O. (1987). Epidemiology of dental fluorosis in Kenya. *J. R. Soc. Health* 107, 242–243.

Chidambaram, S., Ramanathan, A.L. and Vasudevan, S. (2003). Fluoride removal studies in water using natural materials -Technical Note. *Water SA* 29, 339–344.

Chung, F.H. (1974). Quantitative interpretation of X-ray diffraction patterns of mixtures. I. matrix-flushing method for quantitative multicomponent analysis. *J. Appl. Crystallogr.* 7, 519–525.

Clozel, B., Allard, T. and Muller, J.-P. (1994). Nature and stability of radiation - induced defects in natural kaolinites: new results and a reappraisal of published works. *Clays Clay Miner.* 42, 657–666.

Coetzee, P.P., Coetzee, L.L., Puka, R. and Mubenga, S. (2006). Characterisation of selected South African clays for defluoridation of natural waters. *Water SA* 29, 331–338.

Coetzee, P.P., Haarhoff, J. and Chibi, C. (2004). Removal of fluoride from water with clay-based defluoridators. Johannesberg, South Africa.

Das, N., Pattanaik, P. and Das, R. (2005). Defluoridation of drinking water using activated titanium rich bauxite. *J. Colloid Interface Sci.* 292, 1–10.

Deshmukh, W.S. and Attar, S.J. (2008). Equilibrium analysis f or batch studies of adsorption of fluoride in water using activated alumina R and D 6S1-X. *Int. J. Chem. Sci.* 6, 1900–1912.

Díaz-Nava, C., Olguín, M.T. and Solache-Ríos, M. (2002). Water defluoridation by Mexican heulandite-clinoptilolite. *Separation Sci. Technol.* 13, 3109–3128.

El-Said, G.F. and Draz, S.E.O. (2010). Physicochemical and geochemical characteristics of raw marine sediment used in fluoride removal. *J. Environ. Sci. Health. A. Tox. Hazard. Subst. Environ. Eng.* 45, 1601–15.

Emekli-alturfan, E., Yarat, A. and Akyuz, S. (2009). Fluoride levels in various black tea, herbal and fruit infusions consumed in Turkey. *Food Chem. Toxicol.* 47, 1495–1498.

Erdem, M. (2004). Removal of hexavalent chromium by using heat-activated bauxite. *Miner. Eng.* 17, 1045–1052.

Erdemoglu, S.B., Türkdemir, H. and Gücer, S. (2000). Determination of total and fluoride bound aluminium in tea infusions by ion selective electrode and flame atomic absorption spectrometry. *Anal. Lett.* 33, 1513–1529.

Evangelou, V.P. (1998). Environmental Soil and Water Chemistry: Principles and Applications. John Wiley & Sons, Inc., New York.

Færgestad, E.M., Langsrud, Ø., Høy, M., Hollung, K. and Mat, N. (2009). Analysis of megavariate data in functional genomics, in: Reedjik, J. (Ed), Reference module in chemistry, molecular sciences and chemical engineering comprehensive chemometrics: chemical and biochemical data analysis. Elsevier B.V., Amsterdam, pp. 221–278.

Falaras, P., Lezdou, F., Seiragakis, G. and Petrakis, D. (2000). Bleaching properties of alumina-pillared acid-activated montemorillonite. *Clays Clay Miner.* 48, 549–556.

Fan, X., Parker, D.J. and Smith, M.D. (2003). Adsorption kinetics of fluoride on low cost materials. *Water Res.* 37, 4929–4937.

Farrah, H., Slavek, J. and Pickering, W.F. (1987). Fluoride interactions with hydrous aluminum oxides and alumina. *Aust. J. Soil Res.* 25, 55–69.

Feng, L., Xu, W., Liu, T. and Liu, J. (2012). Heat regeneration of hydroxyapatite / attapulgite composite beads for defluoridation of drinking water. *J. Hazard. Mater.* 221-222, 228–235.

Fey, M.V. and Dixon, J..B. (1981). Sybthesis and properties of hydrated aluminous goethites. *Clays Clay Mine*r. 29, 91–100.

Fifield, F.W. and Kealey, D. (2000). Principles and practice of analytical chemistry, 5th ed. Blackwell Sciences Ltd, Paris.

Ford, R.G., Bertsch, P.M. and Seaman, J.C. (1997). Goethite morphologies investigated via x-ray diffraction of oriented samples. *Clays Clay Miner.* 45, 769–772.

Frini-Srasra, N. and Srasra, E. (2010). Acid treatment of south Tunisian palygorskite: removal of Cd(II) from aqueous and phosphoric acid solutions. *Desalination* 250, 26–34.

Gao, S., Sun, R., Wei, Z., Zhao, H., Li, H. and Hu, F. (2009). Size-dependent defluoridation properties of synthetic hydroxyapatite. *J. Fluor. Chem.* 130, 550–556.

Gikunju, J.K., Mbaria, J.M., Murcithi, W., Kyule, M.N. and Maitho, T.E. (1995). Water fluoride in the Molo Division of Nakuru District, Kenya. *Fluoride* 28, 17–20.

Gikunju, J.K., Simiyu, K.W., Gathura, P.B., Kyule, M. and Kanja, L.W. (2002). River water fluoride in Kenya. *Fluoride* 35, 193–196.

Giles, C.H., MacEwan, T.H., Nakhwa, S.N. and Smith, D. (1960). Studies in adsorption. Part XI: a system of classification of solution adsorption isotherms, and its use in diagnosis of adsorption mechanisms and in measurement of specific surface areas of solids. *J. Am. Chem. Soc.* 786, 3973–3993.

Girgis, B.A.Y. (2005). Reuse of discarded deactivated bleaching earths in the bleaching of oils. *Grasas y Aceites* 56, 34–45.

Gitonga, J.N. and Nair, K.R. (1982). Rural water fluorides project. Technical Report. Nairobi.

Glotch, T.D. and Kraft, M.D. (2008). Thermal transformations of akaganéite and lepidocrocite to hematite□: assessment of possible precursors to Martian crystalline hematite. *Phys. Chem. Miner.* 35, 569–581.

Gogoi, P.K. and Baruah, R. (2008). Fluoride removal from water by adsorption on acid activated kaolinite clay. *Indian J. Chem. Technol.* 15, 500–503.

Gopal, V. and Elango, K.P. (2007). Equilibrium, kinetic and thermodynamic studies of adsorption of fluoride onto plaster of Paris. *J. Hazard. Mater.* 141, 98–105.

Goromo, K., Zewgw, F., Hundhammer, B. and Megersa, N. (2012). Fluoride removal by adsorption on thermally treated lateritic Soils. *Bull. Chem. Soc. Ethiop.* 26, 361–372.

Goswami, A. and Purkait, M.K. (2011). Kinetic and equilibrium study for the fluoride adsorption using pyrophyllite. *Sep. Sci. Technol.* 46, 1797–1807.

Gueu, S., Yao, B., Adouby, K. and Ado, G. (2007). Kinetics and thermodynamics study of lead adsorption on to activated carbons from coconut and seed hull of the palm tree. *Int. J. Environ. Sci. Tech.* 4, 11–17.

Hamdi, N. and Srasra, E. (2007). Removal of fluoride from acidic wastewater by clay mineral□: Effect of solid – liquid ratios. Desalination 206, 238–244.

Hamdi, N. and Srasra, E. (2009). Retention of fluoride from industrial acidic wastewater and NaF solution by three tunisian clayey soils. *Fluoride* 42, 39–45.

He, Z.L., Zhang, G.K. and Xu, W. (2013). Enhanced adsorption of fluoride from aqueous solution using an iron-modified attapulgite adsorbent. *Water Environ. Res.* 85, 167–174.

Hiemstra, T. and Riemsdijk, W.. H.V. (2000). Fluoride aAdsorption on goethite in relation to different types of surface sites. *J. Colloid Interface Sci.* 104, 94–104.

Ho, Y.S. (2014). Comments on " Elimination of bisphenol A from water via graphene oxide adsorption." *Acta Physico-Chimica Sin.* 30, 1391–1391.

Huang, Y., Shih, Y.-J. and Chang, C.C. (2011). Adsorption of fluoride by waste iron oxide: the effects of solution pH, major coexisting anions, and adsorbent calcination temperature. *J. Hazard. Mater.* 186, 1355–9.

Hyun, S.P., Cho, Y.H. and Hahn, P.S. (2005). An electron paramagnetic resonance study of Cu(II) sorbed on kaolinite. *Appl. Clay Sci.* 30, 69–78.

Ibrahim, H.S., Jamil, T.S. and Hegazy, E.Z. (2010). Application of zeolite prepared from Egyptian kaolin for the removal of heavy metals: II. Isotherm models. *J. Hazard. Mater.* 182, 842–7.

Ibrahim, M., Shaltout, A.A., Atta, D.E., Jalbout, A.F. and Soylak, M. (2009). Removal of COOH, Cd and Pb using water hyacinth: FTIR and Flame Atomic Absorption Study. *J. Iran. Chem. Soc.* 6, 364–372.

Ingallinella, A.M., Pacini, V.A., Fernández, R.G., Vidoni, R.M. and Sanguinetti, G. (2011). Simultaneous removal of arsenic and fluoride from groundwater by coagulation-adsorption with polyaluminum chloride. *J. Environ. Sci. Health. A. Tox. Hazard. Subst. Environ. Eng.* 46, 1288–96.

Jackson, P.J., Harvey, P.W. and Young, W.F. (2002). Chemistry and bioavailability aspects of fluoride in drinking water. Medmenham, Marlow, Bucks.

Jha, S.K., Singh, R.K., Damodaran, T., Mishra, V.K., Sharma, D.K. and Rai, D. (2013). Fluoride in groundwater: toxicological exposure and remedies. *J. Toxicol. Environ. Health. B. Crit. Rev.* 16, 52–66.

Jiménez-Becerril, J., Solache-Ríos, M. and García-Sosa, I. (2011). Fluoride removal from aqueous solutions by boehmite. Water, Air, Soil Pollut. 223, 1073–1078.

Kahama, R.W., Kariuki, D.N., Kariuki, H.N. and Njenga, L.W. (1997). Fluorosis in children and sources of fluoride around Lake Elementaita region of Kenya. *Fluoride* 30, 19–25.

Kaimenyi, J.T. (2004). Oral health in Kenya. *Int. Dent. J.* 54, 378–382.

Kang, D.H., Hyun, S., Kim, J.G. and Kim, S.J. (2011). Adsorptive removal of aqueous fluoride and ferrocyanide by liner minerals from SPL landfill leachate: Effect of pH and adsorptive competition. *Desalination* 267, 82–87.

Karthikeyan, M., Kumar, K.K.S. and Elango, K.P. (2012). Studies on the defluoridation of water using conducting polymer/montmorillonite composites. *Environ. Technol.* 33, 733–9.

Kenya National Bureaou of Statistics (2010). Kenya Population and Housing 2009 Census Results: Population Distribution by Political Units (vol. 1B). Ministry of Planning, Nairobi, Kenya.

Korir, H., Mueller, K., Korir, L., Kubai, J., Wanja, E., Wanjiku, N. and Waweru, J. (2009). The development of bone char based filters for the removal of fluoride from drinking water, in: Shaw, R. (Ed.) 34th WEDC International Conference, Addis Ababa, Ethiopia, 2009: Water, Sanitation and Hygiene - Sustainable Development and Multusectoral Approaches. Addis Ababa, Ethiopia, pp. 1–6.

Lagassé, P., Goldman, L., Hobson, A. and Norton, S.R. (Eds.) (2012). Calcareous soils, in: The Columbia lectronic Encyclopedia. William B. Strachan, Columbia, pp. 23-38.

Larsen, M.J. and Pearce, E.I.F. (2002). Defluoridation of drinking water by boiling with brushite and calcite. *Caries Res.* 36, 341–346.

Lavecchia, R., Medici, F., Piga, L. and Rinaldi, G. (2012). Fluoride removal from water by adsorption on a high alumina content bauxite. *Chem. Eng. Trans.* 26, 225–230.

Levy, M., Rafferty, J., Hosch, W.L., Rodgers, K., Curley, R. and Hayes, D. (Eds.) (2008). Rocks and minerals. Encyclopedia Britanica, Inc., London.

Li, Y., Zhang, P., Du, Q., Peng, X., Liu, T., Wang, Z., Xia, Y., Zhang, W., Wang, K., Zhu, H. and Wu, D. (2011). Adsorption of fluoride from aqueous solution by graphene. *J. Colloid Interface Sci.* 363, 348–354.

Liang, W., Zhan, L., Piao, L. and Rűssel, C. (2011). Fluoride removal performance of glass derived hydroxyapatite. *Mater. Res. Bull.* 46, 205–209.

Loganathan, P., Vigneswaran, S., Kandasamy, J. and Naidu, R. (2013). Defluoridation of drinking water using adsorption processes. *J. Hazard. Mater.* 248-249, 1–19.

MacDonald, L.H. (2011). An integrated approach to address endemic fluorosis in Jharkhand, India. *J. Water Resour. Prot.* 03, 457–472.

Mahramanlioglu, M., Kizilcikli, I. and Bicer, I. (2002). Adsorption of fluoride from aqueous solution by acid treated spent bleaching earth. *J. Fluor. Chem.* 115, 41–47.

Mahvi, A.H., Heibati, B., Mesdaghinia, A. and Yari, A.R. (2012). Fluoride adsorption by pumice from aqueous solutions. E-Journal Chem. 9, 1843–1853.

Maiti, A., Basu, J.K. and De, S. (2011). Chemical treated laterite as promising fluoride adsorbent for aqueous system and kinetic modeling. *Desalination* 265, 28–36.

Makhoukhi, B.B., Didi, M., Villemin, D. and Azzouz, A. (2009). Acid activation of bentonite for use as a vegetable oil bleaching agent. *Grasasy Aceites* 60, 343–349.

Malakootian, M., Moosazadeh, M., Yousefi, N. and Fatehizadeh, A. (2011). Fluoride removal from aqueous solution by pumice□: case study on Kuhbonan water. *African J. Environ. Sci. Technol.* 5, 299–306.

Malkoc, E. and Nuhoglu, Y. (2006). Removal of Ni(II) ions from aqueous solutions using waste of tea factory□: adsorption on a fixed-bed column. *J. Hazard. Mater.* 135, 328–336.

Malvern Instruments (2014). Zeta potential an introduction in 30 minutes (No. MAK654-01), Zetasizer Nano Series Technical Note. Worcestershire.

Márquez-Mendoza, S., Jiménez-Reyes, M., Solache-Ríos, M. and Gutiérrez-Segura, E. (2011). Fluoride removal from aqueous solutions by a carbonaceous material from pyrolysis of sewage sludge. Water, Air, Soil Pollut. 223, 1959–1971.

Martı, C.E., Mcbride, M. and Hendershot, W. (1998). Adsorption of free lead (II) by pedogenic oxides, ferrihydrite, and leaf compost ′. *Soil Sci. Soc. Am. J.* 64, 595–599.

Mascarenhas, A.K. (2000). Risk factors for dental fluorosis□: a review of the recent literature. *Am. Acad. Pediatr. Dent.* 269 22, 269–277.

Meenakshi, S., Sundaram, C.S. and Sukumar, R. (2008). Enhanced fluoride sorption by mechanochemically activated kaolinites. *J. Hazard. Mater.* 153, 164–72.

Miretzky, P., Mun, C. and Cantoral-uriza, E. (2011). Cd^{2+} adsorption on alkaline-pretreated diatomaceous earth□: equilibrium and thermodynamic studies. *Environ. Chem. Lett.* 9, 55–63.

Mohan, D. and Pittman, C.U. (2007). Arsenic removal from water/wastewater using adsorbents--a critical review. *J. Hazard. Mater.* 142, 1–53.

Mohapatra, D., Mishra, D., Mishra, S.P., Chaudhury, G.R. and Das, R.P. (2004. Use of oxide minerals to abate fluoride from water. *J. Colloid Interface Sci.* 275, 355–359.

Mohapatra, M., Anand, S., Mishra, B.K., Giles, D.E. and Singh, P. (2009). Review of fluoride removal from drinking water. *J. Environ. Manage.* 91, 67–77.

Mohapatra, M., Padhi, T., Anand, S. and Mishra, B.K. (2012). CTAB mediated Mg-doped nano Fe_2O_3□: synthesis, characterization, and fluoride adsorption behavior. *Desalin. Water Treat.* 50, 376–386.

Mohapatra, M., Rout, K., Gupta, S.K., Singh, P., Anand, S. and Mishra, B.K. (2009). Facile synthesis of additive-assisted nano goethite powder and its application for fluoride remediation. *J. Nanoparticle Res.* 12, 681–686.

Moturi, W. (2004). Household water sources and their contribution towards fluoride consumption in Njoro Division, Nakuru household water sources and their contribution towards fluoride. *African J. Aquat.* Sci. 29, 275–277.

Moturi, W.K., Tole, M.P. and Davies, T.C. (2002). The contribution of drinking water towards dental fluorosis□: a case study of. Environ. Geochem. *Health* 24, 123-130.

Mourabet, M., El Rhilassi, A., El Boujaady, H., Bennani-Ziatni, M., El Hamri, R. and Taitai, A. (2012). Removal of fluoride from aqueous solution by adsorption on Apatitic tricalcium phosphate using Box–Behnken design and desirability function. *Appl. Surf. Sci.* 258, 4402–4410.

Murithi, G., Onindo, C.O., Wambu, E.W. and Muthakia, G.K. (2014). Removal of cadmium(II) ions from water by adsorption using aater hyacinth (*Eichhornia crassipes*) biomass. *BioRes.* 9, 3613–3631.

Murray, H.H. (2007). Applied clay mineralogy: occurrence, processing and application of koalins, bentonites, palygorskit-sepiolite, and common clays, 5th ed. Elsevier B.V., Amsterdam, The Netherlands.

Murugan, M. and Subramanian, E. (2006). Studies on defluoridation of water by tamarind seed , an unconventional biosorbent. *J. Water Health* 4, 453–461.

Murutu, C.S., Onyango, M.S., Ochieng, A. and Otieno, F.O. (2009). Investigation on limestone-derived apatite as a potential low cost adsorbent for drinking water defluoridation [WWW Document]. Capacit. Build. Knowl. Shar. Arm WISA. URL http://www.ewisa.co.za/literature/files/148_101 Murutu.pdf (accessed 7.28.14).

Mutisya, P.K., Maranga, S.M. and Ikua, B.W. (2012). An insight into the sources of the bentonite used in the local drilling industry [WWW Document]. Jomo Kenyatta Univ. Sci. Agric. Technol. -Open Resour. URL http://jkuat.ac.ke/departments/library/?page_id=345 (accessed 7.24.14).

Mwaniki, D.L. (1992). Fluoride sorption characteristics of different grades of bone charcoal, based on batch tests. *J. Dent. Res.* 71, 1310–1315.

Nair, K.R., Manji, F. and Gitonga, J.N. (1984). The occurrence and distribution of fluoride in groundwaters of Kenya. *East Afr. Med. J.* 61, 503–12.

Nath, S.K. and Dutta, R.K. (2010). Enhancement of limestone defluoridation of water by acetic and citric acids in fixed bed reactor. *CLEAN - Soil, Air, Water* 38, 614–622.

Nevill, L.B. and Brass, W. (1953). Preliminary report on dental fluorosis in Kenya European children. *East Afr. Med. J.* 30, 235–242.

Ng'ang'a, P.M. and Valderhaug, J. (1993). Prevalence and severity of dental fluorosis in primary schoolchildren in Nairobi, Kenya. *Community Dent Oral Epidemiol.* 21, 15–18.

Nie, Y., Hu, C. and Kong, C. (2012). Enhanced fluoride adsorption using Al (III) modified calcium hydroxyapatite. J. Hazard. Mater. 233-234, 194–199.

Nielsen, J.M. and Dahi, E. (1995). The occurrence of fluoride contaminated magadi (trona) in Kenya and Tanzania, in: Dahi, E. and Breghoj, H. (Eds.), Proceedings of the 1st International Workshop on Fluorosis Prevention and Defluoridation of Water. The International Society fo Fluoride Research, Ngurdoto, Tanzania, pp. 17–22.

Olajire, A.A. and Imeokparia, F.E. (2001). Water quality assessment of osun river: studies on inorganic nutrients. *Eviron. Monit. Assess.* 69, 17–28.

Onyango, M., Masukume, M., Ochieng, A. and Otieno, F. (2010). Functionalised natural zeolite and its potential for treating drinking water containing excess amount of nitrate. *Water SA* 36, 655–662.

Onyango, M.S., Kojima, Y., Aoyi, O., Bernardo, E.C. and Matsuda, H. (2004). Adsorption equilibrium modeling and solution chemistry dependence of fluoride removal from water by trivalent-cation-exchanged zeolite F-9. *J. Colloid Interface Sci.* 279, 341–50.

Onyango, M.S. and Matsuda, H. (2006). Fluoride removal from water using adsorption technique, in: Tressaud, A. (Ed.). Advances in fluorine science□: fluorine and the environment —Agrochemicals, Archaeology, Green Chemistry & Water. Elsevier B.V., pp. 1–48.

Opinya, G.N., Pameijer, C.H. and Grön, P. (1987). Simple defluoridation procedures for Kenyan borehole water. *Community Dent. Oral Epidemiol.* 15, 60–62.

Oyaro, N., Juddy, O., Murago, E.N.M. and Gitonga, E. (2007). The contents of Pb , Cu , Zn and Cd in meat in Nairobi , Kenya. *J. Food, Agric. Environ.* 5, 119–121.

Pasteur, L. (2000). The history of drinking water treatment. *Public Health* 40, 1–4.

Patel, G., Pal, U. and Menon, S. (2009). Removal of fluoride from aqueous solution by CaO nanoparticles. *Sep. Sci. Technol.* 44, 2806–2826.

Payne, K.B. and Abdel-Fattah, T.M. (2004). Adsorption of divalent lead ions by zeolites and activated carbon: effects of pH, temperature, and ionic strength. *J. Environ. Sci. Heal. Part A- Toxic/Hazardous Subst. Environ. Eng.* A39, 2275–2291.

Pekař, M. (2008). Fluoride anion binding by natural lignite (South Moravian Deposit of Vienna Basin). *Water. Air. Soil Pollut.* 197, 303–312.

Rajeshwar, K. and Ibanez, J.G. (1997). Environmental electrochemistry□: fFundamentals and applications in pollution sensors. Elsevier science & Technology books, Amsterdam.

Ramdani, A., Taleb, S., Benghalem, A. and Ghaffour, N. (2010). Removal of excess fluoride ions from saharan brackish water by adsorption on natural materials. *Desalination* 250, 408–413.

Rao, N. (2003). Fluoride and environment- a review, in: Bunch, M.J., Suresh, V.M. and Kumaran, T.V. (Eds.), Proceedings of the third international conference on environment and health, Chennai, India, 15-17 December, 2003. Department of Geography, University of Madras and Faculty of Environmental Studies, York University, Chennai, India, pp. 386–399.

Reardon, E.J. and Wang, Y. (2000). A limestone reactor for fluoride removal from wastewaters. *Environ. Sci. Technol.* 34, 3247–3253.

Reich, T.J., Das, S., Koretsky, C.M., Lund, T.J. and Landry, C.J. (2010). Surface complexation modeling of Pb(II) adsorption on mixtures of hydrous ferric oxide, quartz and kaolinite. *Chem. Geol.* 275, 262–271.

Richards, L.A., Vuachère, M. and Schäfer, A.I. (2010). Impact of pH on the removal of fluoride , nitrate and boron by nanofiltration/reverse osmosis. *Desalination* 261, 331 337.

Robbins, C.W. (1986). Adsorption by a saline sodic soil irrigated with a high F water. *Irrig. Sci.* 7, 107–112.

S´Rodon, J., Drits, V.A., Mccarty, D.K., Hsieh, J.C.C. and Eberl, D.D. (2001). Quantitaitve x-ray diffraction analysis of clay-bearing rocks from random preparations. *Clays Clay Miner.* 49, 514–528.

S´rodoń, J.J. (2006). Identification and quantitative analysis of clay minerals, in: Bergaya, F., Theng, B.K.G. and Lagaly, G. (Eds.), Handbook of clay science: developments in clay science, Vol. 1. Elsevier Ltd, Amsterdam, pp. 765–787.

Samatya, S., Yüksel, Ü., Yüksel, M. and Kabay, N. (2007). Removal of fluoride from water by metal ions (Al^{3+}, La^{3+} and ZrO^{2+}) loaded natural zeolite. *Sep. Sci. Technol.* 42, 2033–2047.

Sarkar, M., Banerjee, A., Pramanick, P.P. and Sarkar, A.R. (2006. Use of laterite for the removal of fluoride from contaminated drinking water. *J. Colloid Interface Sci.* 302, 432–41.

Sasaki, K., Yoshida, M., Ahmmad, B., Fukumoto, N. and Hirajima, T. (2013). Sorption of fluoride on partially calcined dolomite. *Colloids Surfaces A Physicochem. Eng. Asp.* 435, 56–62.

Schaller, M.S., Koretsky, C.M., Lund, T.J. and Landry, C.J. (2009). Surface complexation modeling of Cd(II) adsorption on mixtures of hydrous ferric oxide, quartz and kaolinite. *J. Colloid Interface Sci.* 339, 302–9.

Sen Gupta, S. and Bhattacharyya, K.G. (2011). Kinetics of adsorption of metal ions on inorganic materials: A review. *Adv. Colloid Interface Sci.* 162, 39–58.

Seyfried, M.S., Sparks, D.L., Bar-Tal, A. and Feigenbaum, S. (1989). Kinetics of calcium-magnesium exchange on soil using a stirred-flow reaction chamber. *Soil Sci. Soc. Am. J.* 53, 406.

Shawabkeh, R. (2003). Experimental study and modeling of basic dye sorption by diatomaceous clay. *Appl. Clay Sci.* 24, 111–120.

Sheng, G., Dong, H. and Li, Y. (2012). Characterization of diatomite and its application for the retention of radiocobalt: role of environmental parameters. *J. Environ. Radioact.* 113, 108–15.

Sivasamy, A, Singh, K.P., Mohan, D. and Maruthamuthu, M. (2001). Studies on defluoridation of water by coal-based sorbents. *J. Chem. Technol. Biotechnol.* 76, 717–722.

Srimurali, M., Pragathi, A. and Karthikeyan, J. (1998). A study on removal of fluorides from drinking water by adsorption onto low-cost materials. *Environ. Pollut.* 99, 285–289.

Stumm, W. and Morgan, J.J. (1996). Aquatic chemistry, 3rd ed. John Wiley & Sons, Inc., Toronto.

Sugita, H., Komai, T., Okita, S., Tokanaga, S. and Matsunaga, I. (2005). Analysis on adsorption behavior of fluorine on clay minerals using Freundlich isotherm. *J. Min. Mater. Process. Inst. Japan* 121, 416–422.

Sujana, M.G. and Anand, S. (2010). Iron and aluminium based mixed hydroxides: A novel sorbent for fluoride removal from aqueous solutions. *Appl. Surf. Sci.* 256, 6956–6962.

Sujana, M.G. and Anand, S. (2011). Fluoride removal studies from contaminated ground water by using bauxite. Desalination 267, 222–227.

Sujana, M.G., Pradhan, H.K. and Anand, S. (2009). Studies on sorption of some geomaterials for fluoride removal from aqueous solutions. *J. Hazard. Mater.* 161, 120–5.

Sujana, M.G., Thakur, R.S. and Rao, S.B. (1998. Removal of fluoride from aqueous solution by using alum sludge. J. Colloid Interface Sci. 206, 94–101.

Sulaiman, A., Gupta, A. and Basheer, A. (2009). A fixed bed sorption system for defluoridation of ground water. *J. Urban Environ. Eng.* 3, 17–22.

Sun, Y., Fang, Q., Dong, J., Cheng, X. and Xu, J. (2011). Removal of fluoride from drinking water by natural stilbite zeolite modified with Fe (III). *Desalination* 277, 121–127.

Sushela, A.K., Kumar, A., Bhatnagar, M. and Bahadur, R. (1993). Prevalence of endemic fluorosis with gastrointerstinal manifestations in people living in some North-Indian villages. *Fluoride* 26, 97–104.

Tang, Y., Guan, X., Wang, J., Gao, N., McPhail, M.R. and Chusuei, C.C. (2009). Fluoride adsorption onto granular ferric hydroxide: effects of ionic strength, pH, surface loading, and major co-existing anions. *J. Hazard. Mater.* 171, 774–779.

Tang, Y., Wang, J. and Gao, N. (2010). Characteristics and model studies for fluoride and arsenic adsorption on goethite. *J. Environ. Sci.* 22, 1689–1694.

Teutli-Sequeira, A., Solache-Ríos, M. and Balderas-Hernández, P. (2011). Modification effects of hematite with aluminum hydroxide on the removal of fluoride ions from water. *Water, Air, Soil Pollut.* 223, 319–327.

Thole, B., Mtalo, F. and Masamba, W. (2012). Effect of particle size on loading capacity and water quality in water defluoridation with 200 ° C calcined bauxite, gypsum, magnesite and their composite filter. *African J. Pure Appl. Chem.* 6, 26–34.

Tor, A. (2006). Removal of fluoride from an aqueous solution by using montmorillonite. *Desalination* 201, 267–276.

Tsai, W.T., Hsien, K.J., Chang, Y.M. and Lo, C.C. (2005). Removal of herbicide paraquat from an aqueous solution by adsorption onto spent and treated diatomaceous earth. *Bioresour. Technol.* 96, 657–63.

Turner, B.D., Binning, P. and S. Stipp, B.D. (2005). Fluoride removal by calcite: evidence for fluorite precipitation and surface adsorption. *Environ. Sci. Technol.* 29, 9561–9568.

Turner, B.D., Binning, P.J. and Sloan, S.W. (2008). A calcite permeable reactive barrier for the remediation of Fluoride from spent potliner (SPL) contaminated groundwater. *J. Contam. Hydrol.* 95, 110–20.

Turner, B.D., Binning, P.J. and Sloan, S.W. (2010). Impact of phosphate on fluoride removal by calcite. *Environ. Eng. Sci.* 27, 643–650.

Umlong, I.M., Das, B., Devi, R.R., Borah, K., Saikia, L.B., Raul, P.K., Banerjee, S. and Singh, L. (2011). Defluoridation from aqueous solution using stone dust and activated alumina at a fixed ratio. *Appl. Water Sci.* 2, 29–36.

United Nations (2008). The millennium development goals report. New York.

Vannela, R. and Verma, S.K. (2006). Cu^{2+} removal and recovery by Spi SORB: batch stirred and up-flow packed bed columnar reactor systems. *Bioprocess Biosyst. Eng.* 29, 7–17.

Vijaya, Y., Popuri, S.R., Reddy, A.S. and Krishnaiah, A. (2011). Synthesis and characterization of glutaraldehyde-crosslinked calcium alginate for fluoride removal from aqueous solutions. *J. Appl. Poly. Sci.* 120, 3443–3452.

Vijayaraghavan, K., Padmesh, T.V.N., Palanivelu, K. and Velan, M. (2006). Biosorption of nickel(II) ions onto sargassum wightii: application of two-

parameter and three-parameter isotherm models. *J. Hazard. Mater.* 133, 304–308.

Wambu, E.W., Agong, S.G., Anyango, B., Akuno, W. and Akenga, T. (2014). High fluoride water in Bondo-Rarieda area of Siaya County, Kenya: a hydro-geological implication on public health in the Lake Victoria Basin. *BMC Public Health* 14, 462–470.

Wambu, E.W., Muthakia, G.K., Wa-Thiong'o, J.K. and Shiundu, P.M. (2011). Kinetics and thermodynamics of aqueous Cu(II) adsorption onto heat regenerated spent bleaching earth. *Bull. Chem. Soc. Ethiop.* 25, 181–190.

Wambu, E.W., Muthakia, G.K., wa-Thiong'o, J.K., Shiundu, P.M. and Joseph, K. (2009). Regeneration of spent bleaching earth and its adsorption of copper (II) ions from aqueous solutions. *Appl. Clay Sci.* 46, 176–180.

Wambu, E.W., Onindo, C.O., Ambusso, W. and Muthakia, G.K. (2013). Removal of fluoride from aqueous solutions by adsorption using a siliceous mineral of a Kenyan origin. *CLEAN - Soil, Air, Water* 41, 340–348.

Wang, Y., Chen, N., Wei, W., Cui, J. and Wei, Z. (2011). Enhanced adsorption of fluoride from aqueous solution onto nanosized hydroxyapatite by low-molecular-weight organic acids. *Desalination* 276, 161–168.

Weber, W.J.J. and Morris, J.C. (1963). Kinetics of adsorption on carbon from solution. J. Sanit. Eng. Div. *Am. Soc. Civ. Eng.* 89, 31–60.

Wei, S. and Xiang, W. (2012). Surface properties and adsorption characteristics for fluoride of kaolinite , ferrihydrite and kaolinite-ferrihydrite association. *J. Food, Agric. Environ.* 10, 923–929.

Weng, C. (2004). Modeling Pb(II) adsorption onto sandy loam soil. *J. Colloid Interface Sci.* 272, 262–270.

Weng, C.-H., Tsai, C., Chu, S.-H. and Sharma, Y.C. (2007). Adsorption characteristics of copper(II) onto spent activated clay. *Sep. Purif. Technol.* 54, 187–197.

Williamson, M.M. (1953). Endemic dental fluorosis in Kenya. a preliminary report. *East Afr. Med. J.* 24, 217–233.

World Health Organization (2011). Guideline for drinking water quality, 4th ed. World Health Organization, Geneva.

Wu, H., Chen, L., Gao, G., Zhang, Y., Wang, T. and Guo, S. (2010). Treatment effect on the adsorption capacity of alumina for removal fluoride. *Nano Biomed. Eng.* 2, 231–235.

Wu, Z., Li, C., Sun, X., Xu, X., Dai, B., Li, J. and Zhao, H. (2006). Characterization, acid activation and bleaching performance of bentonite from Xinjiang. *Chinese J. Chem. Eng.* 14, 253–258.

Xu, X., Li, Q., Cui, H., Pang, J., An, H., Wang, W. and Zhai, J. (2012). Column-mode fluoride removal from aqueous solution by magnesia-loaded fly ash cenospheres. *Environ. Technol.* 33, 1409–1415.

Xu, X., Li, Q., Cui, H., Pang, J., Sun, L., An, H. and Zhai, J. (2011). Adsorption of fluoride from aqueous solution on magnesia-loaded fly ash cenospheres. *Desalination* 272, 233–239.

Xu, Y.H., Ohki, A. and Maeda, S. (2000). Removal of arsenate , phosphate , and fluoride ions by aluminium-loaded shirasu-zeolite. *Toxicol. Environ. Chem.* 76, 111–124.

Yang, M., Hashimoto, T., Hoshi, N. and Myoga, H. (1999). Fluoride removal in a fixed bed packed with granular calcite. *Water Res.* 33, 3395–3402.

Zevenbergen, C., van Reeuwijk, L.P., Frapporti, G., Louws, R.J. and Schuiling, R.D. (1996. A simple method for defluoridation of drinking water at village level by adsorption on ando soil in Kenya. *Sci. Total Environ.* 188, 225–32.

Zhang, G., He, Z. and Xu, W. (2012). A low-cost and high efficient zirconium-modified-Na-attapulgite adsorbent for fluoride removal from aqueous solutions. *Chem. Eng. J.* 183, 315–324.

Zhang, J., Xie, S. and Ho, Y. (2009). Removal of fluoride ions from aqueous solution using modified attapulgite as adsorbent. J. Hazard. Mater. 165, 218–22.

Zhu, M., Ding, K., Jiang, X. and Wang, H. (2007). Investigation on co-sorption and desorption of fluoride and phosphate in a red soil of China. *Water. Air. Soil Pollut.* 183, 455–465.